Maren Elise Bengtson

Assessment of Impact of Dredging on Sediment Transport at Borg Port

Master's thesis in Marine Civil Engineering
Supervisor: Raed Lubbad
June 2019

Master's thesis

NTNU
Norwegian University of Science and Technology
Faculty of Engineering
Department of Civil and Environmental Engineering

NTNU
Norwegian University of
Science and Technology

Maren Elise Bengtson

Assessment of Impact of Dredging on Sediment Transport at Borg Port

Master's thesis in Marine Civil Engineering
Supervisor: Raed Lubbad
June 2019

Norwegian University of Science and Technology
Faculty of Engineering
Department of Civil and Environmental Engineering

NTNU
Norwegian University of
Science and Technology

Abstract

The purpose of this research was to model sediment transport during dredging operations. A numerical model for a selected case study, which is a dredging project at Borg Port, has been created using MIKE 21, powered by DHI. The hydrodynamic module of MIKE21 was used to calculate the current speed and it was validated using measurements at site. The particle tracking module of MIKE21 was used to simulate the suspended and sedimented sediments during the dredging process. It uses the output from the hydrodynamic module. Our numerical model was validated by comparing our results to results from SINTEF (research organisation) using their in-house software "DREAM".

The operating window, the discharge from the river, the wind speed and the wind direction were investigated. It was found that discharge from the river is the governing parameter for the current speed. The operating window, based on the discharge data and current speed, excludes June and parts of May.

The effect of the size of the release area were investigated and it only has an effect on the results if the area is changed with a magnitude of 100 or more. A sensitivity analysis for two parameters, namely the settling velocity and the sediment release rate, was performed. It showed that the release rate has a large effect on the results. This shows the importance of knowing with certainty that the release rate for the equipment are not higher than what is described in this report. The sensitivity analysis also shows the significant influence of the settling velocity on the results, as with a lower settling velocity than what has been used in the previous modelling, the sediments will spread over a large area and be difficult to control, especially in May.

For further work, attention should be given to three-dimensional (3D) modelling, to account for effects of flow stratification, which is important at Borg Port, as a estuarine circulation is formed at the river inlet, dividing the water colon in layers with different salinity levels.

Acknowledgements

The author would like to thank the supervisor, Raed Lubbad, for his patience, guidance and support. The author would also like to thank Tore Lundestad, Port director at Borg Port Authority, Ragnhild Daae from SINTEF, Aud Helland from Rambøll and Jens Laugesen from DNV GL for taking their time to answer questions and meetings, it has been essential for this report. The author would also like to thank Dennis Monteban from DTU/NTNU who has been of great help with the practical work with MIKE. Lastly the author would like to thank her husband, Olav Ingvaldsen Bengtson, for his patience and support throughout the work of this master thesis.

Sammendrag på norsk

Målet for denne masteroppgaven har vært å modellere hvordan sedimenter spres under mudringsoperasjoner. En numerisk modell for et utvalgt prosjekt, Borg Havns planlagte mudringsprosjekt, er blitt utarbeidet ved å bruke MIKE21 fra DHI. Den hydrodynamiske modulen i MIKE21 ble brukt til å beregne strømningshastigheten og ble validert ved å sammenligne med lokale målinger. Partikkelsporingsmodulen i MIKE21 ble brukt til å simulere de suspenderte og sedimenterte sedimentene under mudringsprosessen. Modulen benytter resultatene fra den hydrodynamiske modulen. Vår numeriske modell ble validert ved å sammenligne våre resultater med SINTEF (forskningsorganisasjon) sine resultater fra deres simuleringer i programvaren DREAM.

Tidsrommet, strømningen fra elva, vindhastigheten og vindretningen ble undersøkt og det ble funnet at strømningen fra elva er den viktigste parameteren for strømningshastigheten. Undersøkelsene av mulig tidsrom, basert på strømning fra elva og strømningshastigheten, ekskluderer juni og deler av mai.

Effekten av størrelsen på mudringsområdet ble undersøkt og det har kun påvirkning på resultatet hvis det endres i en størrelsesorden på 100 eller mer. En sensitivitetsanalyse ble utført for to parametere, fallhastighet og utslippsrate. Undersøkelsene viste at utslippsraten har stor effekt på resultatene og det er derfor viktig å forsikre seg om at utstyret som brukes har den utslippsraten som er beskrevet i denne oppgaven eller lavere. Sensitivitetsanalysen viste også at fallhastigheten har stor effekt på resultatet, hvis den er lavere enn hva som er brukt tidligere (0.1 mm/s) vil sedimentene spre seg over store områder og være vanskelig å kontrollere.

Videre arbeid bør fokusere på å utvikle den tredimensjonale modellen videre slik at effekten av strømningslagdeling blir inkludert. Dette er viktig da området ligger slik til at det dannes en estuarinsirkulasjon ved innløpet til elva, som deler vannkolonnen inn i lag med ulik salinitet.

Contents

List of Figures

List of Tables

Chapter 1

Introduction

1.1 Background

In any dredging operation there will be spreading of a certain amount of sediments, which may cause harm to the surrounding environment mainly due to turbidity and lack of passage of light. Therefore, there are certain limits as to how much spreading of sediments is allowed while dredging. These limits can be monitored by measuring the turbidity in the water. Prior to dredging operations it is essential to know whether the sediment spreading pose a risk to the environment. To assess this, one can numerically simulate the dredging process and the consequences of spreading of sediments. By simulating different scenarios, we can find out which option is the best and if it is safe for the environment.

In Borg Port, located in Fredrikstad, the fairway will be deepened and parts of it will be relocated. This will be done by dredging and blasting. It's the Norwegian Coastal Administration that are responsible for the project. The project is planned to be executed in the upcoming years. One of the problematic aspects of this project is contaminated sediments. There are also several habitats of rare species that need to be protected throughout the project.

This area and project forms an interesting case study for simulating dredging processes. In this thesis, a numerical model will be used to simulate the spreading of sediment during dredging at Borg Port and to study its effects on the environment.

1.2 Problem statement

MIKE21, powered by DHI, was used to analyse the hydrodynamic conditions in Borg Port (mainly currents) and to simulate the transport of sediments during dredging.

The initial part of the study was focused on the calibration and validation of the model using in situ data and previously available results from a numerical model by SINTEF (research organization).

A sensitivity analysis for the sediment transport rates in the fairway was carried out. The influence of some of the parameters governing sediment transport was analysed and described.

1.3 Approach

Available literature on the subject was gathered and reviewed. The university and especially the university's library service, Oria, were very helpful. Google Scholar was useful for finding relevant articles and books.

The co-supervisor, Tore Lundestad, Port Director at Borg Port Authority was of great help to gather the data needed for the case study. In addition, people from several companies (that have been involved in the Borg Port dredging project) has been contacted and they provided

valuable input. This includes Ragnhild Daae from SINTEF, Jens Laugesen from DNV GL (classification society) and Aud Helland from Rambøll.

Data for the discharge from Glomma river and wind data were gathered by the help of The Norwegian Institute for Water Research (NIVA) and from The Norwegian Meteorological Institute (MET). Tidal data were generated by MIKE21 and verified by comparison to local measurement. The data were analysed and used as input to the hydrodynamic module of MIKE21. The output of the hydrodynamic module is mainly depth-averaged current velocity. After the current velocity was calculated, the sediment transport module of MIKE21 was configured. By using this module to simulate the same dredging operations as had already been done by SINTEF, the sediment transport module was validated.

The sediment transport module was then used for a sensitivity analysis, and the results were studied. The results were discussed, conclusions were drawn and further work was proposed.

Prework

As a part of the course TBA4550, "Marine Civil Engineering, Specialization Project", preparations for the master thesis was done in the fall of 2018. The work consisted of two main parts, clarification and preparation. The goal of the first part was to clarify the scope of the thesis and define a problem statement. The goal of the second part was to prepare for the master thesis, including deciding upon and installing the software needed, acquiring the right theoretical knowledge, acquiring the information about the case study, getting in contact with key people in the case study project and getting familiarized with the software.

The results of this project report is partly included in this master thesis.

1.4 Structure of the report

This report consists of eight chapters:

- **Chapter 1: Introduction**: Describes the background of the project, the approach that has been used and an overview of the content of the report.
- **Chapter 2: Sediment transport**: Describes sediment transport and the physics of how sediments spread. Advection, diffusion, flux, plumes and fall velocity are presented.
- **Chapter 3: Dredging**: Describes what dredging is, the different type of dredging equipment and gives information about the dredging that is planned in Borg Port. Spreading of polluted sediments are described briefly.
- **Chapter 4: Borg Port**: Introduces the history of the expansion project in Borg Port, the previous modeling, the estuarine circulation, the input data for the numerical modeling and the analysis of the data.
- **Chapter 5: Numerical Modelling**: Introduces the software that will be used for the numerical modelling, MIKE software package, powered by DHI. Explains the assumptions, modules and solution technique used in the software. Lists the required input and the possible outputs.
- **Chapter 6: Validation**: Describes the set-up and results of the simulations that were run to validate the MIKE model by comparing to results from SINTEF in their DREAM (Dose-related Risk and Effects Assessment Model) model.
- **Chapter 7: Results and discussions**: Presents the results of the sensitivity analysis of the configured model and discuss the relevant aspects of the theory, validation and results.

- **Chapter 8: Conclusion and recommendations for further work**: Shortly captures the work that has been done and lists recommendations for further work.

Chapter 2

Sediment transport

"Sediment is a naturally occurring material that is broken down by processes of weathering and erosion, and is subsequently transported by the action of wind, water, or ice or by the force of gravity acting on the particles" (Wikipedia, 2018b). Sediment transport can be defined as "the movement of sediment from sediment sources to sedimentary deposits, often interrupted by various types of temporary sediment storage" (Matthews, 2014). The sediments can be moved by wind, water or ice. In more technical terms it can be defined as "a strong and non-linear function of the current velocity and orbital motion" (Roelvink, Reniers, 2011). Orbital motion is motion around a fixed point moving in a circular pattern. Sediment transport can be divided into bed load transport and suspended load transport. In figure 2.1, the different mechanisms of sediment transport on land is visualized, where we see that when the sediment has a creep movement it is mainly driven by bed load transport, and when it is in suspension it is mainly driven by suspended load transport (Roelvink, Reniers, 2011). The sediment transport in water is similar to what happens on land. When a sediment is moved in saltation a mix of bed load transport and suspended load transport is affecting the sediment.

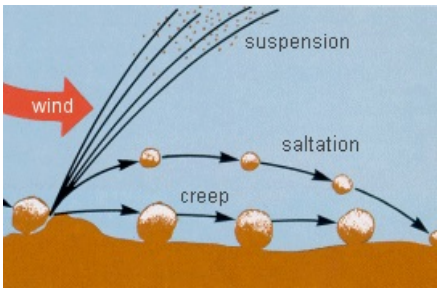

Figure 2.1: Definition sketch of particle creep, saltation and suspension (Carson, 2011)

Bed load transport is the activity just above the bed and is responsible for 50% of the sediment transport (Roelvink, Reniers, 2011; Matthews, Owen, 2014). This transport reacts quickly to the local conditions. It's usually sand and gravel, but it can also transport some finer particles such as mud and silt (Matthews, Owen, 2014).

Suspended load transport is a slower process and is mainly following the water motion in a flow (Roelvink, Reniers, 2011; Matthews, Boulton, 2014), which means that it depends on time or space to be picked up or settle down. Turbulent flow is created by the eddies in the main flow, which keeps the sediments suspended. The particles are >0.2mm in diameter in rivers and streams.

There are some general trends for sediment transport (Roelvink, Reniers, 2011):

- Sand tends to go in the direction of the near-bed current.
- If the current increases, the transport increases by some power greater than 1.

- On a sloping bed transport tends to be diverted downslope.
- The orbital motion stirs up more sediment and thus increases the transport magnitude.
- In shallow water, the wave motion becomes asymmetric in various ways, which leads to a net transport term in the direction of wave propagation or opposed to it.

Turbidity is the interference of passage of light through air or water (Matthews, 2014). In water it is suspended particles that causes the turbidity. Turbidity in water can be measured with turbidity meters and sensors which assess the degree of cloudiness.

2.1 Plumes and jets

A plume is a boundary layer flow originating from a source of buoyancy (Lund University, 2010). A buoyant jet is a forced plume with a boundary layer flow originating from a source of momentum and buoyancy.

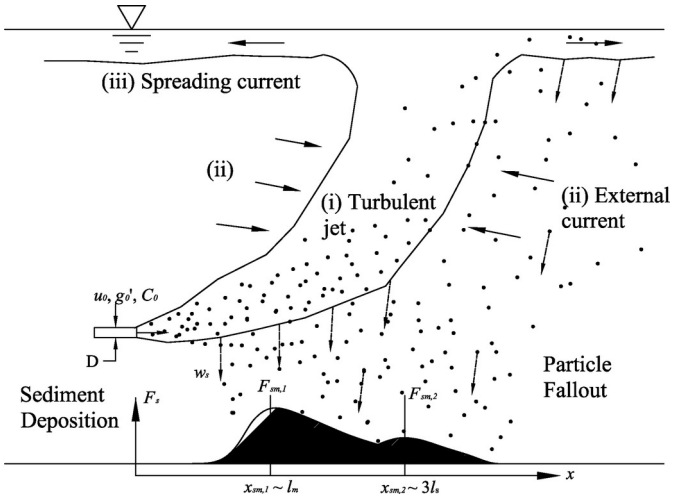

Figure 2.2: Horizontal sediment-laden buoyant jet (Chan, Lee, 2016)

A result of marine disposal of dredged soil is sediment-laden turbulent buoyant jets (Chan, Lee, 2016). A jet can either sink or rise when discharged into a marine environment. If the effluent has a higher density than the surrounding fluid it will sink as a negatively buoyant plume (Gildeh et al., 2014). It will look similar to the plume in figure 2.2, where u_0 is the jet initial velocity, $g_0{}' = (\Delta\rho/\rho)g$ is the jet initial reduced gravity, c_0 is the initial sediment concentration, D is the jet diameter, F_s is the deposition rate per unit distance along jet direction with peaks at $F_{sm,1}$ and $F_{sm,2}$ at distance $x_{sm,1}$ and $x_{sm,2}$.

To calculate the settling of particles from a sediment-laden turbulent buoyant jet we both have to calculate the turbulent fluctuations and the mean flow-in particular particle re-entrapment due to the external irrotational flow induced by the jet (Chan, Lee, 2016).

It has been observed through experimental studies that a vertically downward discharging sediment jet's sectional particle velocity and concentration follows a Gaussian distribution. It was also found that the spreading of particle jet depends on particle size and loading (Chan, Lee, 2016).

2.2 Settling velocity

To describe the movement of sediments in suspension we need the settling velocity and the associated drag force (Swamee, Ojha, 1991). The settling velocity occurs as a constant speed

when the submerged weight is in equilibrium with the drag force. Which is the friction between the particle and the substance around it (Swamee, Ojha, 1991; Johansen, 1993), as shown in figure 2.3, and described mathematically as:

$$\rho V g - \rho_w V g = \frac{1}{2}\rho_w {w_s}^2 C_D A \tag{2.1}$$

where ρ is the density of the particle, ρ_w is the density of the surrounding fluid, g is gravity, w_s is the settling velocity, C_D is the drag coefficient and A and V is defined as:

$$A = \pi {D_n}^2 \tag{2.2}$$

$$V = \frac{\pi {D_n}^3}{6} \tag{2.3}$$

where D_n is the diameter of the particle. We then get:

$$\frac{\pi {D_n}^3}{6} g(\rho - \rho_w) = \frac{1}{2}\rho_w {w_s}^2 C_D \frac{\pi {D_n}^2}{4} \tag{2.4}$$

and finally:

$$w_s = \sqrt{\frac{4(s-1)gD_n}{3C_D}} \tag{2.5}$$

where $s = \frac{\rho}{\rho_w}$.

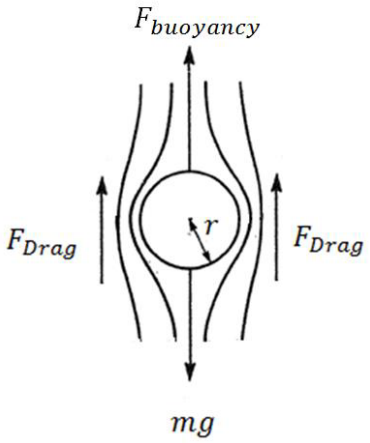

Figure 2.3: Drag, buoyancy and gravity forces on a particle in a fluid (Saremi, 2016)

When the particles have a spherical shape and the Reynold's number is $Re < 1$, $C_D = 24/Re$ can be used when calculating the settling velocity (Johansen, 1993). This gives Stokes equation:

$$w_s = \frac{{D_n}^2}{18\mu} g \Delta\rho \tag{2.6}$$

where $\Delta\rho = \rho - \rho_w$ and μ is the dynamic viscosity of the surrounding liquid. This law is well fitted with experimental data for fine sediments ($d < 0.01mm$).

2.2.1 Drag coefficient

One parameter that is difficult to decide in these equations is the drag coefficient. The drag coefficient is closely connected to the Reynold's number (Re):

$$Re = \frac{w_s D_n}{v} \tag{2.7}$$

where v is the kinematic viscosity:

$$v = \frac{\mu}{\rho_w} \tag{2.8}$$

There has been done a lot of experiments in order to find C_D empirically. Some relations for the Reynolds number has been found:

Table 2.1: Drag coefficients for different Reynolds numbers

Re	C_D
Very low	$\frac{24}{Re}$
$1 - 2,000$	$\frac{130}{Re}^{0.45}$
$2,000 - 2 \cdot 10^4$	$0.133 \cdot Re^{0.125}$
$2 \cdot 10^4 - 1.5 \cdot 10^5$	0.5

2.2.2 Flocculations

Flocculation is "a process, also known as coagulation, which causes clay particles to form aggregates (also known as flocs)" (Wohlfarth, 2014). One example of how flocculation occurs is when electrically charged colloidal clays mixes with saline water that carries electrically charged particles.

2.3 Bed load transport

Bed load transport, which takes place in a thin layer above the bed, can always be assumed to react directly to local flow conditions (Roelvink, Reniers, 2011). The bed shear stress that is created due to the flow acting on sediment grains is often expressed as the dimensionless Shields parameter:

$$\theta = \frac{\sigma_s}{\rho_w g \Delta D_{50}} \tag{2.9}$$

where σ_s is the bed shear stress, ρ_w the water density, g the acceleration of gravity, $\Delta = (\rho - \rho_w)/\rho_w$ is the relative sediment density, and D_{50} is the median grain diameter. The dimensionless Shields parameter reflects the balance between lifting forces, which are proportional to shear stress and grain surface, and gravity, which is proportional to the relative density, g and the grain volume.

A general form of bed load transport formulation is given by:

$$q_b \approx \sqrt{\Delta g {D_{50}}^3} \theta^{b/2} (m\theta - n\theta_{cr})^{c/2} (1 - \alpha \frac{\partial z_b}{\partial s}) \tag{2.10}$$

where q_b is the transport rate and θ_{cr} is the critical shear stress. The coefficient m represents a ripple efficiency factor, which depends on the ratio of skin friction to form drag, and n may represent a factor for hiding and exposure in graded sediments. A number of bed load transport formulae are captured by this formulation, e.g. Meyer-Peter and Muller (1948) (c=3,b=0) , van Rijn (1984) (b=0,c=3-4). And:

$$\alpha \approx \frac{\tilde{c}_{eq}}{\tilde{c}} \tag{2.11}$$

where $\tilde{c}$ is the depth-averaged concentration, $\tilde{c_{eq}}$ is the equilibrium depth-averaged concentration.

2.4 Suspended load transport

Advection is here defined as the movement of fluid particles due to the resolved flow processes (MIKE, powered by DHI, 2017e). Convection is often used as a synonym to advection, but can also be described as the movement of fluid due to density gradients created by thermal gradients. Dispersion is here defined as scattering of fluid particles due to non-resolved flow processes and is divided in shear, which is caused by the spatial velocity gradients and diffusion, which is caused by the molecular motion and turbulence (Wikipedia, 2018a; MIKE, powered by DHI, 2017e).

2.4.1 Flux

Fickian dispersion describes the spreading of solute mass in a fluid at rest (Arntsen, McClimans, 2003). The transport of any tracer across a unit area is the sum of advected concentration due to the flow in the direction normal to the area and dispersion of tracer proportional to the concentration gradient in the direction normal to the area.

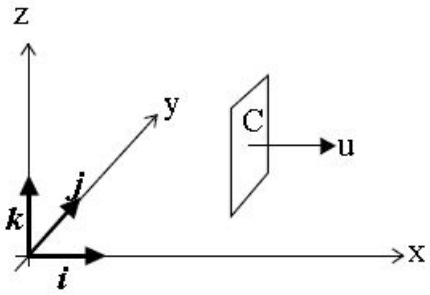

Figure 2.4: Flux of material across a plane C normal to the x-axis (Arntsen, McClimans, 2003)

When considering a unit area normal to the x-axis in a standard Cartesian co-ordinate system, as shown in figure 2.4, the flux through this unit (q) can be described as:

$$q = uc - D\frac{\partial c}{\partial x} \tag{2.12}$$

where uc is the advective part (c is the mass concentration of the tracer in the fluid and u is the instantaneous current velocity vector at position x and time t). The second term on the right-hand side of equation 2.12 is the diffusive part where D is the dispersion coefficient.

2.4.2 Transport

When calculating sediment transport the advection-dispersion equation is used. It can be used in several dimensions, but is usually either used in two or three dimensions. The general equation in i dimensions is (MIKE, powered by DHI, 2017e):

$$\frac{\partial c}{\partial t} + \frac{\partial u_i c}{\partial x_i} = \frac{\partial}{\partial x_i}(D_i \frac{\partial c}{\partial x_i}) + SS \tag{2.13}$$

where c is the concentration of the substance, t is time, D_i is the dispersion coefficients and SS is the sink-source term. The source-sink term, SS, represents the exchange with the bottom (Roelvink, Reniers, 2011), and defined by Galappatti and Vreugdehnhil in 1985 as (Galappatti, 1985):

$$SS = \frac{h(\tilde{c_{eq}} - \tilde{c})}{T_s} \tag{2.14}$$

where h is the water depth, $\tilde{c}$ is the depth-averaged concentration, $\tilde{c_{eq}}$ is the equilibrium depth-averaged concentration and T_s is a typical timescale, which can be expressed as:

$$T_s = T_{sd}\frac{h}{w_s} \tag{2.15}$$

where w_s is the settling velocity and T_{sd} is a dimensionless factor that depends on the ratio of shear velocity to settling velocity.

When calculating the sediments in suspension we use the 3D version of the advection-dispersion equation (Roelvink, Reniers, 2011):

$$\frac{\partial c}{\partial t} + u\frac{\partial c}{\partial x} + v\frac{\partial c}{\partial y} + (w - w_s)\frac{\partial c}{\partial z} - \frac{\partial}{\partial z}(D_s\frac{\partial c}{\partial z}) - \frac{\partial}{\partial x}(D_h\frac{\partial c}{\partial x}) - \frac{\partial}{\partial y}(D_h\frac{\partial c}{\partial y}) = SS \tag{2.16}$$

where u is the flow velocity in x-direction, v is the flow velocity in y-direction, w is the flow velocity in z-direction, w_s is the settling velocity, D_s is the vertical dispersion coefficient and D_h is the horizontal dispersion coefficient.

It can be argued that the horizontal variations is of higher importantance than the vertical non-uniformities when calculating the suspended load and we can use the depth-averaged 2D version of the equation (Roelvink, Reniers, 2011):

$$\frac{\partial h\tilde{c}}{\partial t} + \tilde{u}\frac{\partial h\tilde{c}}{\partial x} + \tilde{v}\frac{\partial h\tilde{c}}{\partial y} - \frac{\partial}{\partial x}(D_h\frac{\partial h\tilde{c}}{\partial x}) - \frac{\partial}{\partial y}(D_h\frac{\partial h\tilde{c}}{\partial y}) = SS \tag{2.17}$$

where $\tilde{u}$ and $\tilde{v}$ is the depth-averaged velocities.

2.4.3 Boundary conditions

For the bottom boundary condition of a sandy bed the flux (q) of sediment between the bed and the flow can be described as (Roelvink, Reniers, 2011):

$$q_z = -D_s\frac{\partial c}{\partial z} - w_s c \tag{2.18}$$

where the concentration gradient can be approximated by:

$$\frac{\partial c}{\partial z} \approx \frac{c(z_{ref} + \Delta z) - c_{ref}}{\Delta z} \tag{2.19}$$

where c_{ref} is the reference concentration, z_{ref} the reference depth and Δz the difference between the depth and the reference depth.

When defining equation 2.18 and 2.19 it becomes evident that with increasing shear stress the sediment flux from the bed to the water column will be positive. When the shear stress decreases the settling flux term will be dominant.

2.4.4 Spreading of polluted sediments

For this chapter, only spreading of polluted sediments in water, not in air, is covered. The spreading of pollution is usually driven by the difference in the density between the pollution and the medium it is spreading in (Johansen, 1993). This phenomenon is also called reduced gravity and is described by g' given as:

$$g' = g(\rho_w - \rho)/\rho_w \tag{2.20}$$

where g is gravity ρ_w is the density of the surrounding water and ρ is the density of the sediments.

Passive pollution is defined as when the pollution does not affect the currents in the water. This usually happens at a later state in the pollution process. First the pollution is spreading

and dilution is decided by convection currents, which is caused by the buoyancy of the pollution. Further away from the source, the pollution will be so diluted that the density difference will not matter any more, and only the turbulence is further diluting the pollution concentration. To calculate the spread in these cases the advection-dispersion equation (equation 2.13) is used. The simplest case with a one dimensional dispersion in one direction with a constant current u in the x-direction is described by equation:

$$\frac{\partial c}{\partial t} + u\frac{\partial c}{\partial x} = \frac{\partial}{\partial x}(D\frac{\partial c}{\partial x}) + SS \tag{2.21}$$

where c is the concentration of the polluted substance, D is the dispersion coefficient. For molecular dispersion D is assumed to be substance-constant, in other words a feature of the substance that it disperses. This equation is rather hard to hand calculate and are therefore often solved numerically.

If constant current U is assumed in the surrounding area, the transported distance X is determined by:

$$X = U\tau \tag{2.22}$$

where:

$$\tau = h/w_s \tag{2.23}$$

where h is the water depth and w_s is the settling velocity.

As the current vary in time, the spreading of the particles will depend on the time of discharge. The current varies in two directions and therefore X has two components, x and y, which is the eastward u and the northward v components of the current U. The position of $X = (x, y)$ can be evaluated as a distribution function:

$$(X(\tau)) = \left(\int_0^{t_i+\tau} U dt - \int_0^{t_i} U dt\right)_{i=1,n} \tag{2.24}$$

where t_i is the time of the current measurement.

When assuming that this set of positions are normally distributed and symmetrical fit around the center of gravity, the distribution can be presented by the middle position $X_m = U_m t$ and the standard deviation in the radial direction $\sigma(\tau)$. The deposition pattern of the particles with a falling time of τ will be uncertainty ellipses with a center of gravity and variance that can be decided using statistical analysis of current measurements in the area. The total particle deposition pattern (with a certain particle distribution) will be a weighted sum of those uncertainty ellipses.

When the particles are released at a depth of 5m, they have approximately an entrapment depth of 20m, where the underwater cloud divides into two parts (Daae et al., 2018):

- The first part is spreading horizontally in the entrapment depth. This part consists of dissolved compounds that doesn't sink and solid particles that are so small that the settling velocity is neutralized by the Brownian motion.
- The other part of the discharge sinks to the bottom. This part can consist of bigger particles with chemical components attached.

The process is shown in figure 2.5 where SINTEF has modelled an example of such a discharge. The discharge is in the top left corner and the water depth is 400m.

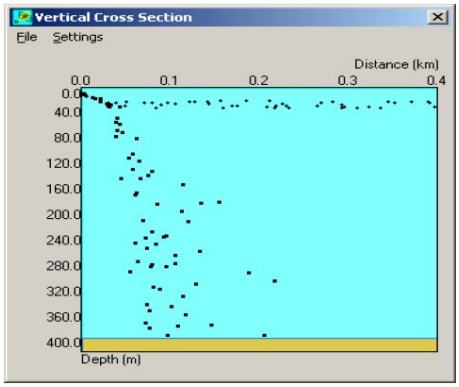

Figure 2.5: SINTEF's modeled example of discharge (Daae et al., 2018)

To find the concentration of the polluted sediments equation 2.21 is used and a mass M is assumed. The result is:

$$c(r,t) = c_0 e^{-\frac{r^2}{2\sigma^2}} \tag{2.25}$$

where r is the radial distance, c_0 is the concentration in the center ($r = 0$) and defined as:

$$c_0 = \frac{M}{2\pi\sigma^2} \tag{2.26}$$

and the variance, σ^2, can be described as:

$$\sigma^2 = 2Dt \tag{2.27}$$

where t is the time of dispersion and D the dispersion coefficient.

The dispersion coefficients have to be found empirically in the case of horizontal turbulence. This is due to the large variance in size of the vortices, which makes it difficult to decide the characteristic length.

Discharge

Generic types of discharges to water can be classified as (Arntsen, McClimans, 2003):

- Buoyant (e.g. sewerage, river, oil)
- Neutral (e.g. chemicals, radioactivity, trace metals)
- Dense (e.g. mine tailings, slurries, brine, cold seawater, marine particles).

The amount of heavy metals that is available for organism uptake in the water column depends highly on the acid-volatile sulfides (AVS), organic content, and particle size of the sediment particles brought into suspension (Bach et al., 2016). Metal concentrations are generally highest in fine fraction (particle size <63 μm) of aquatic sediments because of the large surface area to volume ration and the availability of binding phases, such as organic carbon and sulfides. The fine fraction is the sediment fraction that is most easily brought into suspension and which may stay in suspension for the longest time. Usually the major part of the fine-grained material is transported away from the construction site and its vicinity. This could imply that the heavy metals that are bound to this material were transported away and became mobilized far away from the construction site. When in suspension, the contaminated sediments may be subject to chemical changes, such as increased redox potential or decreased pH, thus acting to increase the bioavailabiity of metals.

Chapter 3

Dredging

Dredging can be described as a process with three stages (Manap, Voulvoulis, 2014). The three stages are excavation at site, transport and disposal at site, as shown in figure 3.1. Dredging is in other words sediments being moved from one place, most often in water, to another place, either in water or on land.

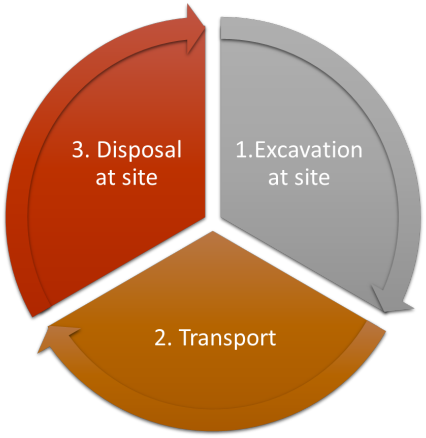

Figure 3.1: The three stages of dredging (modified based on (Manap, Voulvoulis, 2014))

There are mainly three reasons for dredging. The first one is remedial dredging, also called environmental dredging, which is removal of contaminated sediments in water (Wang, Feng, 2007). The second reason is maintenance, where the goal is to sustain the water depth or similar actions (Fettweis et al., 2011). The third reason is capital, where the goal is to create a new area, change a fairway, create a new trench or similar actions.

When dredging contaminated sediments, there are a lot of aspects to consider. First the contaminated layer must be removed. One of the aspects to consider when removing the sediments is to not overdredge, as this causes unnecessary turbidity and expenses. Another aspect is the spreading of these contaminated sediments. As it is important that they don't spread, the method chosen should be carefully evaluated.

All three aforementioned stages of dredging bring with them different impact on the environment around as can be seen in figure 3.2. One of the most visible effects of the turbidity caused by the dredging is the reduction of sunlight penetration (Ansa, Akinrotimi, 2018).

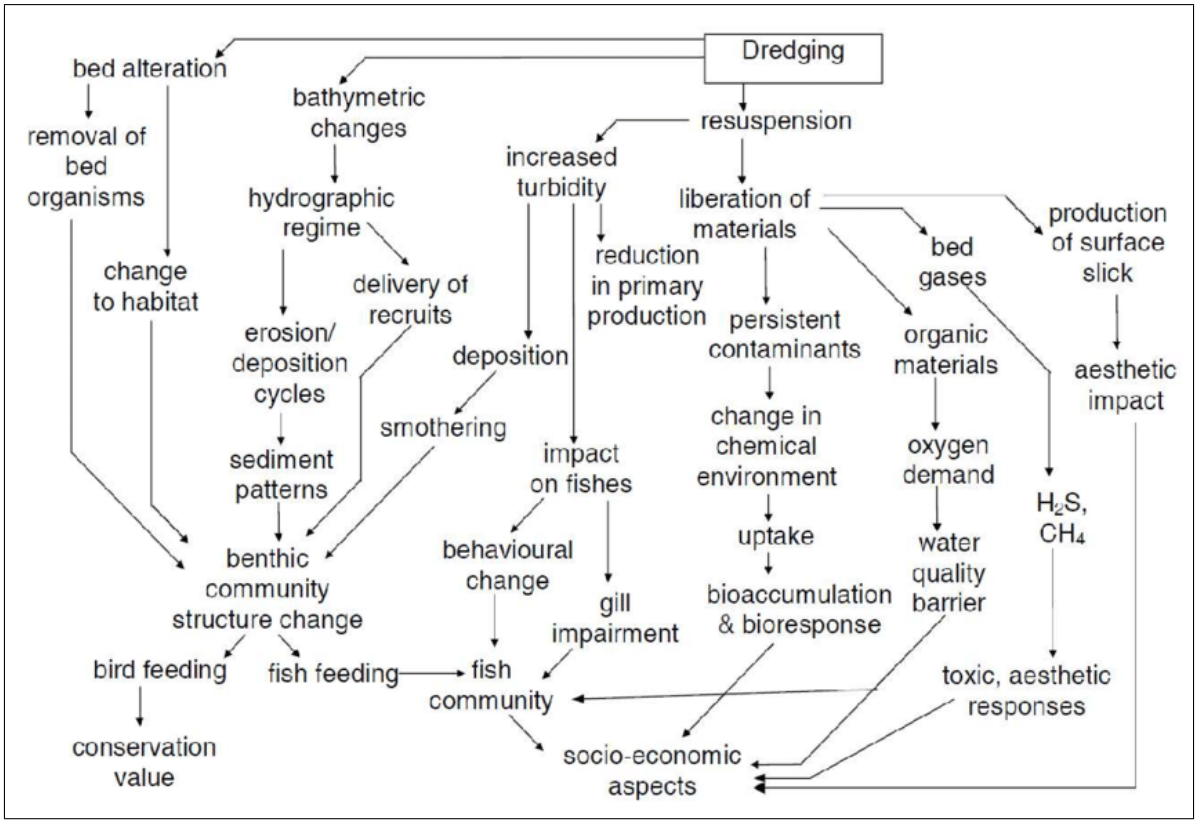

Figure 3.2: Potential environmental impacts of marine dredging (Elliot, Hemingway, 2018)

3.1 Dredging equipment

There are two main type of dredgers: Mechanical and hydraulic (European Dredging Association, 2018). There is also a need to define a third category, other, as not all dredgers fit in one of the two first categories.

3.1.1 Mechanical

The mechanical dredgers are bucket dredgers, grab dredgers and backhoe dredgers. There are several types of grabs and backhoes which are developed to fit different types of sediments. The two half-shells of the grab can either be operated by wire or (electro)-hydraulically. A grab in wire is illustrated in figure 3.3. A backhoe dredger is a backhoe that is installed on a pontoon (Jan de Nul, 2014), an example of a backhoe dredger is illustrated in figure 3.4. One of the backhoe dredgers that are used a lot is the long-range backhoe dredger, which allows for dredging at deeper areas.

Figure 3.3: Grab in wire (MyNewsDesk, 2014)

Figure 3.4: Backhoe dredger (Jan de Nul, 2014)

When doing environmental dredging a grab is usually used (from personal communication with Jens Laugesen, Chief Specialist Environment, DNV GL). It is important to use a grab that leaves a flat level, also called a horizontal level cut. This is needed to not stir up the contaminated sediments. The grab should also be closed on top, so the sediment spreading is reduced.

3.1.2 Hydraulic

The hydraulic category consists of suction dredger (see figure 3.5), cutter suction dredger, trailing hopper suction dredger and reclamation dredger. They all have in common that they raise the sediments up to the surface using a pipe system connected to a centrifugal system. This makes it a good option for fine sediment, but not for coarser sediments. Some sediments need to be loosened either by mechanical dredgers or water jets before using the pump. One example is the cutter suction dredger where the material is first loosened with a rotating cutter at the bed. Other sediments can be sucked up without loosening.

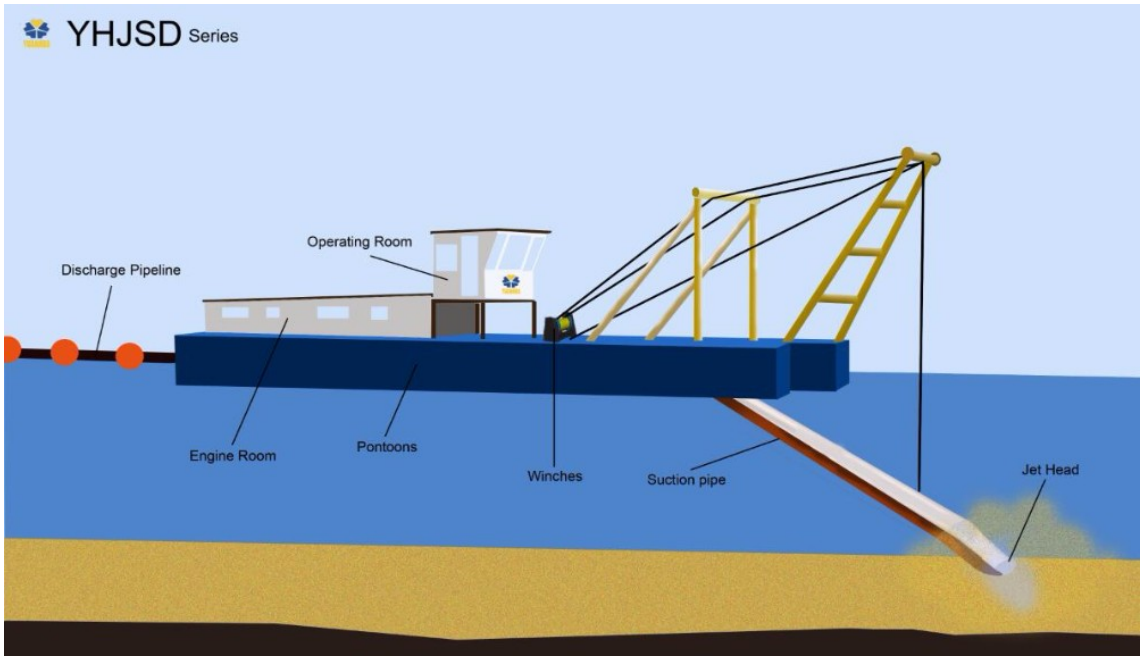

Figure 3.5: Suction deepwater sand dredger (Yuanahua, 2019)

3.1.3 Other

The other dredgers that don't fit in the two first categories are jet-lift dredgers, air-lift dredgers, augur suction dredgers, pneumatic dredgers, amphibious dredgers and water injection dredgers. Some of these are a mix of mechanical and hydraulic and some use different principles. These specialized dredgers are usually small in size and output.

3.2 Resuspended sediments during dredging

Dredging operations generate resuspension, sediments being stirred up from the bed. The rate of resuspension varies greatly. The amount of resuspension is dependent on the interaction between the dredging method (both the excavation and the discharge method), the sediment (particle size distribution, water content, cohesive strength, etc.) and water and soil conditions (Daae et al., 2018). The rate of resuspension can be expressed as a fraction of the dredging rate (Høy-Petersen, 2008). The sediment resuspension rate (SRR, kg/hr or ton/hr) is expressed as:

$$SRR = Q \cdot \chi \cdot \gamma \tag{3.1}$$

where Q is the volume dredging rate (m^3/hr), χ the sediment solids content ($dry - ton/m^3$ or $dry - kg/m^3$) and γ the fractional resuspension. The fractional resuspension is generally between 0.01 and 0.1 (Høy-Petersen, 2008). The fractional resuspension depends on sediment conditions (sediment grain size or fines content, sediment bulk density or moisture content, and sediment mineralogy and organic content), current conditions and on choice of dredging operation method.

3.3 Dredging in Borg Port

In the case of the dredging project for Borg Port Authority the main goal is to change the fairway, which is considered capital dredging. As there are contaminated sediments there will have to be remedial dredging. Maintenance dredging is done almost every year at Borg Port and some of the dredging done during this project will also be maintenance dredging (communication

with Tore Lundestad, Borg Port director). Overdredging is not an issue as the dredging depth will be deeper than the contaminated layer (The Norwegian Environment Agency, 2018).

Chapter 4

Borg Port

Borg Port is the case study chosen for this project. They will be doing an expansion project, including dredging a large amount of sediments, in the upcoming years. The port is located in Fredrikstad, Hvaler and Sarpsborg, in Østfold, Norway. The area is shown in Figure 4.1.

Figure 4.1: Borg Port in Fredrikstad, Norway (Google Earth, 2018)

The area is at the end of the river Glomma, which is Norway's longest river, with a length of 619 km and a catchment area of 41 857 m^2 (SNL - Great Norwegian Encyclopedia, 2019). There has been a lot of industrial activity along the river, leading to contamination being brought with the river, to Borg Port, throughout the years.

The port has been operated by Borg Port Authority since 1993 (Borg Havn IKS, 2018). It is used for multiple purposes; cruise, container, recreational, etc.

4.1 Borg Port Dredging Project

The combined maintenance and capital dredging project for Borg Port Authority began already in 2006, when the users of the port saw the need for a deeper, wider and safer fairway (personal communication with Tore Lundestad, Borg Port director), see Figure 4.2. In addition, a need to enlarge the turning basin was identified. One of the reasons for changing the fairway is the current restrictions on night sailing for ships longer than 165 m, which has a negative influence on the attractiveness of the port. Ships have to wait for daylight, which increases the cost and causes delays for the larger service ships that are operating weekly. One of the goals is to be able to handle a higher load of large ships also for the night sailing. Several causes has delayed the project until now.

Figure 4.2: The fairway to Borg Port, Røsvikrenna, marked in yellow, the turning base, Fuglevikbukta, in red and the deposit areas, Møkkalasset and Svaleskjær, in blue (Google Earth, 2018). Borg 2 is defined as the area from Flyndregrunnen (at the bottom of the yellow circle) to Duken (7km south of the map).

The turning basin, shown in Figure 4.3, will be extended to handle ships up to 250 m, compared with 20 m today. The project includes dredging 750 000 m^3 of contaminated sediments, 2 560 000 m^3 of clean sediments, blasting 250 450 m^3 of bedrock and the disposal of the rock and sediments (The Norwegian Environment Agency, 2018). The new depth is from 11.3 m to 16.3 m at different areas. At the shallowest point, the current depth is less than 1 m. After the dredging, ships up to 205 m will be able to use the fairway also during night time.

Figure 4.3: Turning basin at Borg Port (Google Earth, 2018)

The pollutants in the contaminated sediments mainly come from persistent point discharges, from industry and drains from urban areas (Daae et al., 2018). These are mainly metals and organic toxic waste. These metals and organic toxic waste has been detected: Arsenic, chromium, copper, mercury, lead, nickel, zinc, PAH16, PCB7 and TBT.

The sediments consists mainly of silt, clay, sand and some organic material. The clean sediments are defined as sediments that are in class 1 to class 3 according to the Norwegian classification system for metals and organic toxic in water and sediments (Miljødirektoratet, 2016). These sediments will be disposed of in two disposal locations, called Møkkalasset and Svaleskjær, see Figure 4.2. These are both seabed disposal sites. The contaminated sediments are going to a landfill called Frevar.

Another aspect that makes this project difficult is all the different species that currently live in the area which will be affected by the work. Rambøll has done a thorough analysis of the habitat of the species currently living there (Helland, 2018).

The project is now being evaluated by the Norwegian Environment Agency (The Norwegian Environment Agency, 2018). This is needed due to the contaminated sediments and the endangered habitats. There are many interested parties that have shown interest by voicing their opinions at the public hearing during the fall of 2018. In the proposal the project is divided into two main parts and consists of multiple smaller parts (The Norwegian Environment Agency, 2018). The first part is called Borg 1 and includes the area closes to the port called Røsvikrenna and the turning basin at Fuglevikbukta, see Figure 4.2. The second part is called Borg 2 and covers the area called Flyndregrunnen to the area called Duken.

It is important to find out the amount of contaminated and non-contaminated sediments as this will highly affect the price of the dredging process (Hjermann, 2018). Several companies has been involved in order to calculate the amounts of sediments with as little uncertainty as possible. The results are presented in Table 4.1.

Table 4.1: Dredged sediments and volume available for spreading in the water column

	Confidence interval	Dredged volume	Volume available for spreading
Total contaminated sediments	80% 95%	742 433 m^3 963 728 m^3	37 122 m^3 48 186 m^3
Total non-contaminated sediments	80% 95%	2 545 293 m^3 2 354 985 m^3	185 656 m^3 171 822 m^3
Total volume dredged and available for spreading	80% 95%	3 287 726 m^3 3 318 713 m^3	222 777 m^3 220 008 m^3

In this project there are several aspects to be aware of and take into consideration. The main goal of the project is to do capital dredging to increase the depth. This will give a larger clearance under the ships and allow the port to receive bigger vessels. Another goal is to change parts of the fairway, which will lead to a safer and more visible passage for the ships. This is planned to be done by blasting. In conjunction with this project the maintenance dredging of the harbor must also be considered.

4.2 Previous modelling

SINTEF has modelled the dredging process using their own particle based model called DREAM with a detailed set of data for the current generated by SINTEF's numerical 3D model SINMOD (Daae et al., 2018). The different types of materials were calculated based on an 85 percentile and a 95 percentile.

For the fall velocity a value of 0.1 mm/s was used (Daae et al., 2018). This value has been calculated based on the flocculation potential for the sediments which has been analysed by Deltares.

For the modelling that has been done by SINTEF, the remedial dredging was done by a long-range backhoe at Fuglevika and with two backhoes at Borg 1 (Daae et al., 2018). For the dredging of the non-contaminated sediments, grab in wire, small suction dredger and big suction dredger were used (Daae et al., 2018). The diffusion was modelled using a pipe diffusor. In previous reports (Daae et al., 2018) the modelling has also covered diffusion through split barge, which caused too high turbidity in the water and was therefore not considered an option.

4.3 Input data for numerical modeling

The input data needed to create the numerical model for this study was gathered as follows:

- **Bathymetry**: In order to get the bathymetry the Norwegian Mapping Authority (Kartverket) sent a request to The Norwegian Armed Forces as they are responsible for the safety of the information. The area specified in the request is shown in Figure 4.4 (20.26 km^2). The format is specified as ascii .xyz, UTM coordinates, with $1m$ resolution.
- **Wind data**: The wind data was gathered from Strømtangen Fyr, by the Norwegian Meterological Institute (MET).
- **Discharge from the river**: The discharge was measured at Sarpsfossen, the data was gathered by Glommen and Laagens user union.
- **Tidal information**: The tidal data from the software will be compared with measurments from a local weather station.

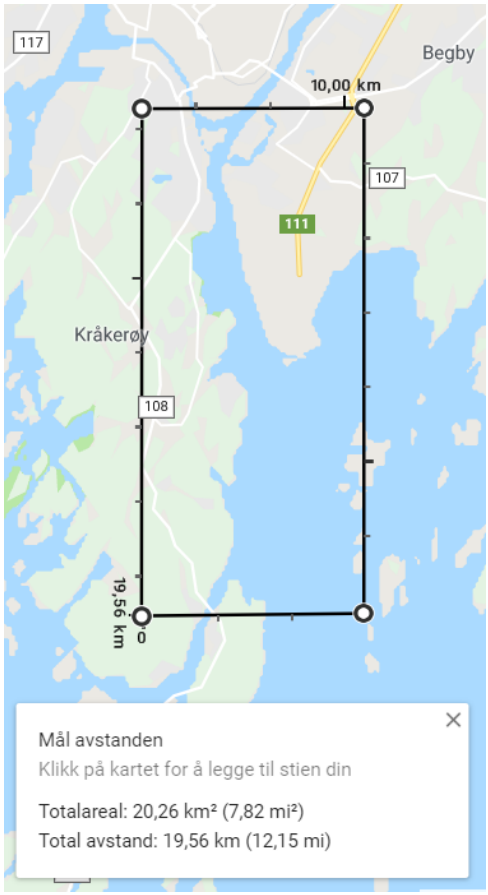

(a) Measurement of the area

(b) Area covered in the black box

Figure 4.4: The area specified in the bathymetry application to The Norwegian Armed Forces (Google Maps, 2018).

The current in the port area will be modelled using the wind data, the discharge from the river and tidal information. The model will be validated against the measured current data in the port area. The port and fairway is well protected from waves and waves will therefore be neglected in the planned modelling.

4.4 Data analysis

4.4.1 Discharge data

The discharge data have been gathered from Sarpsfossen, Figure 4.5, from Glommen and Laagens user union.

Figure 4.5: Location of Sarpsfossen measuring station

The data ware collected once a day from 1964 to 2018, which accumulate to 54 years of data with 365 occurrences per year, see Figure 4.6. The data were sorted into months and the maximum, minimum and average discharges were plotted, see Figure 4.7.

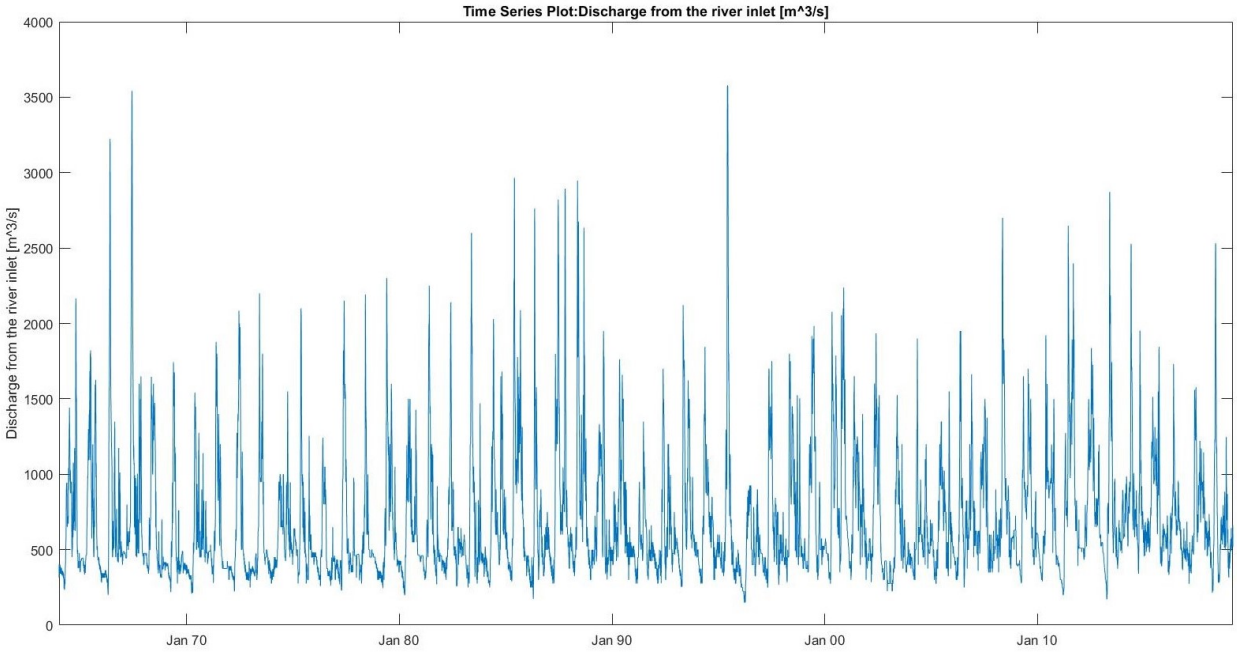

Figure 4.6: Discharge from Glomma, from 1st of Jan 1964 to 10th of Mar 2019 (raw data)

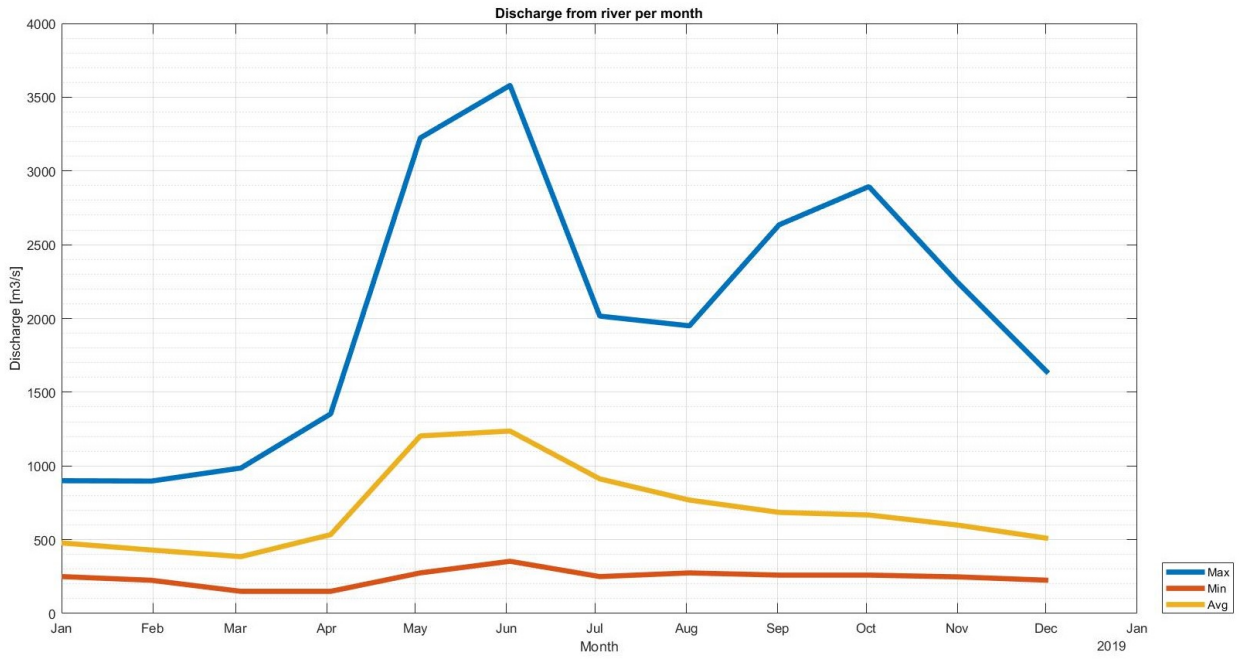

Figure 4.7: Discharge from Glomma, from 1st of Jan 1964 to 10th of Mar 2019 (raw data sorted by month)

In order to analyse the data and see the extreme events we need to find the 100-, 50- and 20-year return period value for the current. To ensure the independence of the data points, the annual maxima method was chosen for the analysis (Goda, 2010). Which means that the maximum from each year is used for the probability distribution. Using the annual maxima method gives a mean rate of 1. The mean rate is defined as:

$$\lambda = \frac{N_T}{K} \tag{4.1}$$

where N_T is number of events with occurrences and K is number of years.

To find the 20-, 50- and 100-year return value for the discharge a transformation of the coordinate axes was preformed (Kamphuis, 2010). This was done to fit a Gumbel distribution:

$$P = exp(-exp(-\frac{Q-\gamma}{\beta})) \tag{4.2}$$

where P is the probability, Q is a specified discharge volume, γ the mean and β the standard deviation.

There are several probability distributions that could have been used; normal, log-normal, Frechét, maximal Weibull, generalized extreme-value and Weibull are the most common for this type of analysis (Kamphuis, 2010; Goda, 2010). As controlling the fit for each of these distributions is a time consuming process and this is not the main aspect of this master thesis, Gumbel was chosen as a distribution that is rather easy to perform and at the same time has the complexitiy needed for this dataset.

The values was grouped in bins and the Gumbel probability for each bin was calculated based on these equation:

$$P = P(Q' < Q) \tag{4.3}$$

where Q' is any discharge volume.

$$Y = -ln(ln\frac{1}{P}) = G \tag{4.4}$$

where G is the Gumbel Reduced Variate and Y defines the Y-axis.

The X-axis is defined as:

$$X = Q \tag{4.5}$$

With these transformed axis a linear regression analysis could be performed using the equation:

$$Y = AX + B \tag{4.6}$$

giving a value for A and B which can be used to find γ and β:

$$A = \frac{1}{\beta} \qquad B = -\frac{\gamma}{\beta} \tag{4.7}$$

The plotted results of the Gumbel distribution and the linear regression analysis is shown in Figure 4.8. The results of the analysis can be found in Table 4.2.

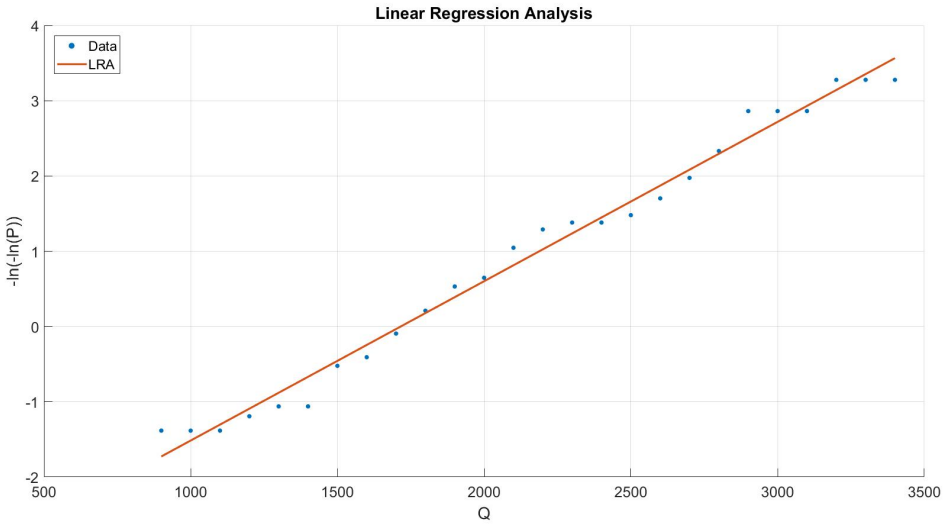

Figure 4.8: Linear regression of the extreme value analysis using the annual maxima

Table 4.2: Extreme Value Analysis of the discharge using the annual maxima

Type	m^3/s
Maximum	3580
Minimum	925
Mean	2071
100 year discharge	3784
50 year discharge	3458
20 year discharge	3023

A similar analysis was done for each month to evaluate at what time the wind and the discharge will be largest to find the operational window for the dredging operations. The results can be found in Table 4.3 and Figure 4.9. R2 is a measurement of fitting for the linear regression to the point data used, and R2 closer to 1 means a better fit.

Table 4.3: Daily discharge $[m^3/s]$ values calculated based on months

Type	Jan	Feb	Mar	Apr	May	Jun	Jul	Aug	Sep	Oct	Nov	Dec
Maxi	900	897	986	1353	3224	3580	2016	1950	2635	2894	2238	1629
Min	343	275	225	375	600	775	524	425	363	375	350	350
Mean	541	490	478	812	1846	1741	1274	1014	922	1006	793	608
100y	921	822	898	1649	3607	3755	2388	2109	2613	2662	2076	1295
50y	847	757	818	1499	3280	3392	2176	1904	1887	2355	1836	1146
20y	750	671	710	1277	2843	2908	1895	1631	1302	1946	1516	947
R2	0.986	0.965	0.969	0.988	0.961	0.976	0.941	0.984	0.959	0.972	0.944	0.827

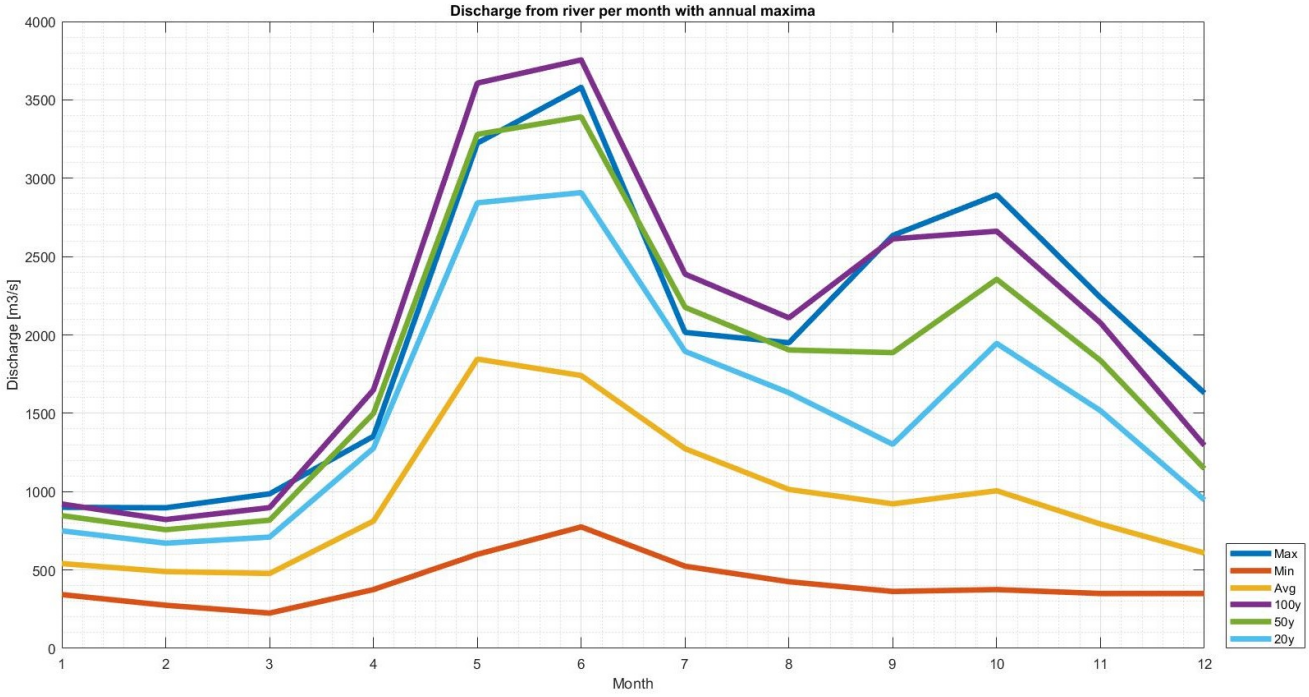

Figure 4.9: Discharge - Extreme value analysis per month

4.4.2 Tidal data

Tides are defined as short term water level fluctuations that alternate and regularly rises and lowers the sea level in oceans and other large bodies (Kamphuis, 2010). These changes are caused by the gravitational attraction of the moon and, to a lesser extent, of the sun on the earth.

Tidal analysis consists of separating a measured tide into as many of its constituents (contributing forces) as can be identified from the length of the record available. The tide-generating potential is a complicated function of time, which may be resolved into the sum of large number of harmonic constituents. The tidal water level (η_τ) at time t can be calculated as:

$$\eta_\tau(t) = \sum_{i=1}^{l} a_i cos(\omega_i t + \alpha_i) \tag{4.8}$$

where a_0 is the mean water level, a_i and α are the amplitudes and phase angles of the tidal constituents (from tidal analysis) and ω_i is the angular frequency. This equation can be used to predict future tides.

Tidal currents are the horizontal movement of water due to the tidal effect. The tidal waves are very long compared to the water depth, therefore the shallow water formulation of the linear wave theory can be used to calculate the velocity (C) of the propagation of the tidal currents:

$$C = \sqrt{gd} \tag{4.9}$$

where g is gravity and d is water depth.

The length (L) of the tidal wave is:

$$L = CT \tag{4.10}$$

where $T = 24.41hrs$ for the semi-diurnal constituent. Since the length of the tidal waves are substantially large, the propagation of such waves must be effected by the earth rotation (the Coriolis force). In other words, the tides do not propagate in a straight line, but rotate. Some tide constituents resonate (the amplitude is amplified) due to the different land mass topography and this leads to different coastal shapes yielding different tides.

The tidal data used in the simulations are based on MIKE's tidal prediction model (the Global Tide Model from MIKE21 Toolbox). This was done to produce timeseries at various points along the borders at any time. The results at point '611983, 6557836' (UTM-32) were compared with measured data from Viker measuring station (Kartverket, 2019), see Figure 4.10.

Figure 4.10: The blue is where the tidal data has been compared. The red mark is where the tidal has been measured by kartverket

The comparison can be found in Figure 4.11. The data from Kartverket (sehavniva.no) is taken from the measurements at Viker measuring station, multiplied by 1.05 and adjusted by 6 minutes. The two are not a 100% fit, but it's close enough to use the tidal prediction from MIKE for the simulations.

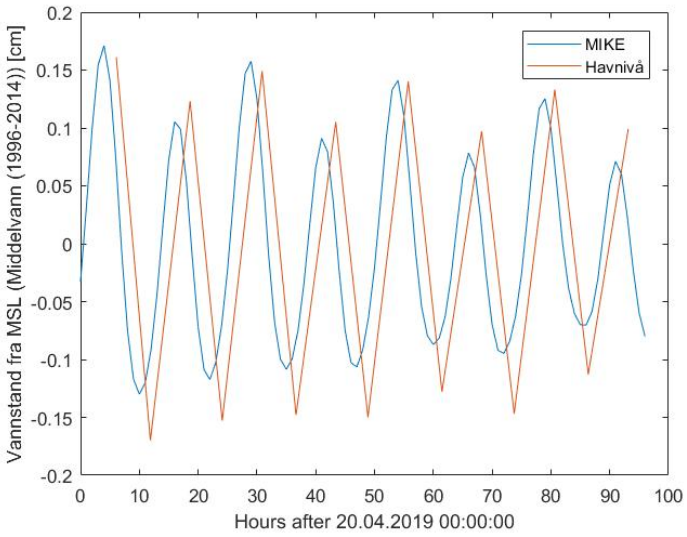

Figure 4.11: Comparison of tidal data from MIKE21 Toolbox and measurment from Viker measuring station gathered from sehavniva.no

The Global Tide Model from MIKE21 Toolbox was used with a 0.125x0.125 degree resolution grid for the major 10 tidal constituents in the tidal spectra (MIKE, powered by DHI, 2017d).

4.4.3 Wind

The wind was measured at Strømtangen Fyr, see Figure 4.12. The data were gathered from MET (Norwegian Meterological Institute, 2019). The wind was measured every hour from 1.1.2009 to 1.1.2019, giving ten years of data with 8760 occurrences per year. The raw data is shown in Figure 4.13 and the raw data sorted into months and given as minimum, maximum and average is shown in Figure 4.14.

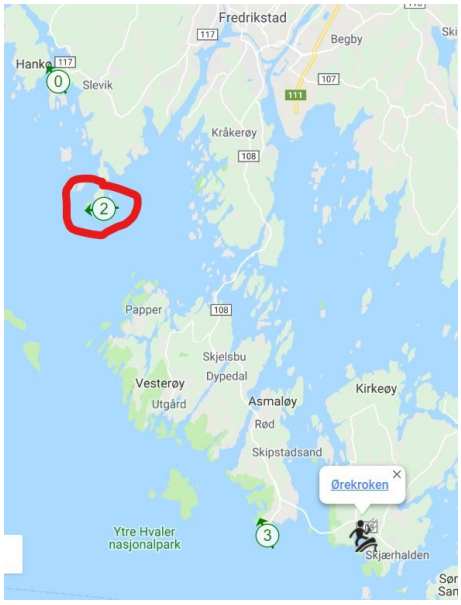

Figure 4.12: The location of Strømtangen Fyr

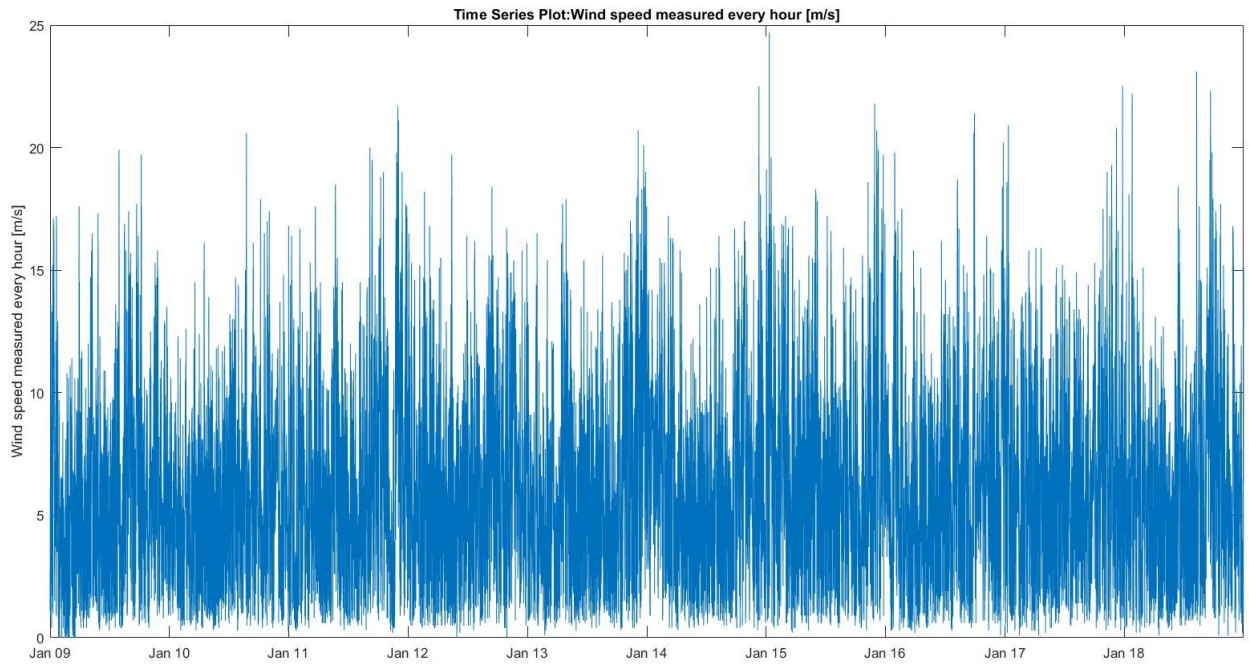

Figure 4.13: Wind speed at 10 meter over the ground from 1st of Jan 2009 to 1st of Jan 2019 (raw data)

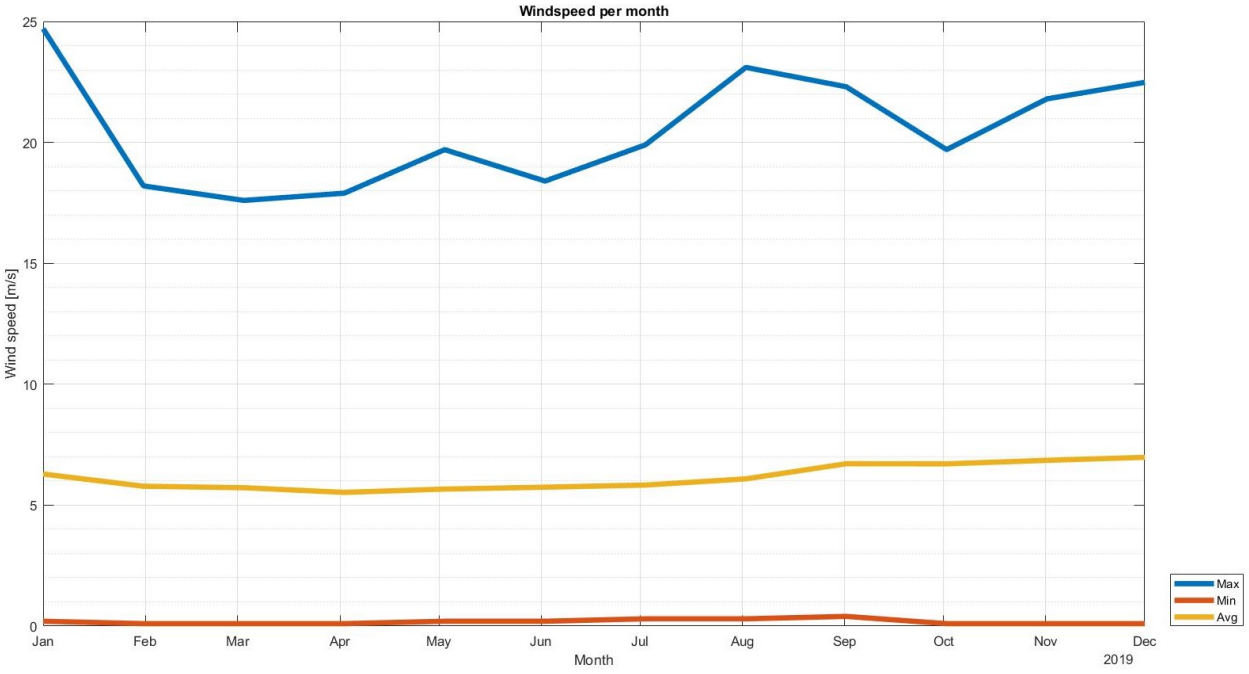

Figure 4.14: Wind speed at 10 meter over the ground from 1st of Jan 2009 to 1st of Jan 2019 (raw data sorted on months)

All the wind data sorted by wind direction in a wind rose can be found in Figure 4.15.

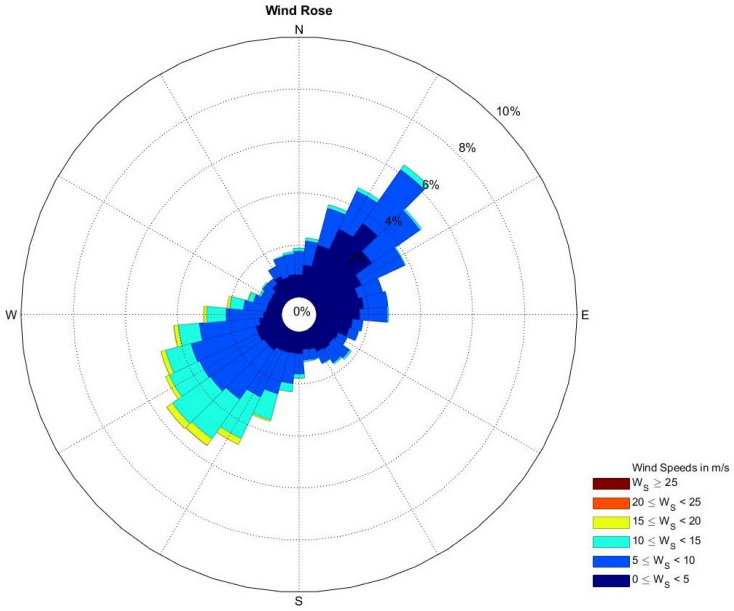

Figure 4.15: Wind rose with all data

To find the extreme values for the wind, the peak over threshold (POT) method was used and a threshold value of 15 m/s was chosen (Goda, 2010; Kamphuis, 2010). The POT method includes all data points with a value higher than the set threshold. This ensures that we get independent data points and a good distribution for fitting. When a threshold of 15 m/s is set the wind rose shift as seen in Figure 4.16.

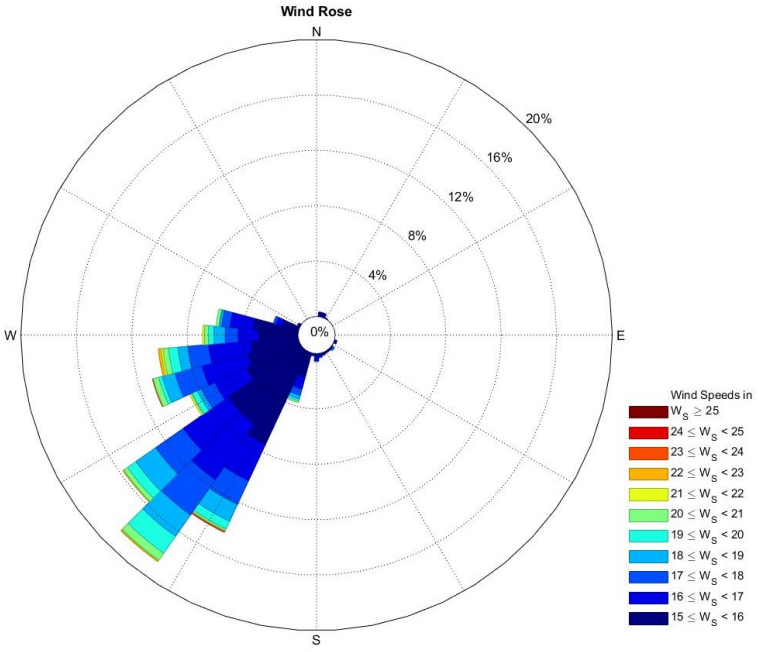

Figure 4.16: Wind rose with a threshold of 15 m/s

Since the data only expands over ten years, the annual maxima method (used for the discharge data) could not be used. When the data are gathered in bins there are a lot of empty bins, resulting in a probability distribution function that are fitted based on too few data points, as can be seen in Figure 4.17 and 4.18, where the annual maxima method was used for the wind data for January and for all the months. When we use 15 m/s as POT, the result of the Linear

Regression Analysis (LRA) becomes what can be seen in Figure 4.19. We clearly see that with the annual maxima we don't have enough data points and there is no good fit, and that with a POT of 15 m/s there is a good fit.

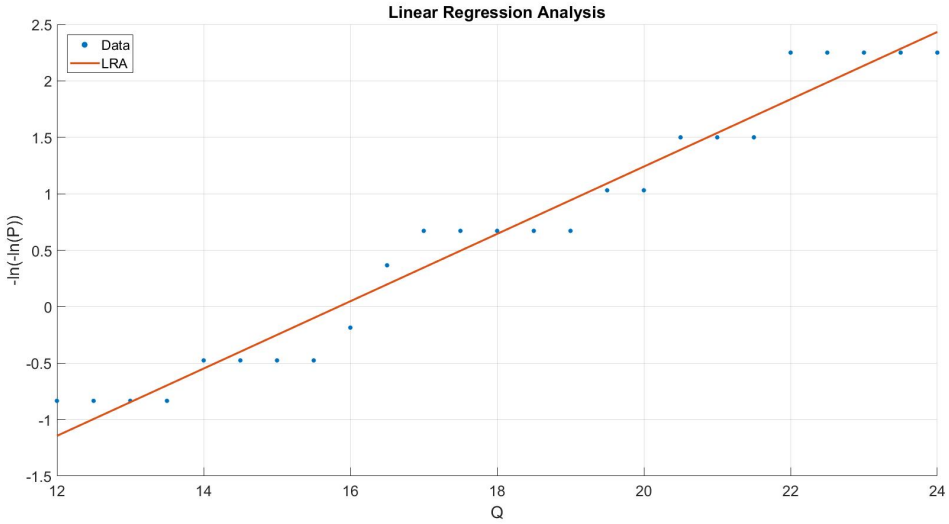

Figure 4.17: Wind analysis for January with annual maxima

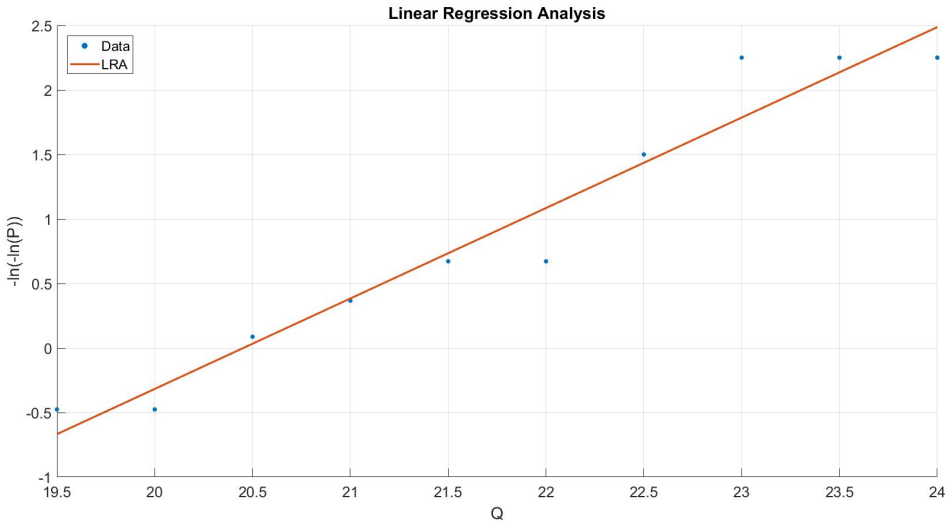

Figure 4.18: Wind analysis for all months with annual maxima

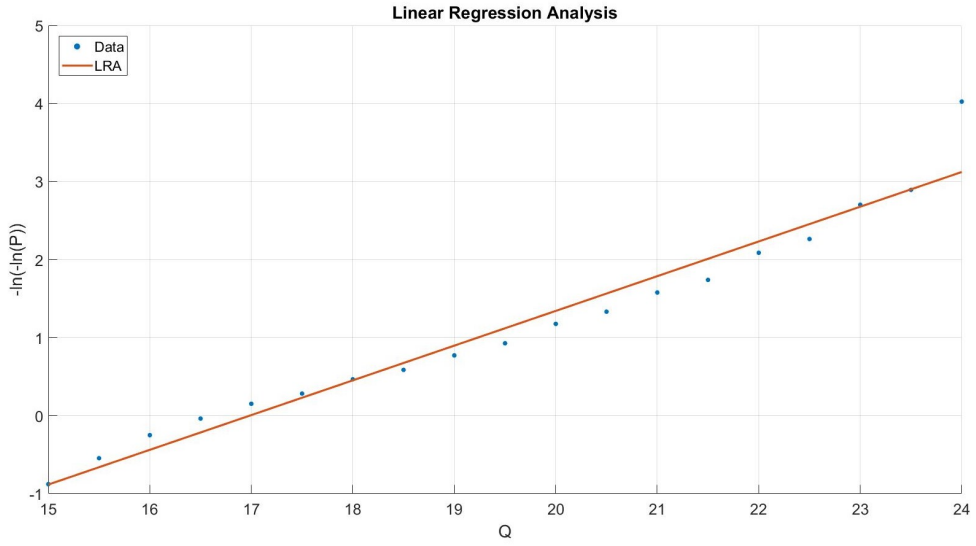

Figure 4.19: Wind analysis for all months with a 15 m/s POT

The maximum wind over the ten last ten years are 24.7 m/s. And the mean wind speed over the ten years is 6.16 m/s. When doing a POT analysis of the wind data for each month the results are as presented in Table 4.4 and Figure 4.20.

Table 4.4: Wind analysis per month with threshold of 15 m/s

Type	Jan	Feb	Mar	Apr	May	Jun	Jul	Aug	Sep	Oct	Nov	Dec
Max	24.7	18.2	17.6	17.9	19.7	18.4	19.9	23.1	22.3	19.7	21.8	22.5
Min	15.1	15.1	15.1	15.1	15.1	15.1	15.1	15.1	15.1	15.1	15.1	15.1
Mean	16.7	15.9	15.9	15.8	16.4	16.5	16.4	16.8	17.0	16.2	16.5	17.0
100y	25.8	19.1	18.9	19.3	21.3	21.4	22.1	25.1	24.6	21.0	22.9	25.7
50y	24.8	18.6	18.5	18.7	20.7	20.8	21.3	24.1	23.8	20.5	22.2	24.9
20y	23.4	18.0	18.0	17.9	19.8	19.9	20.3	22.8	22.7	19.7	21.3	23.8
R2	0.979	0.988	0.960	0.884	0.989	0.968	0.950	0.980	0.955	0.988	0.982	0.989

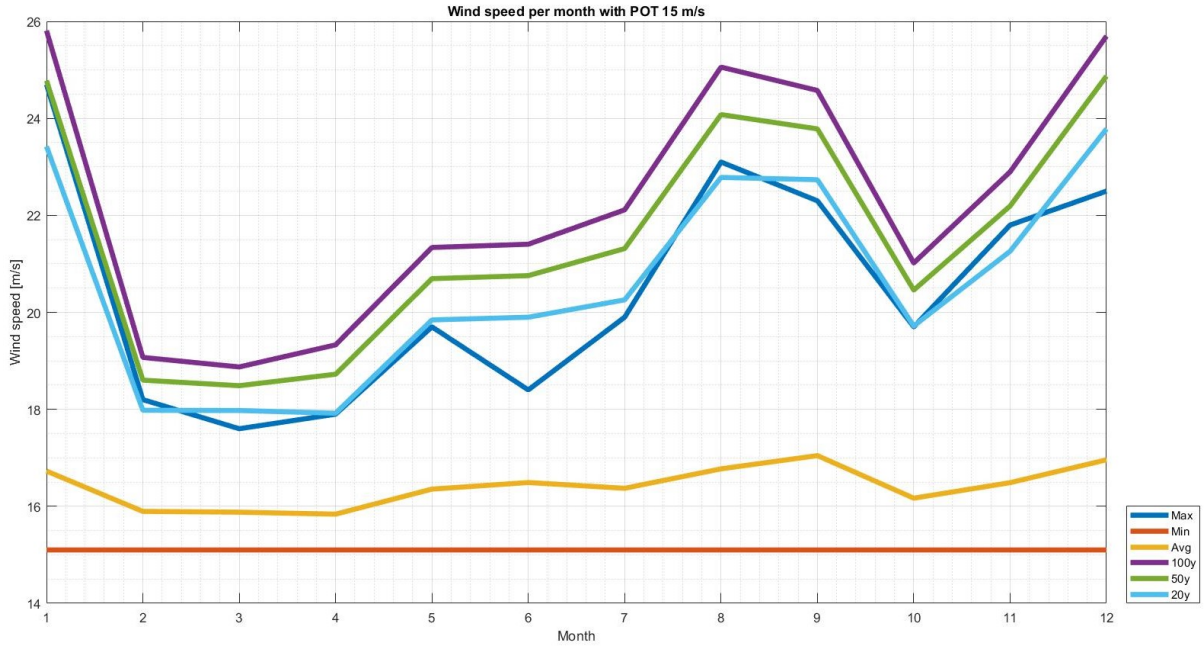

Figure 4.20: Wind analysis per month with threshold of 15 m/s

The wind was also analysed based on direction. When looking at the wind rose for the whole dataset there are two directions that stands out, northeast (25-55 degrees) and southwest (205-245). Therefore the wind was analysed for these two directions. The results are presented in Table 4.5.

Table 4.5: The results of the POT analysis for the two main directions of wind

Degrees	$25-55$	$205-245$
Threshold	10	15
Maximum	15	24.7
Minimum	10.1	15.1
Mean	11.1	16.6
100 year	21.8	37.4
50 year	20.9	35.8
20 year	19.5	33.7
R2	0.985	0.972

4.5 Estuarine circulation

The harbor is located in a river outlet which brings with it many different challenges (from personal communication with Ragnhild Daae from SINTEF). This creates a reverse current bringing saltwater and also partly sediments up the river. The main current is the one coming from the river bringing with it sediments and freshwater down to the sea. The freshwater meeting the saltwater in the sea creates a brackish water.

Estuarine circulation is usually defined by seawater which flows into the estuary where it meets more buoyant fresh water from the river inlet through tidal action (Götz Flöser, 2011). "When tidal mixing is minimal, salty ocean water flows into an estuary at the base of the water

column, promoting water column density stratification and producing a saltwater wedge. (Pike, 2014)"

Chapter 5

Numerical modelling

Due to the complexity of solving fluid hydrodynamic problems, computational fluid dynamics (CFD) has become one of the biggest fields of research in fluid mechanics (Ferziger, Peric, 2002). To solve fluid hydrodynamic problems we need to solve partial differential equations varying both in space and time. This can not be done analytically for most cases and must therefore be found by obtaining an approximate solution numerically. This involves using a discretization method. It's applied on small domains in space and time and the numerical solution provides results at discrete locations.

There exists several software packages that are capable of modelling sediment transport during dredging. The MIKE software package from DHI was chosen as it has well-developed modules for sediment transport and well developed scientific documentation and user guides. MIKE21, MIKE3 and three sediment transport modules are described in this chapter. Further use of the software will only use one of the sediment transport modules, namely the particle tracking module. Figure 5.1 shows a brief overview of how some of these modules are connected to each other:

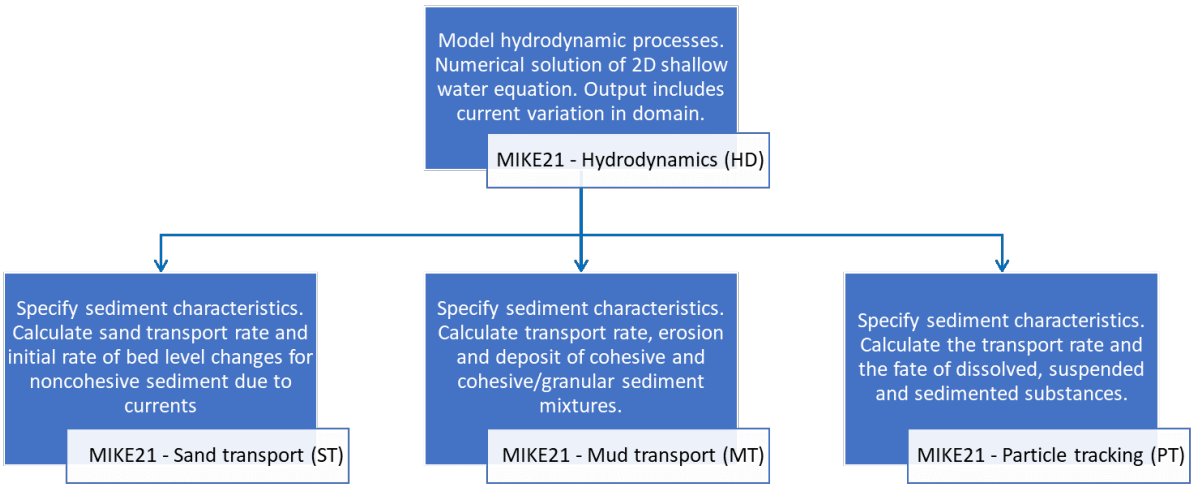

Figure 5.1: MIKE21 - Module flowchart

All the modules shown in Figure 5.1 is part of Flow Model FM in MIKE21, powered by DHI.

5.1 MIKE21

The part of MIKE21 that will be used is the Flow Model FM (Flexible Mesh) (MIKE, powered by DHI, 2017g). MIKE21 is a modular software and the basic modules that will be used is the hydrodynamic (HD) module. "The HD module simulates water level variations and flows in response to a variety of forcing forces." (MIKE, powered by DHI, 2017g)

The Hydrodynamic Module in MIKE21 Flow Model FM is based on the numerical solution of the two-dimensional shallow water equations: The depth-integrated incompressible Reynolds averaged Navier-Stokes equations (MIKE, powered by DHI, 2017b). Thus, the model consists of continuity, momentum, temperature, salinity and density equations. In the horizontal domain both cartesian and spherical coordinates can be used.

The bottom stress is determined by a quadratic friction law (MIKE, powered by DHI, 2017g). The surface stress is determined by the winds above the surface (for areas without ice). The tidal potential is defined as the elevation and is calculated as the sum of the actual elevation and the equilibrium tidal potential.

5.2 MIKE3

MIKE3 allows for modelling in the vertical dimension and is essential for modelling with vertical density gradients. In MIKE3 the free surface is taken into account using a sigma coordinate transformation approach (MIKE, powered by DHI, 2017g).

5.3 Sediment transport

For sediment transport there are mainly three modules (MIKE, powered by DHI, 2017a):

- **Sand Transport (ST) Module**: Allows us to assess the sediment transport rates and inital rates of bed level change for non-cohesive sediments resulting from currents or combined wave-current flows.
- **Mud Transport (MT) Module**: Includes erosion, transport and deposition of cohesive and cohesive/granular sediment mixtures. It also includes a dredging module, which allows dynamical simulations of all stages of the dredging process. For sediments to be defined as mud they have to be $< 65\mu m$ (silt and clay).
- **Particle Tracking (PT) Module**: Can be used to describe the transport and fate of dissolved and suspended substances discharged or spilled anywhere within the water column.

5.4 Assumptions

The assumptions connected to Boussinesq is used (MIKE, powered by DHI, 2017g). These include, amongst other, that the software ignores any other variations in fluid properties than density ρ, and density is only relevant when multiplied by gravity, g. Assumptions connected to the hydrostatic pressure is also used, where it is assumed that for a fluid at rest the pressure is increasing linearly with depth.

In the particle tracking module two assumptions are made (MIKE, powered by DHI, 2017j). The first one is neglecting the interaction between diffusing particles (Fick's dispersion law is not considered). The second is assuming that there is instant acceleration. This results in the particles having velocities according to the surrounding water flow. Numerical diffusion is negligible when using the Lagrangian discrete parcels method.

5.5 Solution Technique

MIKE21 and MIKE3 Flow Model FM use spatial discretiation by subdivision of the continuum into non-overlapping elements (MIKE, powered by DHI, 2017f). A cell-centred finite volume method is used. An unstructured mesh is used in the horizontal plane and the mesh is divided in triangular or quadrilateral elements. For the vertical domain in the 3D model, the mesh is structured, as shown in Figure 5.2.For the time integration an explicit scheme is used. For computation of the convective fluxes an approximate Riemann solver is used (MIKE, powered by DHI, 2017b). This allows for discontinuous solutions.

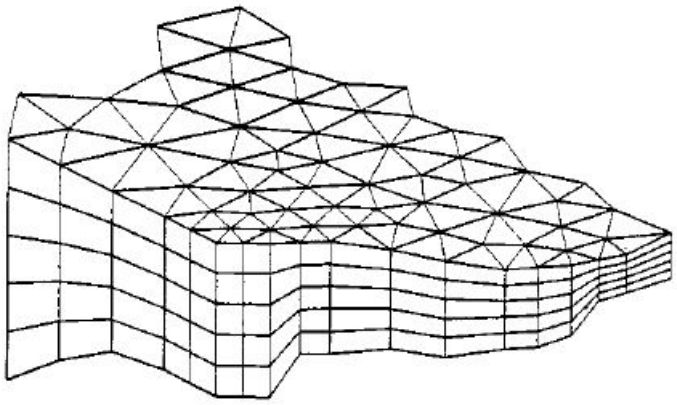

Figure 5.2: Principle of meshing for the three-dimensional case (MIKE, powered by DHI, 2017g)

The simulation of jets and plumes is based on dynamic coupling of nearfield integrated jet solution and farfield hydrodynamic flow model (MIKE 3 Flow Model FM). The near field solution is based on the integral model equations described by (Jirka, 2004), which solves conservation equations for flux and momentum, salinity and temperature under the given ambient conditions.

5.5.1 Sand transport

Sand transport is calculated using a mean horizontal velocity component, assuming the vertical velocity profile to be logarithmic (MIKE, powered by DHI, 2017j). With pure current the sediment transport rates are calculated directly during the simulation based on the actual conditions. The calculations are divided into bed load transport and suspended load transport. When modelling sediment transport only for currents, the equations have to be chosen amongst these alternatives:

- Engelund and Hansen (total load)
- Van Rijn (bed load + suspended load)
- Engelund and Fredsøe (bed load + suspended load)
- Meyer-Peter and Müller (bed load)

5.5.2 Mud transport

The sediment transport formulations are based on the advection-dispersion calculations in the hydrodynamic module (MIKE, powered by DHI, 2017h). The MT solves the advection-dispersion calculations using an explicit, third-order finite difference scheme, known as the

ULTIMATE scheme. The solution of the erosion and the deposition equations are straightforward and do not require special numerical methods. The model is essentially based on the principles that Mehta defined (Metha, 1989). Bed shear stress due to waves have been added.

5.5.3 Particle Tracking

Transport of particles are modelled according to a drift regime and by adding dispersion using a random walk term (MIKE, powered by DHI, 2017i). The equations that are used for the particle tracking is among others the Langevin equation, which is based on Brownian motion. The method is called the Lagrangian Discrete Parcels Method, where the stochastic differential equation is solved with an explicit Euler scheme. The particles are divided into classes with different characteristics and in different layers.

The Lagrange method use discretization both in time and space. In space the discretization is connected to particles. The position of the particle (X) is calculated recursively:

$$X = X + U\Delta t + \varepsilon \tag{5.1}$$

where Δt is the timestep, U is the current velocity, ε represents random walks, which are assumed to be normally distributed with a middle value 0 and a variance:

$$\sigma^2(\Delta t) = 2D\Delta t \tag{5.2}$$

where D is the grain diameter.

It was decided to use the particle tracking module, as opposed to the mud or sand transport module, because it includes turbulence and is the most accurate when the goal is to learn where the particles end up. The mud transport module can only be used for cohesive sediments (and granular mixtures), while the sand transport module can only be used for non-cohesive sediments. Since there is a mix of sediments in this case study, the particle tracking module is the most fitting for the purpose. The particle tracking module also allows us to evaluate the suspension of the particles, while with the two other models we can only track transport rates and bed level changes.

5.6 Hydrodynamic module

5.6.1 Input

The input data can be divided into the following groups (MIKE, powered by DHI, 2017f):

- Domain and time parameters
  - Computational mesh (the coordinate type is defined in the computational mesh file) and the bathymetry
  - Simulation length and overall time step
- Calibration factors
  - Bed resistance
  - Momentum dispersion coefficients
  - Wind friction factors
  - Heat exchange coefficients
- Initial conditions
  - Water surface level

  - Velocity components
  - Temperature and salinity
- Boundary conditions
  - Closed
  - Water level
  - Discharge
  - Temperature and salinity
- Other driving forces
  - Wind speed and direction
  - Tide
  - Source/sink discharge
  - Wave radiation stresses
- Structures
  - Structure type
  - Location
  - Structure data

5.6.2 Output

The output that can be collected can be divided into basic and additional variables. They are calculated for each mesh element and for each time step and consists of:

- Basic variables
  - Water depths and surface elevations
  - Flux densities in main directions
  - Velocities in main directions
  - Densities, temperatures and salinities
- Additional variables
  - Current speed and direction
  - Wind velocity
  - Air pressure
  - Drag coefficient
  - Precipitation/evaporation
  - Courant/CFL number
  - Eddy viscosity
  - Element area/volume

The output results can be saved in defined points, lines and areas. The output is visualized using either the Data Viewer in MIKE Zero or MIKE animator plus.

5.6.3 Mesh generation and bathymetry

The goal of the bathymetry and mesh file is to describe the water depth in the model area, allow result with a desired accuracy and give model simulation times acceptable to the user (MIKE, powered by DHI, 2017k).

To obtain this, the final mesh should have small triangles, without small angles (the perfect mesh has equilateral triangles), have smooth boundaries, have high resolutions in areas of special interest and be based on valid xyz data using the same chart datum.

Part of creating the mesh is choosing what coordinate system to use. Normally a geographical coordinate system with latitude and longitude or a UTM system is used. The Universal Transverse Mercator (UTM) coordinate system uses a 2-dimensioanl Cartesian Coordinate system to give locations on the surface of Earth.

The Courant number (Courant-Friedrichs-Lewy condition) (CFL) is a necessary condition for convergence while solving certain partial differential equations. It arises when explicit time-marching schemes are used for the numerical solution. In order for the simulation to run smoothly the time-step, the mesh and the water depths combined must yield a CFL number that is lower than one for the whole area throughout the simulation. For simulating flow conditions the CFL number is calculated using this equation:

$$CFL_{HD} = (\sqrt{(g * h)} + |u|) * \frac{\Delta t}{\Delta x} + (\sqrt{(g * h)} + |v|) * \frac{\Delta t}{\Delta x} \tag{5.3}$$

where g is gravity, h is the water depth, u and v are the velocity components in the x- and y-direction, Δt is the time step and Δx is the spatial resolution.

When creating the mesh, the boundaries are also marked out. By attributing the nodes with different numbers each boundary gets a code value. All nodes are number 1 by default, which marks a closed boundary (land). By giving the nodes different codes the open boundaries and the inlets can be marked and later used in the other modules.

The bathymetry for Borg Port was created based on the scatter data received from The Norwegian Armed Forces (through Norwegian Mapping Authority). The data were used in MIKE to first create a mesh by drawing around the area, generating a mesh, smoothing the mesh and interpolating it with the scatter data. With the mesh a simple hydrodynamic simulation was run to control that the maximum Courant number was lower than 1.0, and if not changes were made to the mesh. This process was iterated until the maximum Courant number was lower than 1.0 throughout the simulation. The final mesh with the code values can be found in Figure 5.3. In order to both be able to run the model fast and have the overview of the whole area two different models were created. The first covering only Røsvikrenna and the second model covering a larger area below.

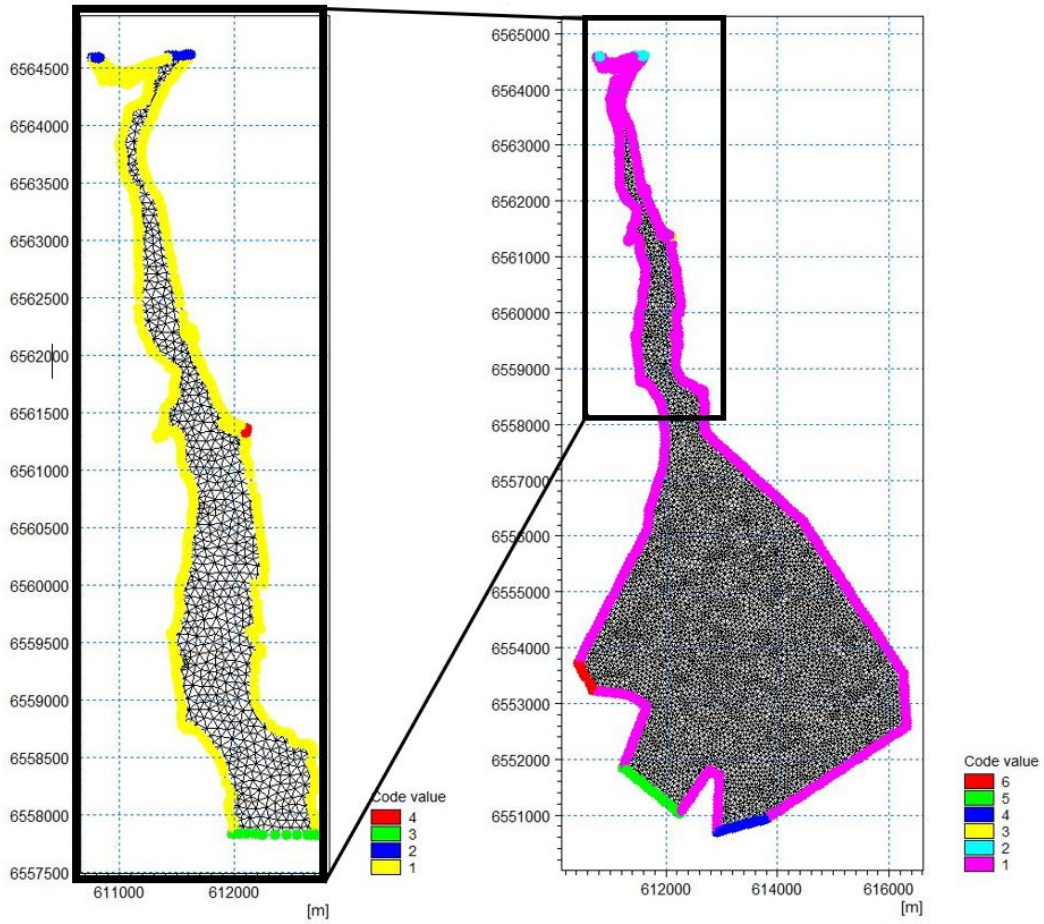

Figure 5.3: Mesh covering only Røsvikrenna and bathymetry covering a larger area including the disposal sites, including code values (1 is land boundary, 2 is inlet and the rest are open boundaries)

Assumptions made when creating the bathymetry:

- The small channel next to Isegran has been excluded.
- The newest measurements were prioritized when interpolating the scatter data into the mesh

The interpolated mesh with the scatter data is the final bathymetry file that will be used in the simulations, see Figure 5.4. The scatter data received from the Norwegian Mapping Authority only covered the area on the left of Figure 5.4. To create the rest of the area that you can see on the right side of the Figure, a MIKE tool called C-map was used. This tool provides sea charts in a digital form.

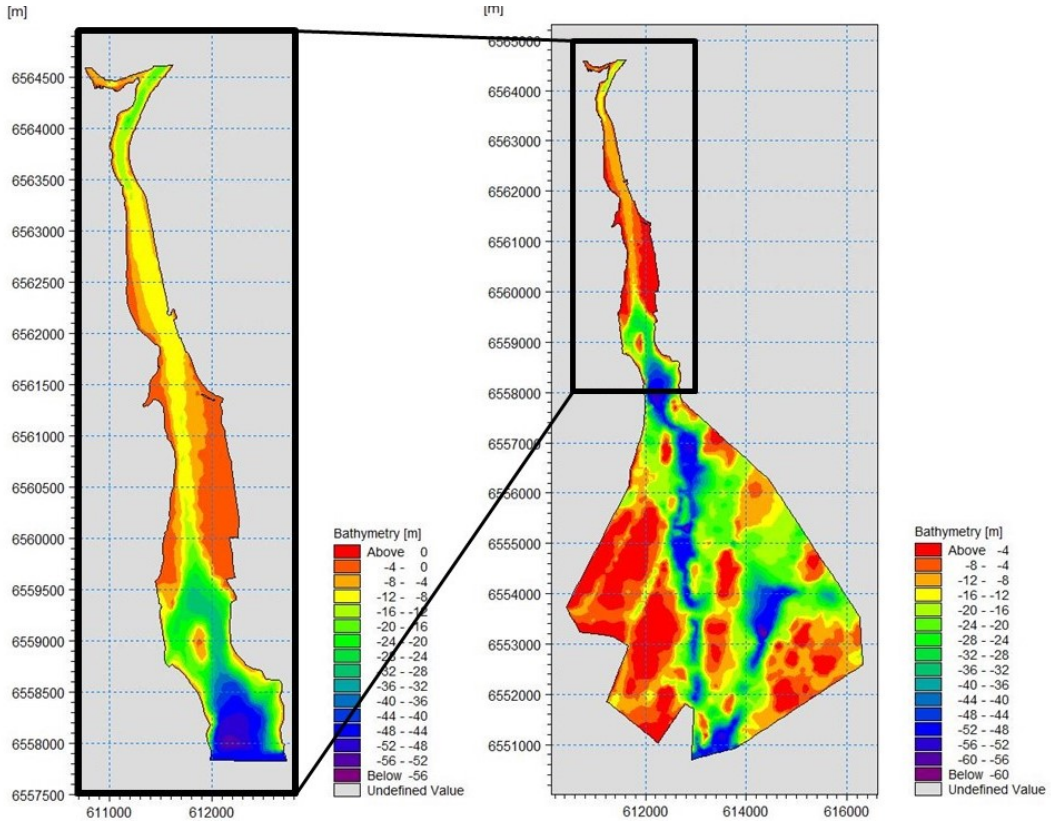

Figure 5.4: Bathymetry covering only Røsvikrenna and bathymetry covering a larger area including the disposal sites

The discharge was used to define the inlet boundary (at the top of the model, shown as code 2 in Figure 5.3). The tidal data collected was used to define the open boundaries, shown as code 3 and 4 in Figure 5.3. The wind data was used to describe the wind forcing. The wind friction was set to 0.001255 for all the simulations as a simplification. This value is based on the graph in Figure 5.5 and the fact that most wind speed values used in the simulations are between 10 and 20.

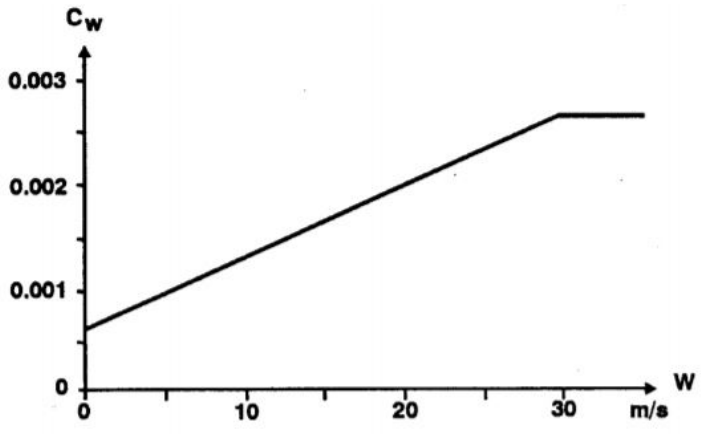

Figure 5.5: Wind friction, C_W is the wind friction factor and W is the wind speed. (MIKE, powered by DHI, 2017c)

The bed resistance was created by using the MIKE21 toolbox to create a map over the area with a Manning number for each mesh element.

The main outcome from the hydrodynamic module was the drift regime that was needed for the particle tracking module. The most important component of this drift regime is the current speed. The current speed gives an indication regarding the spreading of the sediments, which allows us to evaluate whether or not a simulation of sediment spreading in the particle tracking module is useful.

5.7 Particle Tracking Module

The particle tracking module has been used to simulate the sediment spreading during dredging operations. It uses Lagrange discretizaton (MIKE, powered by DHI, 2017i). This method splits all mass into a number of particles which are each given specific 3D coordinates and masses. The particles are then transported according to a drift regime and adding parameters that effect the particle transport. In this case this drift regime is calculated by the hydrodynamic module described in the previous section. An advantage of using the Lagrange method (as opposed to of Euler discretization) is that the Lagrangian approach has negligible numerical diffusion.

The module can be used for all types of sediments and therefore fits our needs as the case study includes several types of sediments.

Simplifications

There are two simplifications that are worth mentioning (MIKE, powered by DHI, 2017i):

- Interaction between diffusing particles is neglected, which means that Fick's dispersion law is not considered. This could affect the accuracy when there is a larger diffusivity in the middle of the stream than on the sides. The particle tracking diffusion would then make a non-homogeneous distribution with more particles on the sides than in the middle of the stream, which should not be physically possible according to Fick's law. This is the case for this project, therefore this needs to be taken into account when evaluating the results.
- Instant acceleration is assumed. This is only significant if the particles are very heavy, which they are not in this case.

Langevin equation

The module uses the Langevin equation, which describes the dynamics of transport and dispersion of particles in terms of stochastic differential equations:

$$dX_t = a(t, X_t)dt + b(t, X_t)\xi_t dt \tag{5.4}$$

where t is time, a is the drift term, b is the diffusion term and ξ_t is a random number.

The molecular diffusion term is a function of temperature and the specie in question. And the turbulent dispersion term is a function of the flow conditions. Sometimes the turbulent dispersion must also cover unresolved turbulence not resolved with the applied discretization.

Classes

A grouping of the particles used for the simulation (MIKE, powered by DHI, 2017i). The properties are decided for each class. Classes can be divided into different fractions of sediment particles, which is how it will be used in this case. It could also be used to classify different organic pollutants with different decay rates.

Drift

The drift is decided by the current, wind drag and bed drag (MIKE, powered by DHI, 2017i). These parameters have been discussed earlier in this chapter and in the particle tracking module we use the outputs from the hydrodynamic module as input.

In the 2D hydrodynamic simulations with depth integrated current fields, the bed shear profile can be applied in the whole water column.

Wind

Several wind parameters can be defined, but this is only relevant for particles that are on the surface, which is not relevant in this case.

Dispersion

Both horizontal and vertical dispersion has been neglected in this case study.

Decay

It's possible to set a decay rate [1/s], either constant or varying in time, for each of the classes. This is needed if there are particles that decay fast and will therefore need to be removed in the simulations after a certain time. This is not relevant for the dredging operations in Borg Port, as these are sediments and pollution that has been there for several years.

Settling

The settling velocity defined in the particle tracking module is for one particle only, not affected by other particles. This is decided by flocculations, which is defined by maximum and minimum concentration for flocculations in kg/m^3 and a gradient coefficient α. The flocculations can also be affected by hindered settling and salinity. Hindered settling is when the concentration is so large that the particles affect each other and the settling velocity lowers due to the dense concentration which prevents the flocculations from falling freely. To include the effect of hindered settling the gelling point C_{gel} is by default defined, but can be changed. In fresh/brackish water the flocculations processes are reduced and the settling velocity is therefore reduced. We can also use Stokes law to calculate the unflocculated settling velocity. To include the effect of salinity the two calibration parameters c_1 and c_2 are by default defined, but can be changed.

In the case of Borg Port, the flocculations in the area including hindered settling and salinity has already been calculated and a settling velocity for the particles of interest in this case defined as 0.0001 m/s. Therefore the option of setting the settling velocity directly will be used.

Erosion

Erosion and resuspension has been neglected for this case study.

Parameters

- Classes
- Sources: For each class: Flux $[g/s]$ (can also be defined as mass $[g]$), Number of particles per timestep.
  - Particle Source specification: Coordinates of the location and a vertical source specification
  - Fixed or moving location

  - Released class term: Constant or varying in time. If the amount of released sediments changes during the simulation

- Decay
- Settling (decided per class included in the simulation) (Alpha)
  - General: The settling velocity has been set to 0.1 mm/s based on extensive research done by Daae for the Borg Port dredging project (Daae et al., 2018). The velocity is based on the analysis of the potential for flocculation done by Deltares.
  - Flocculation: Max and min concenration for flocculation
  - Hindered Settling: Gelling point
  - Salinity: C1 and C2
- Dispersion: Dispersion coefficient formulation or scaled eddy-viscosity formulation (or no dispersion) (decided per class included in the simulation)
  - Vertical
  - Horizontal
- Erosion
- Drift profile (From HD module) (including wind forcing)
- Salinity (From HD module)
- Density (From HD module)
- Bed roughness (From HD module)
- Output

Chapter 6

Validation

In this chapter the validation of the model created in MIKE is presented. The validation has been done by comparing the results in MIKE to previously published results from SINTEF, which is created by using their model, DREAM.

The settling velocity used for the validation is based on calculations of the flocculations at Borg Port (done by Deltares (Daae et al., 2018)) and set to be constant 0.1 mm/s. The currents modelled by the hydrodynamic module in MIKE uses the same discharge from Glomma as the modelling done by SINTEF, but the tides and the wind data are different and this might lead to differences in the results. The wind data in the current study were gathered from MET, while it's not known where Deltares gathered their wind data from. The tides are generated here using Mike Zero Toolbox, while it's not known where Deltares gathered their data on tides. The analysis of the data used in this study can be found in Chapter 4.

6.1 Set-up

SINTEF has simulated five different excavation operations, and three different release operations, as described in Table 6.1 and 6.2. However only the excavation cases was used for the valdidation. The release rate of sediments from the excavation work is based on the production speed and the release of fine-particulated sediments as a percentage of the production speed.

Table 6.1: SINTEF simulations - Excavation

Equipment	*Typeofsediment*	*Area*	Release $[ton/h]$
Long-range backhoe	Polluted	Fuglevika (Turning basin)	0.6
Backhoe	Polluted	Borg 1 and Borg 2	5
Grab in wire	Not polluted	Borg 1 and Borg 2	10
Small suction dredger	Not polluted	Borg 1	49
Large suction dredger	Not polluted	Borg 1 and Borg 2	135

Table 6.2: SINTEF simulationss - Realease with pipe diffuser at Møkkalasset og Svaleskjær

Equipment	Release $[ton/h]$
After grab in wire	83
After small suction dredger	113
After large suction dredger	281

For the excavation operations the simulations where performed from 1st of April 2013 and with a duration of ten days. This is to allow direct comparison between the results from this study and previous studies (Daae et al., 2018).

Details on the different excavation operations mentioned in Table 6.1 are given below:

6.1.1 Long-range backhoe

Dredging polluted sediments in Fuglevika with a long-range backhoe gave a flux of 0,6 ton/h from the dredging operations (Daae et al., 2018). This is based on the production speed of the long-range backhoe being 13 ton/h and the release of fine particulated sediments being 5% of the production speed.

6.1.2 Backhoe

Dredging polluted sediments at Borg 1 and Borg 2 with a backhoe dredger gave a flux of 5 ton/h from the dredging operations (Daae et al., 2018). This is based on the production speed of the backhoe being 101 ton/h and the release of fine particulated sediments is 5% of the production speed.

The backhoes uses eleven days at each location, and there were therefore used two sources to simulate the two backhoes.

6.1.3 Grab in wire

Dredging clean sediments at Borg 1 and Borg 2 with a grab in wire gave a flux of 10 ton/h from the dredging operations (Daae et al., 2018). This is based on the production speed of the backhoe being 210 ton/h and the release of fine particulated sediments is 5% of the production speed.

The simulations included five different sources, where each one was running for two days each.

6.1.4 Small suction dredger

Dredging clean sediments at Borg 1 and Borg 2 with a small suction dredger gave a flux of 49 ton/h from the dredging operations (Daae et al., 2018). This is based on the production speed of the backhoe being 2 426 ton/h and the release of fine particulated sediments is 2% of the production speed.

The simulations included three different sources, where each one was running for four days each (the last location only two days).

6.1.5 Large suction dredger

Dredging clean sediments at Borg 1 and Borg 2 with a grab in wire gave a flux of 135 ton/h from the dredging operations (Daae et al., 2018). This is based on the production speed of the backhoe being 2 031 842 ton/h and the release of fine particulated sediments is 2% of the production speed.

The simulations included three different sources, where each one was running for four days each (the last location only two days).

6.2 Results

The results from the two software packages (MIKE from DHI and DREAM from SINTEF) are not identical, but they are in the same range and we can therefore say that the model has been validated. The reasons for the differences can be attributed to the upstream currents due to the

salinity, which have been modelled in SINTEFs model made with DREAM, while the modelling done with MIKE is so far only 2D and therefore it has not been possible to model this upstream. This leads to the suspended sediments travelling only south, as to the sediments also travelling north in the simulations done by SINTEF.

6.2.1 Long-range backhoe

With the DREAM model SINTEF has used for modelling the sediment transport of contaminated sediments in Fuglevika, the maximum concentration of suspended sediments during the dredging is between 3 and 10ppm, as can be seen in Figure 6.1. When doing the same simulation in MIKE the results are up to 10ppm, as can be seen in Figure 6.2. It is therefore in the same range and is as detailed as we can compare the results.

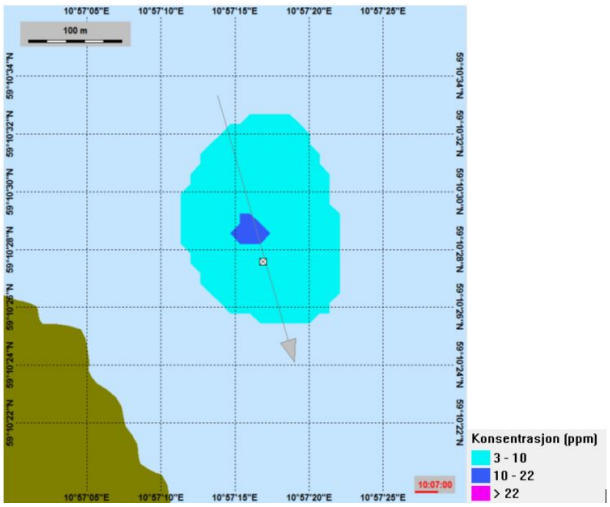

Figure 6.1: Concentration of suspended sediments at Fuglevika while dregding with a long-range backhoe after ten days with DREAM (SINTEF)

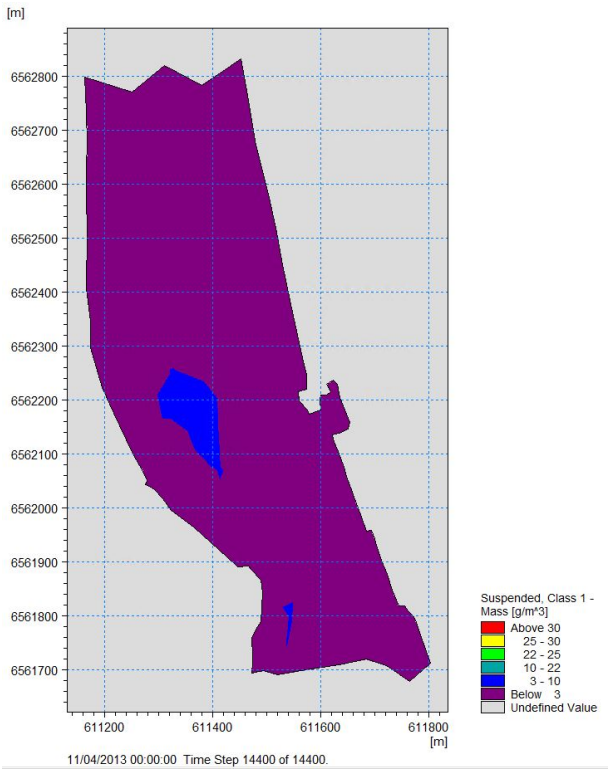

Figure 6.2: Concentration of suspended sediments at Fuglevika while dredging with a long-range backhoe ($1g/m^3 = 1ppm$) after ten days with MIKE21

6.2.2 Backhoe

Spreading of contaminated sediments at Borg 1, with two backhoes. We can see that the spreading is similar in Figure 6.3 and 6.4. The movement of the sediments close to the channel at Øra differs, which indicates that the area around Øra needs more focus in the model.

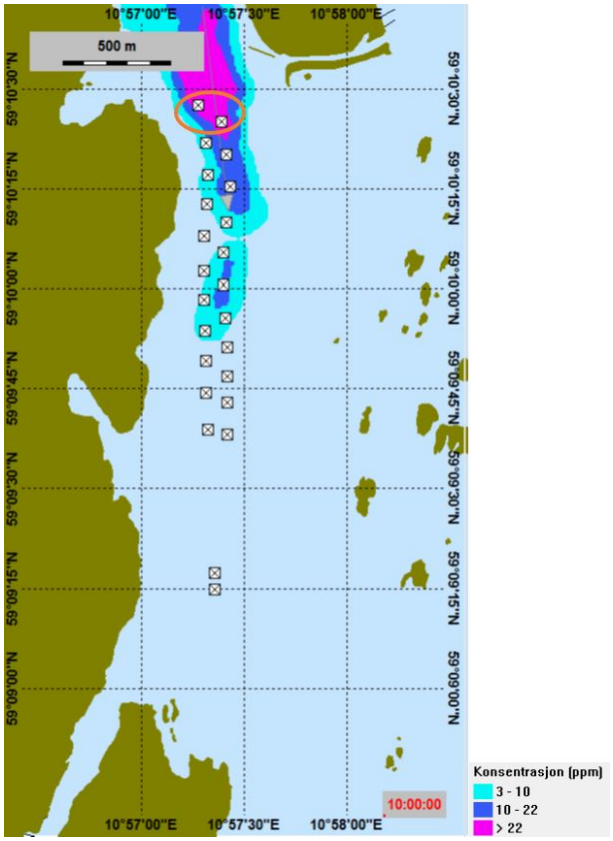

Figure 6.3: Concentration of suspended sediments at Borg 1 while dredging with two backhoes after then days with DREAM (SINTEF)

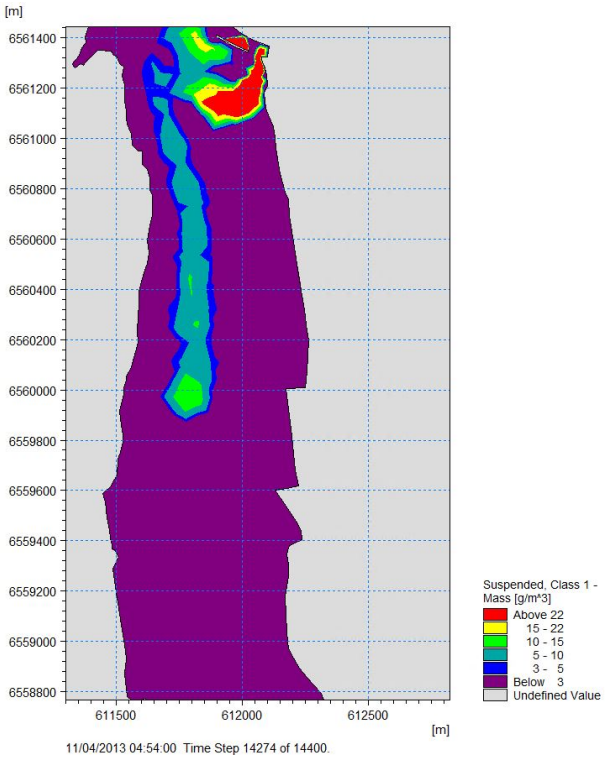

Figure 6.4: Concentration of suspended sediments at Borg 1 while dredging with two backhoes ($1g/m^3 = 1ppm$) after ten days with MIKE21

6.2.3 Grab in wire

Clean sediments at Borg Port. We can see the comparison of the two models for a dredging operation where a grab is used with DREAM in Figure 6.5 and with MIKE in Figure 6.6. The particles travel further south and it seems that there are a greater part of the sediments that are sedimented in MIKE21.

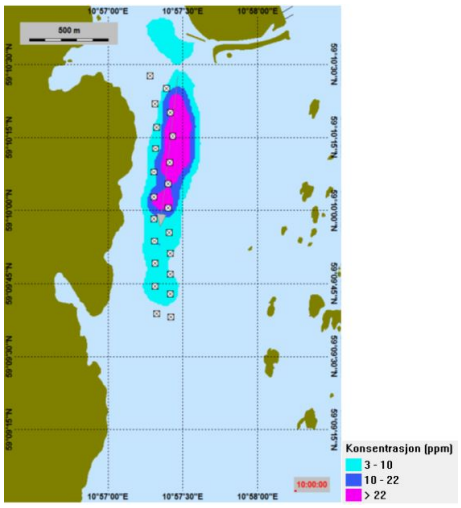

Figure 6.5: Concentration of suspended sediments at Borg 1 while dredging with a grab in wire aften ten days with DREAM (SINTEF)

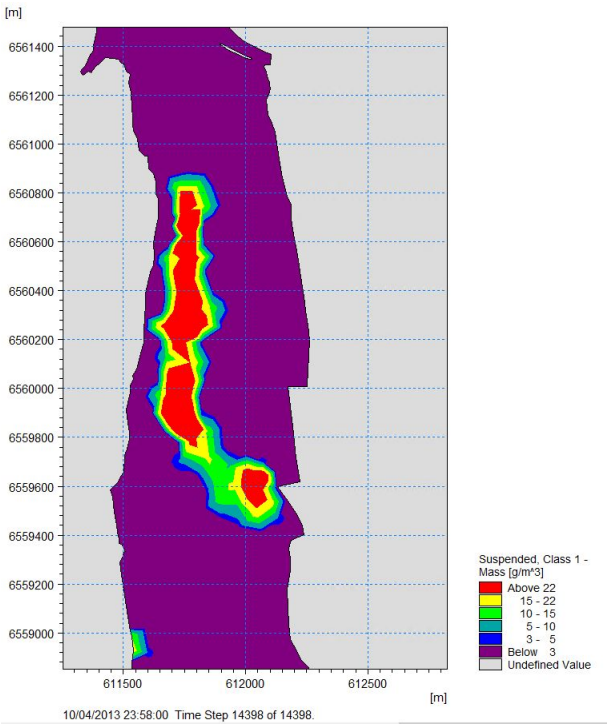

Figure 6.6: Concentration of suspended sediments at Borg 1 while dredging with a grab in wire ($1g/m^3 = 1ppm$) after ten days with MIKE

6.2.4 Small suction dredger

Clean sediments at Borg 1. We can see the comparison of the two models for a dredging operation where a small suction dredger is used with DREAM in Figure 6.7 and with MIKE in Figure 6.8. The particles travel further south and it seems that there are a greater part of the sediments that are sedimented in MIKE21.

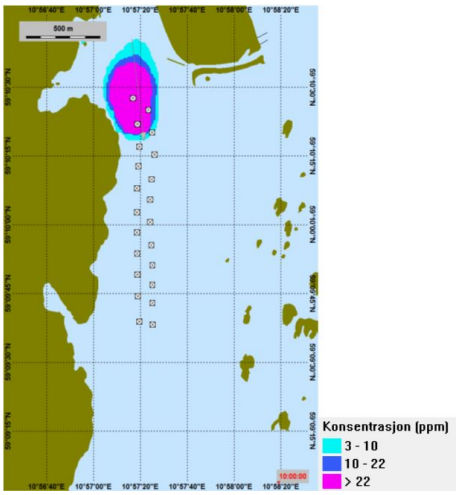

Figure 6.7: Concentration of suspended sediments at Borg 1 while dredging with a small suction dredger after ten days with DREAM (SINTEF)

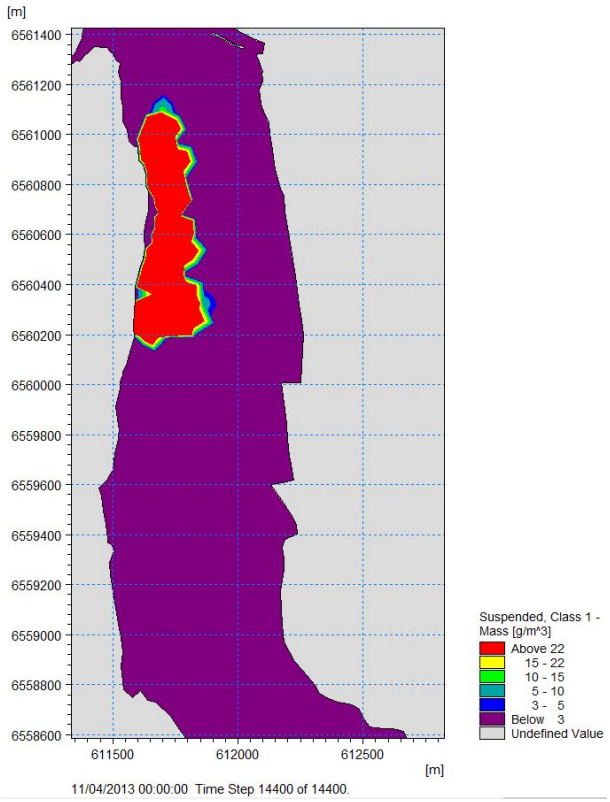

Figure 6.8: Concentration of suspended sediments at Borg 1 while dredging with a small suction dredger ($1g/m^3 = 1ppm$) after ten days with MIKE

6.2.5 Large suction dredger

Dredging of clean sediments at Borg 1. We can see the comparison of the two models for a dredging operation where a large suction dredger is used with DREAM in Figure 6.9 and with MIKE in Figure 6.10. The particles travel further south and it seems that there are a greater part of the sediments that are sedimented in MIKE21. In addition we see that the particles don't move north at all, due to the upstream not being modelled in the MIKE module.

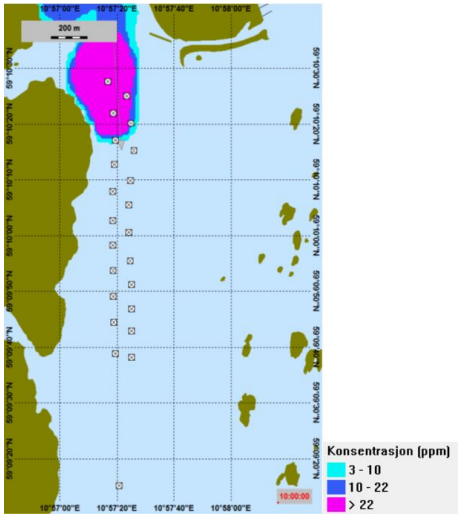

Figure 6.9: Concentration of suspended sediments at Borg 1 while dredging with a large suction dredger after ten days with DREAM (SINTEF)

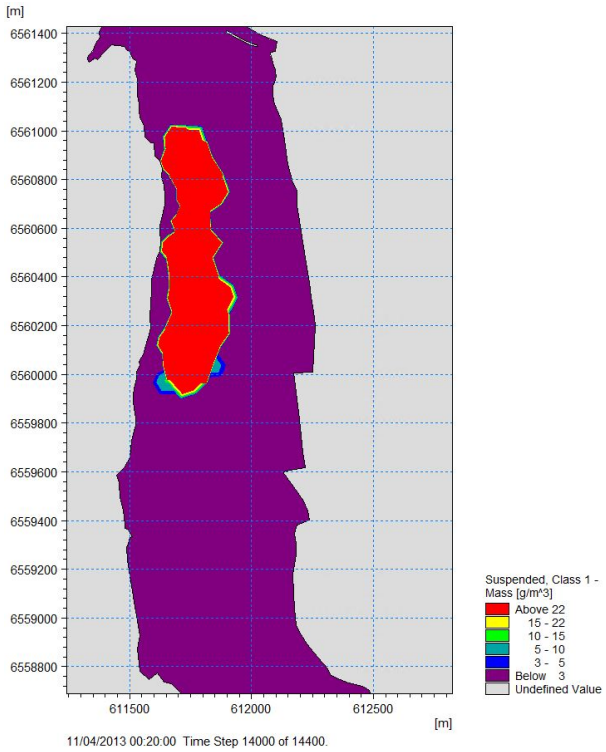

Figure 6.10: Concentration of suspended sediments at Borg 1 while dredging with a large suction dredger ($1g/m^3 = 1ppm$) after ten days with MIKE

6.3 MIKE3

Due to time limitations, the 3D model (using MIKE3 from DHI) was not used to run all the simulations. In order to see the effect of the difference in current speed in the different layers, as well as the difference the salinity has on the z-range, one simulation was done using MIKE3. The simulation was case number two, dredging at Borg 1 with two backhoes, from 1st of April 2013 to 11th of April 2013.

In Figure 6.11 we can see the results from running the same case as when validating the dredging operation with two backhoes. The images was taken at timestep 3000 (of 14 400), which is after two and a half days. It's now visible how the particle spread further and further down the fairway and how there is less and less spreading the closer to the surface we get.

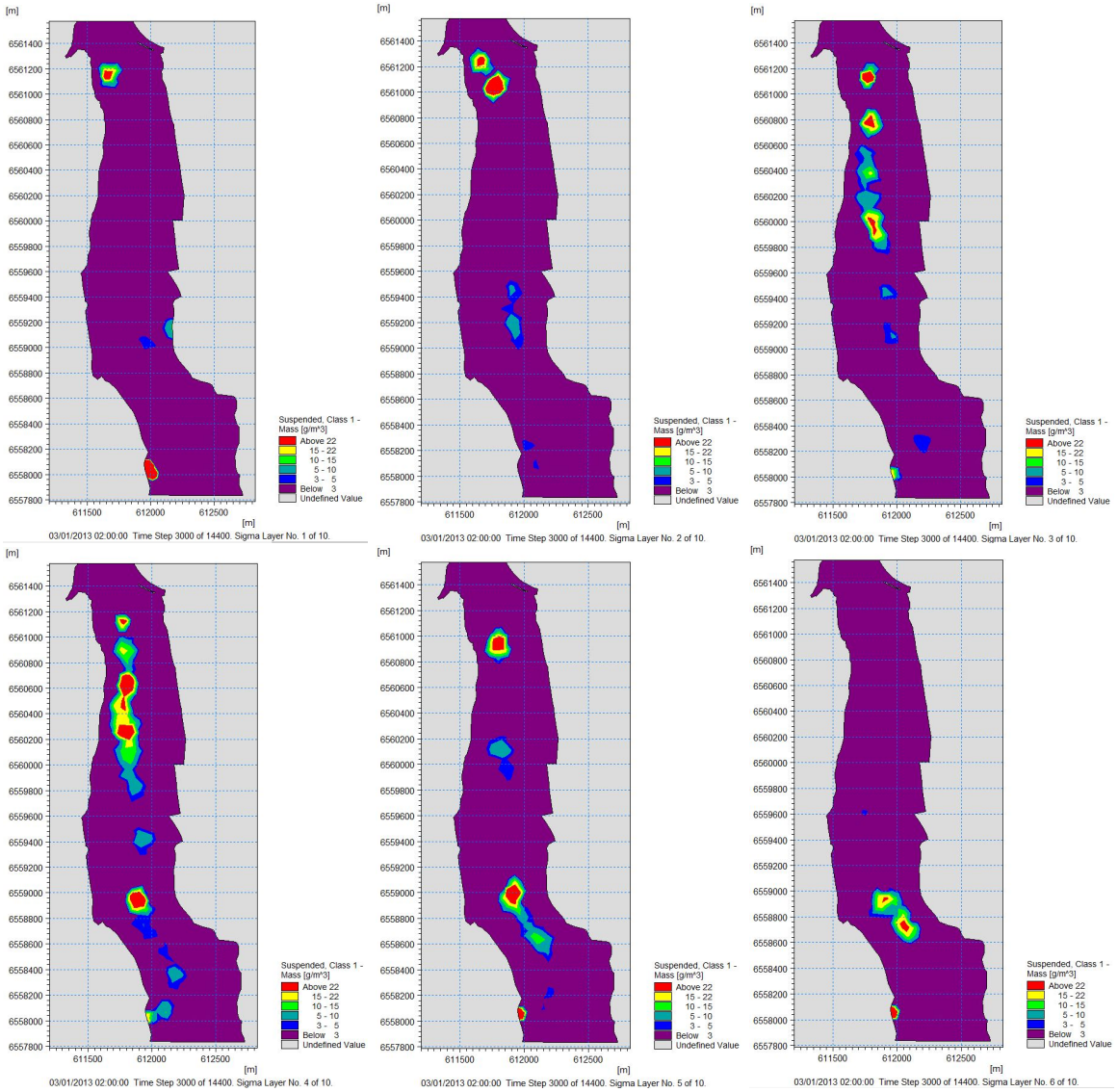

Figure 6.11: Dredging at Borg 1 with two backhoes, 2.5 days into the operation, with MIKE3. Layer 1 is closest to the bottom and layer 10 closest to the surface. $1g/m^3 = 1ppm$

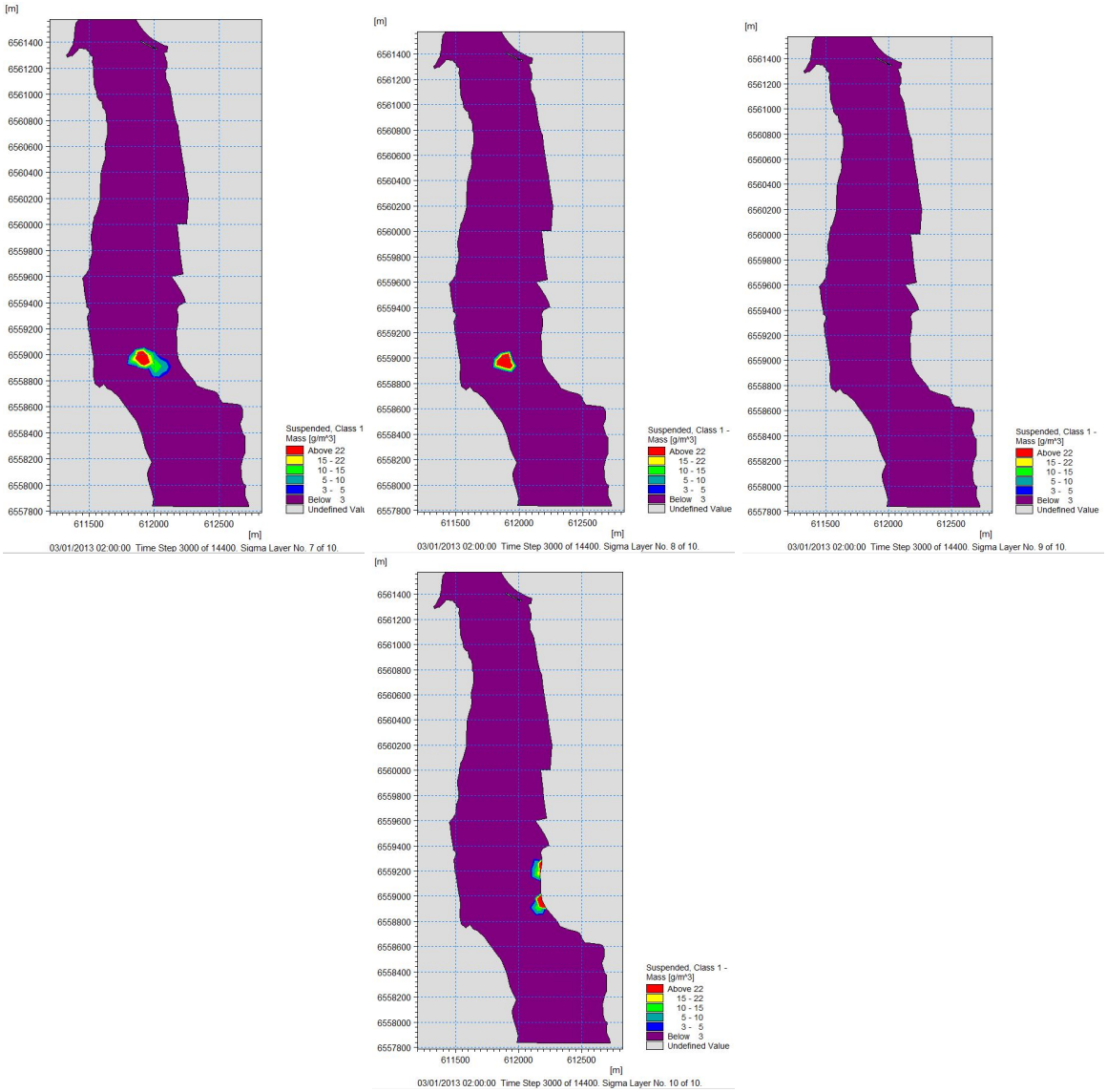

Figure 6.12: Dredging at Borg 1 with two backhoes, 2.5 days into the operation, with MIKE3. Layer 1 is closest to the bottom and layer 10 closest to the surface. $1g/m^3 = 1ppm$

When comparing it with the simulation done in MIKE21 for the same timestep, Figure 6.13, we see that the depth-averaged result only shows the spreading close to the port area, and not further down the fairway. There are a lot of details that are lost.

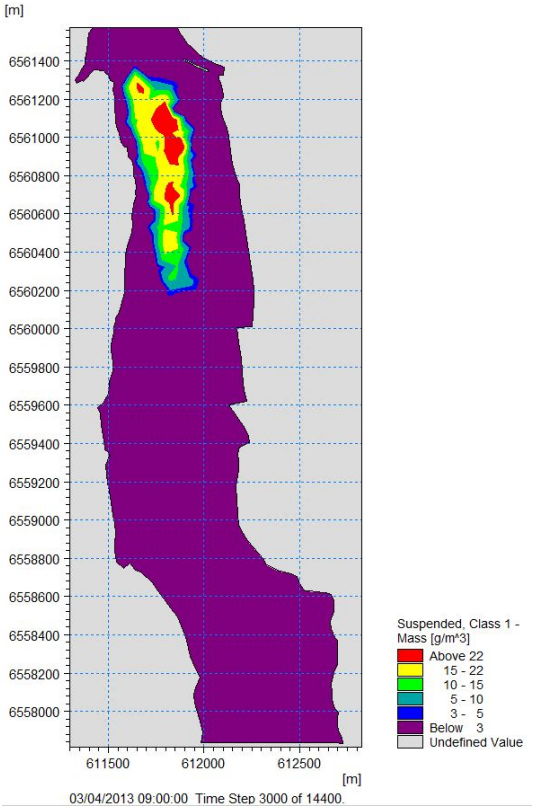

Figure 6.13: Dredging at Borg 1 with two backhoes, 2.5 days into the operation, with MIKE21. $1g/m^3 = 1ppm$

Chapter 7

Results and discussions

7.1 Operating window

To find the right operating window for the dredging work we need to know the current and the sediment spreading for each month. In order to do so we start out by testing some scenarios in the hydrodynamic module, where we will get the current speed as an output. This can be used in the particle tracking module to check the sediment spreading. To find the right input for the hydrodynamic module and learn which parameter has a greater effect various scenarios should be tested. In Table 7.1, some scenarios has been defined.

Table 7.1: Scenarios hydrodynamic

		Wind		Discharge	
	Type	Speed [m/s]	Direction	Type	m^3/s
Scenario 1	100y	21.4	210°	100y	3755
Scenario 2	100y NE	14.6	40°	100y	3755
Scenario 3	Avg	16.5	210°	Avg	1741
Scenario 4	Avg	16.5	210°	100y	3755
Scenario 5	100y	21.4	210°	Avg	1741

In order to create the hydrodynamic model the discharge, tidal and wind (as described in section 4) were used and defined in the model as described in chapter 5. The scenarios described in Table 7.1 were run with the hydrodynamic module. For the validation, described in Chapter 6, time series for discharge and wind were used. When controlling the operating window a steady state analysis was run with constant discharge and wind. The results of this analysis are shown below, in Figure 7.1.

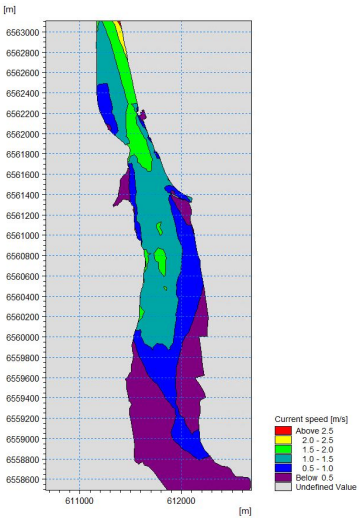

(a) Scenario 1 - 100y discharge and 100y wind

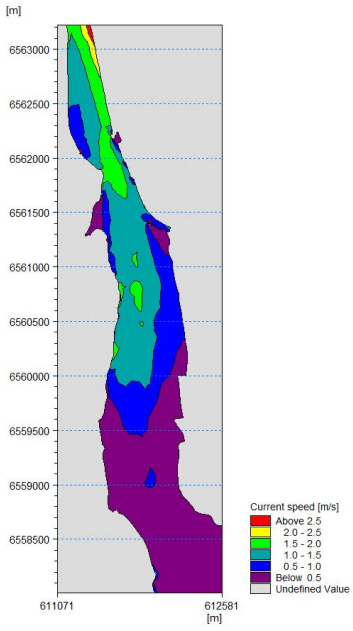

(b) Scenario 2 - 100y discharge and 100y wind from north-east

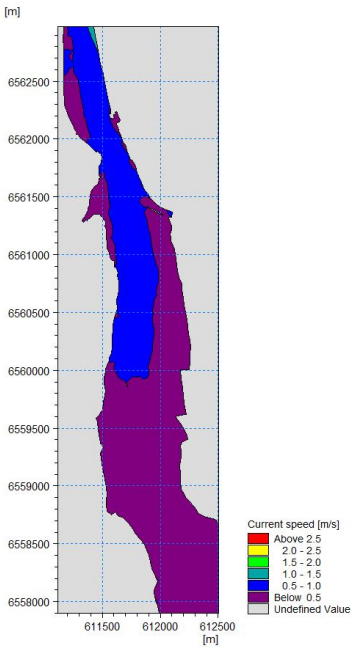

(c) Scenario 3 - Average discharge and average wind

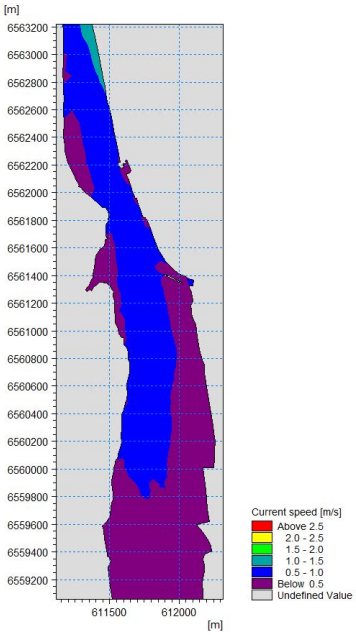

(d) Scenario 4 - Average discharge and 100y wind

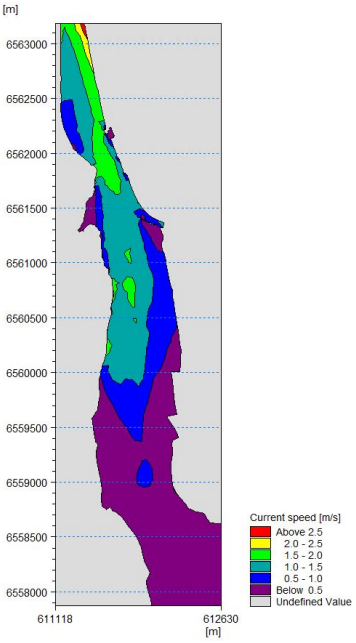

(e) Scenario 5 - 100y discharge and average wind

Figure 7.1: Current speed after two days of steady state simulations

From this we can conclude that the discharge is the dominating parameter when we are looking at the averaged current speed. And we can also see that the current speed is too high with extreme values in June to do any dredging work. Based on these results and the data analysis done in chapter 4 it was decided to do the sensitivity analysis for April and May.

In communication with Borg Port director (Tore Lundestad), the modelled current speed was validated based on their experience and also a measuring of the current speed in May using drifting of their boat as a measuring tool. The measured current speed in late May was 0.75 m/s, while the modelled current speed was 2-2.5 m/s for an extreme weather situation.

Considering also that the current speed measured in situ reflects only the current speed in the top layer, and the current speed in the model is depth averaged, this seems to be a good results, assuming a continuous velocity profile as in Figure 7.2.

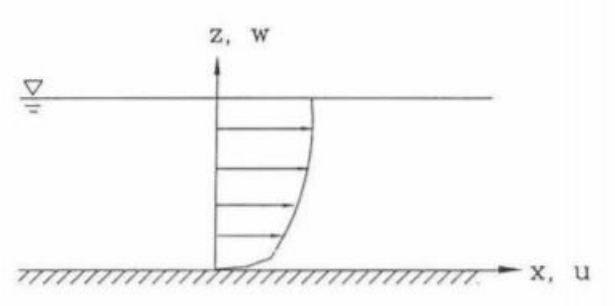

Figure 7.2: Uniform flow in an open channel (Liu, 2001)

7.2 Effect of the size of source area on the results

In order to see the effect of the size of the source area on the results, a few different sizes were tested and there is no visible changes in the results as we can see in Figure 7.3. But if the source size is increased to 100mx100m the effect is visible, as we can see in Figure 7.4.

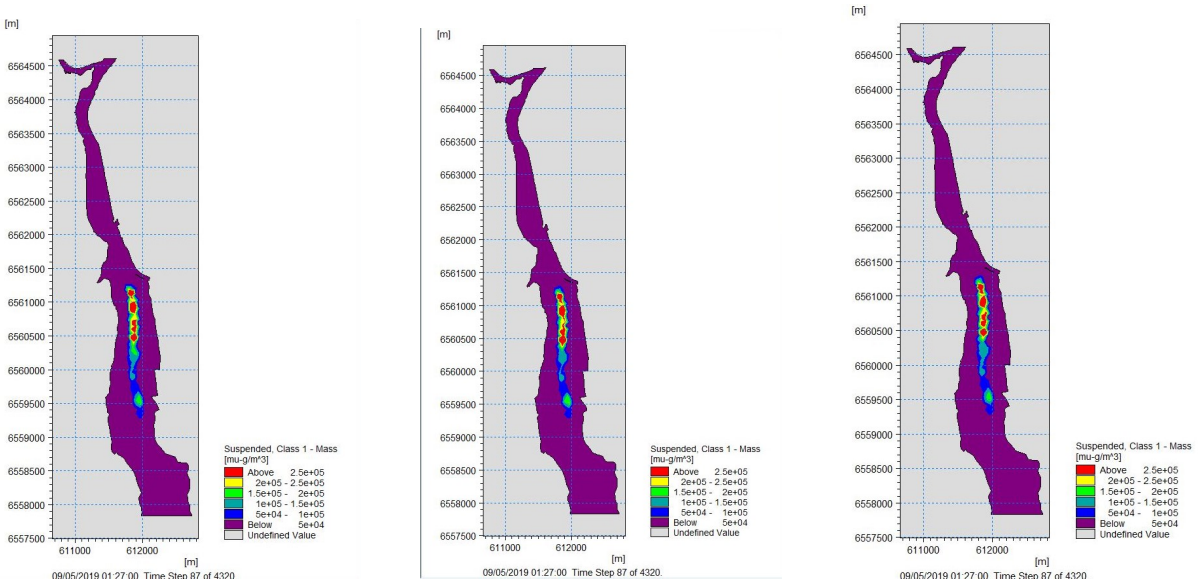

(a) Source size of 5mx5m (b) Source size of 10mx10m (c) Source size of 15mx15m

Figure 7.3: Spreading of suspended particles after 10 days with different size of source area

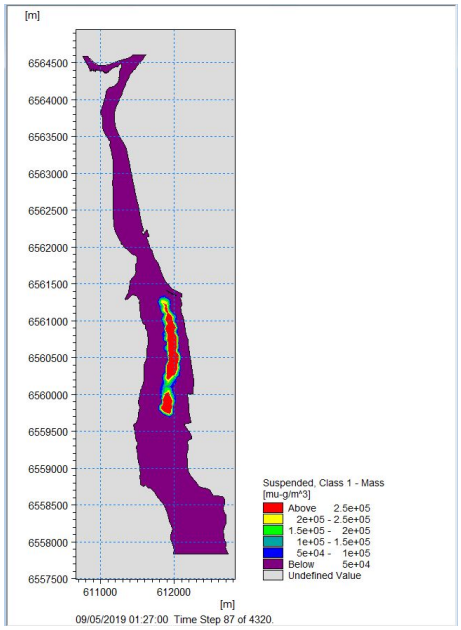

Figure 7.4: Spreading of suspended particles after 10 days with a size of source area 100mx100m

7.3 Sensitivity Analysis

The sensitivity analysis of model was studied to learn which parameters are governing for the dredging operations planned at Borg Port.

As mentioned earlier it was decided to do the sensitivity analysis for two different scenarios, one in April and one in May, defined in Table 7.2. In April the largest discharge from the river was in 2011 and the highest wind speed from 2013. In May the largest discharge from the river was in 1966 and the highest wind speed from 2012. The simulations for each of the scenarios where therefore run during the year defined by the discharge, with tides from that year, and the wind was filled in as constant from the year with the highest wind speed.

Table 7.2: Scenarios Particle Tracking

	Month	Year		Wind	
			Speed [m/s]	Direction	Year
Scenario 1	April	2011	17.9	185°	2013
Scenario 2	May	1966	19.7	200°	2012

The parameters chosen for the sensitivity analysis are settling velocity and release rate of particles from the dredging operation. An overview of the values for the two parameters can be found in Table 7.3.

Table 7.3: Parameters

Parameter	Low	Standard	High
Settling velocity [m/s]	0.00001	0.0001	0.001
Release rate [kg/s]	0.695	1.389	2.778

The results of all the runs at 2 days, 6 days, 10 days, 14 days, 21 days and 30 days can

be found in Appendix A (Scenario 1) and B (Scenario 2). Below is a selection of the figures presented in order to study the differences.

7.3.1 Scenario 1 - April 2011

Settling velocity

If we compare the amounts of suspended and sediments six days into the dredging operation for the three different settling velocities we see that there are large differences. In the first run with a settling velocity of 0.0001 m/s (in Figure 7.5) we see that there are quite a lot of suspended particles, but that they move quite far down before they settle, and there are a lot of sedimented particles. While in the second run, with a settling velocity of 0.00001 m/s (in Figure 7.6) we see that there are a lot more suspended particles, and far less sedimented particles, and that they have spread over a larger area. While if we increase the settling velocity to 0.001, in run 3 (see Figure 7.7) we see that the particle hardly move at all before they are sedimented.

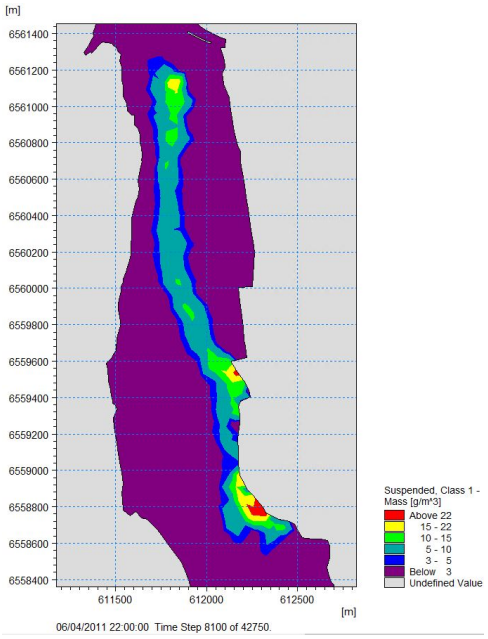

(a) Suspended sediments with a settling velocity $0.0001 m/s$

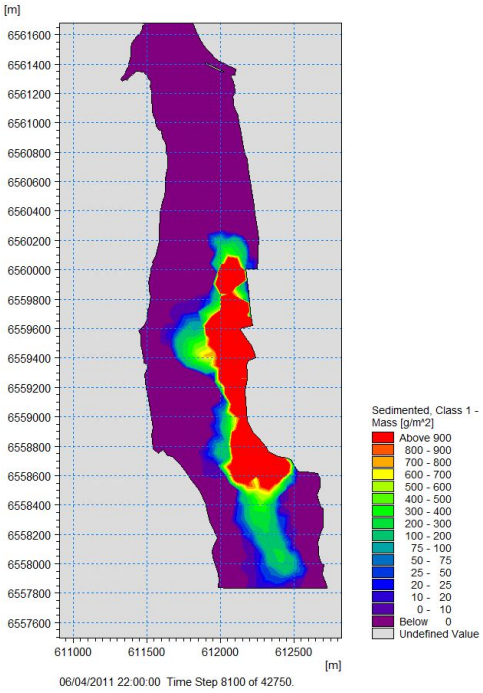

(b) Sedimented sediments with a settling velocity $0.0001 m/s$

Figure 7.5: Concentration of sediments at Borg 1 while dredging with two backhoes in April 2011 ($1 g/m^3 = 1 ppm$) after six days with MIKE

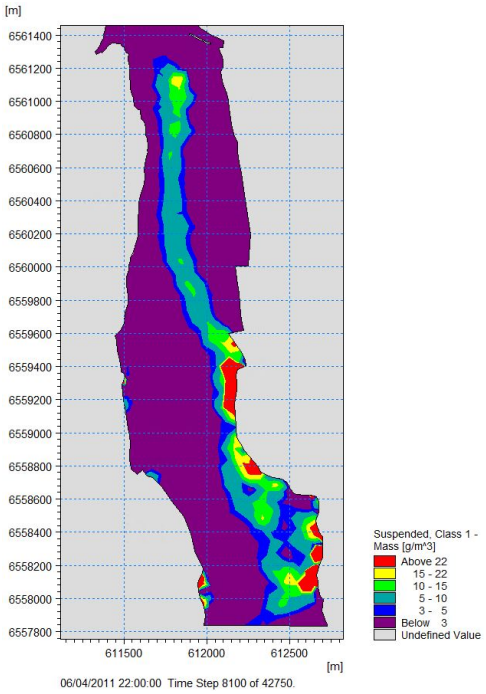

(a) Suspended sediments with a settling velocity $0.00001 m/s$

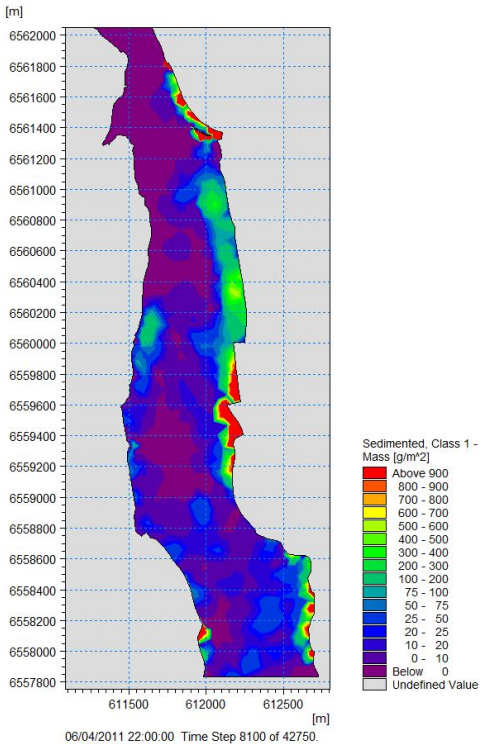

(b) Sedimented sediments with a settling velocity $0.00001 m/s$

Figure 7.6: Concentration of sediments at Borg 1 while dredging with two backhoes in April 2011 ($1 g/m^3 = 1 ppm$) after six days with MIKE

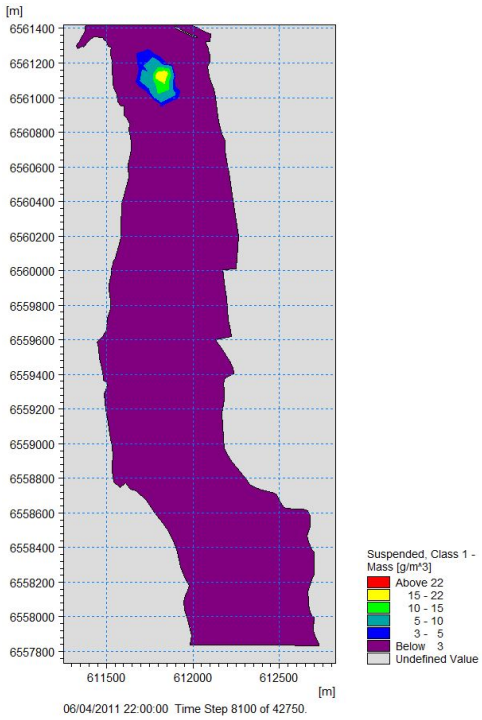

(a) Suspended sediments with a settling velocity $0.001m/s$

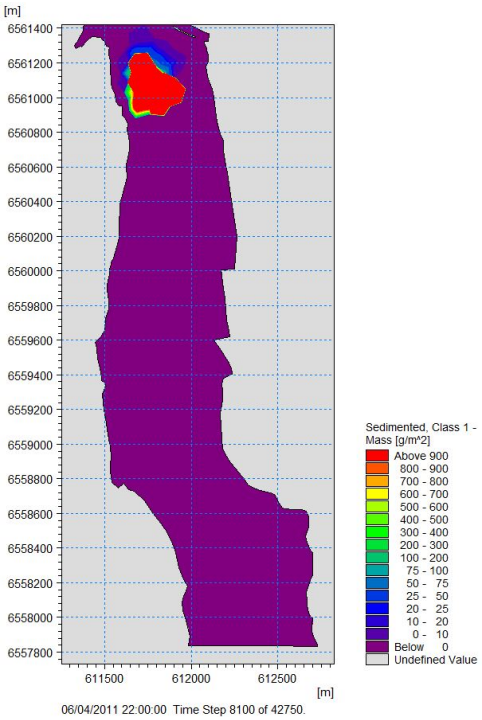

(b) Sedimented sediments with a settling velocity $0.001m/s$

Figure 7.7: Concentration of sediments at Borg 1 while dredging with two backhoes in April 2011 ($1g/m^3 = 1ppm$) after six days with MIKE21

The settling velocity has the biggest impact on the sedimented particles, as we can see in Figure 7.5, 7.6 and 7.7. They are sedimented over a large area with a low settling velocity, and a more controllable area in the case of a higher settling velocity.

Changing the settling velocity by a function of 10 might seem like a lot, but in the case of so many variables, with salinity level, flocculations, hindered settling, particle size etc. these changes can easily happen during the dredging process.

Release rate

When we change the realease rate we clearly see an increase both for the suspended and sedimented sediments when we double the release rate, Figure 7.8. And we can see that the same happens when we half the release rate, the reduction in both suspended and sedimented sediments are clearly visible, Figure 7.9. This is compared to the results with standard release rate of 1,389 (Figure 7.5).

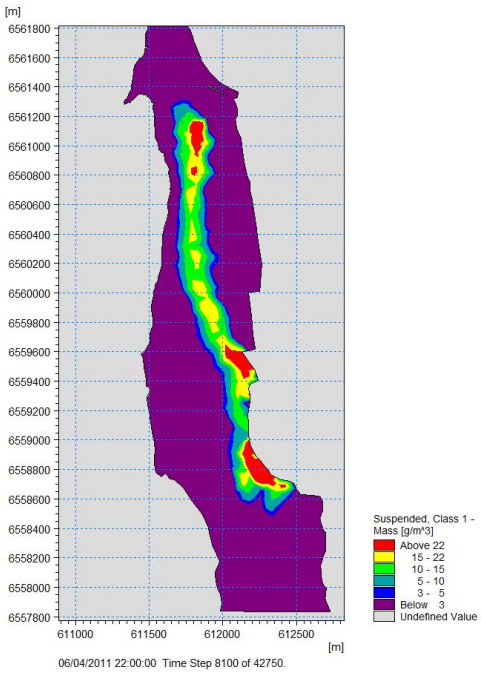

(a) Suspended sediments with a release rate of 2.778 kg/s

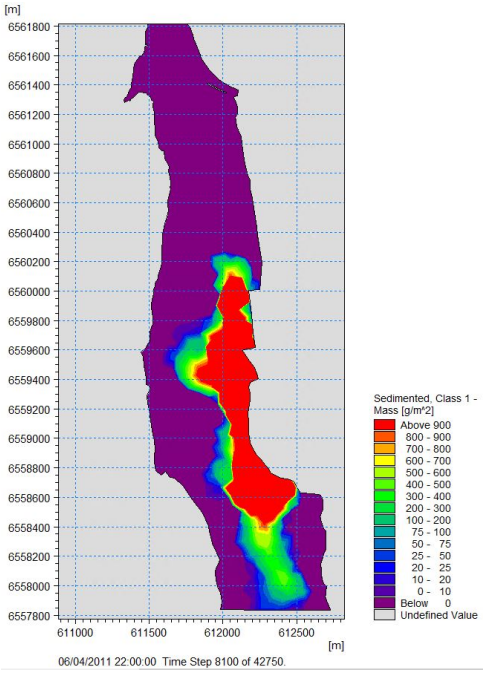

(b) Sedimented sediments with a release rate of 2.778 kg/s

Figure 7.8: Concentration of sediments at Borg 1 while dredging with two backhoes in April 2011 ($1g/m^3 = 1ppm$) after six days with MIKE21

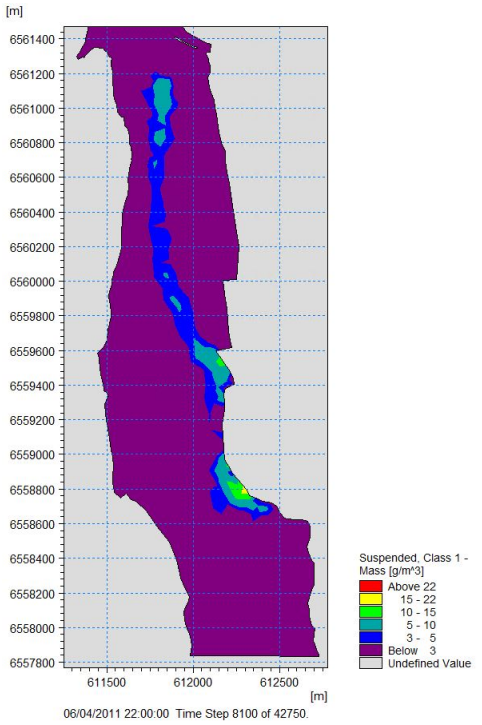

(a) Suspended sediments with a release rate of $0.695kg/s$

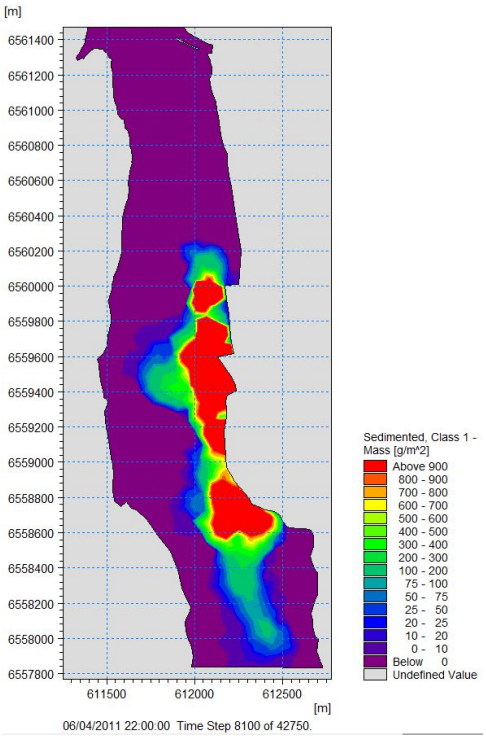

(b) Sedimented sediments with a release rate of $0.695kg/s$

Figure 7.9: Concentration of sediments at Borg 1 while dredging with two backhoes in April 2011 ($1g/m^3 = 1ppm$) after six days with MIKE21

7.3.2 Scenario 2 - May 1966

If we compare what happens in April (Figure 7.5) to what happens in May (Figure 7.10) we can see that the particles are spread further down and are sedimented over a larger area. This is probably due to the current speed, which is increased in May as the discharge is increased (Chapter 4.

This also makes the other parameters more sensitive, so that there is a larger spreading when the settling velocity is reduced, and the amounts that are spread when we increase the release rate are larger.

Settling velocity

In Figure 7.10, 7.11 and 7.12 we can see the differences the change of settling velocity has on the particle spreading in May, with a stronger current than what has been calculated in April. The change in settling velocity was the same as for scenario 1.

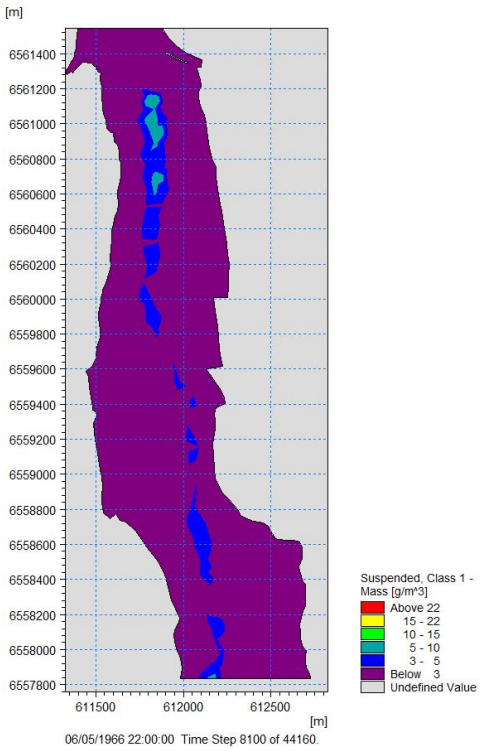

(a) Suspended sediments with a settling velocity $0.0001 m/s$

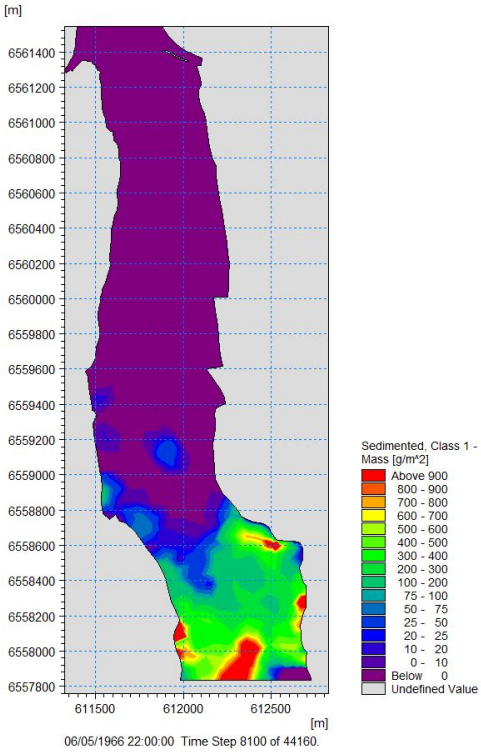

(b) Sedimented sediments with a settling velocity $0.0001 m/s$

Figure 7.10: Concentration of sediments at Borg 1 while dredging with two backhoes in May 1966 ($1 g/m^3 = 1 ppm$) after six days with MIKE21

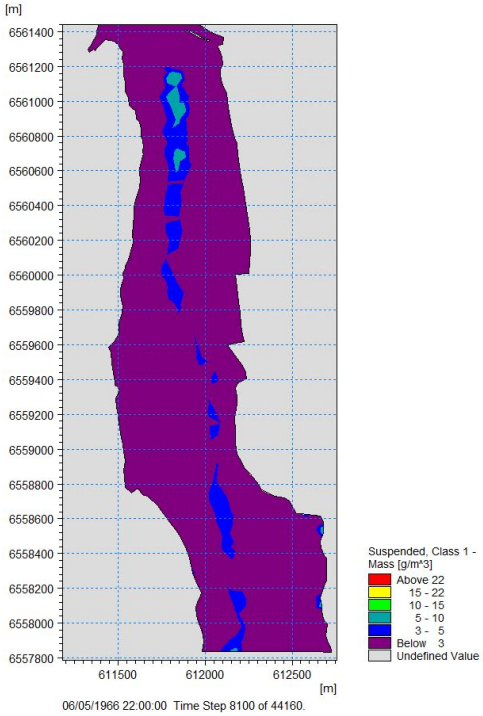

(a) Suspended sediments with a settling velocity $0.00001 m/s$

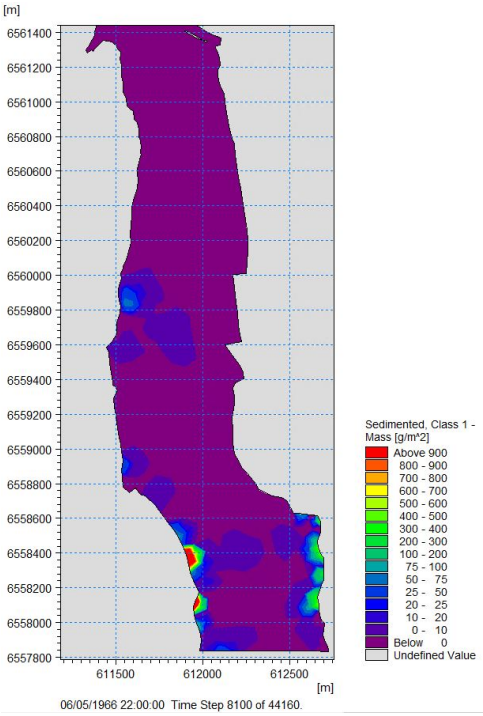

(b) Sedimented sediments with a settling velocity $0.0001 m/s$

Figure 7.11: Concentration of sediments at Borg 1 while dredging with two backhoes in May 1966 ($1 g/m^3 = 1 ppm$) after six days with MIKE21

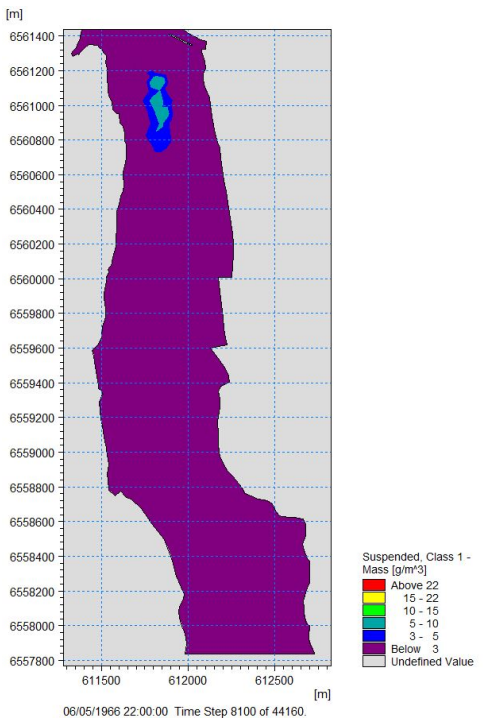

(a) Suspended sediments with a settling velocity $0.001 m/s$

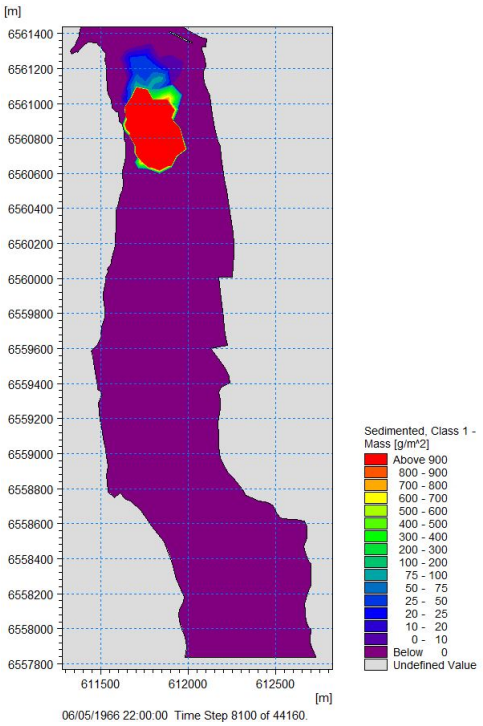

(b) Sedimented sediments with a settling velocity $0.001 m/s$

Figure 7.12: Concentration of sediments at Borg 1 while dredging with two backhoes in May 1966 ($1 g/m^3 = 1 ppm$) after six days with MIKE21

Release rate

In Figure 7.10, 7.13 and 7.14 we can see the differences the change of release rate has on the particle spreading in May, with a stronger current than what has been calculated in April. The change in release rate was the same as for scenario 1.

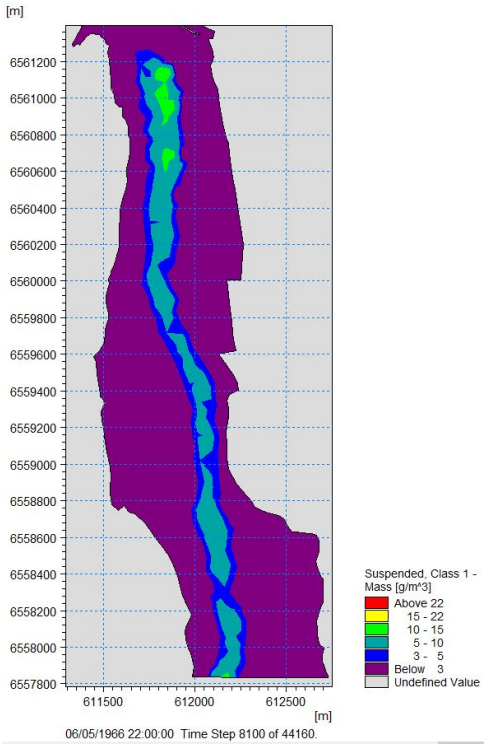

(a) Suspended sediments with a release rate of 2.778 kg/s

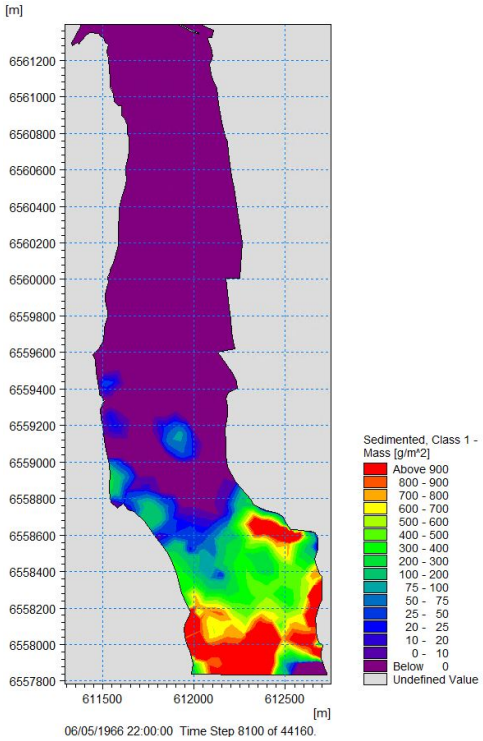

(b) Sedimented sediments with a release rate of 2.778 kg/s

Figure 7.13: Concentration of sediments at Borg 1 while dredging with two backhoes in May 1966 ($1g/m^3 = 1ppm$) after six days with MIKE21

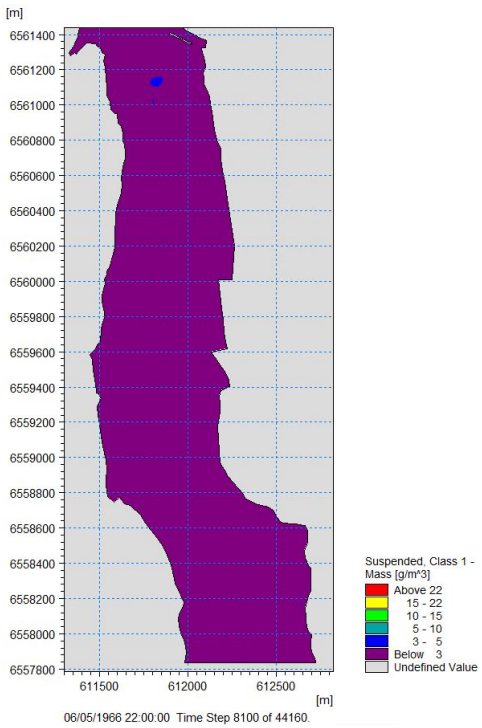

(a) Suspended sediments with a release rate of $0.695 kg/s$

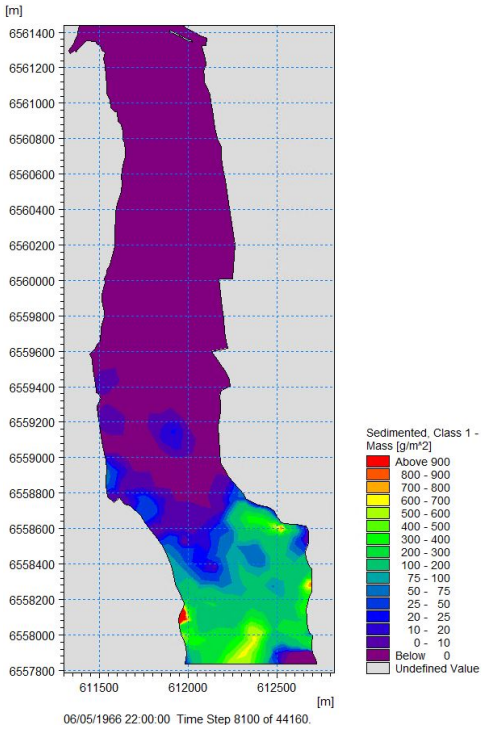

(b) Sedimented sediments with a release rate of $0.695 kg/s$

Figure 7.14: Concentration of sediments at Borg 1 while dredging with two backhoes in May 1966 ($1 g/m^3 = 1 ppm$) after six days with MIKE21

7.4 Discussions

7.4.1 Theory

In this report, there is only a brief presentation of dredging, sediment transport and numerical modelling. The information presented here is what has been evaluated as the most relevant for the work of the master thesis. The dredging chapter mainly focused on the impact dredging has on the bed and in the water, as this is what has be assessed in the sensitivity analysis.

There are many different formula used to describe sediment transport, but the advection-dispersion equation is one of the most essential equations to calculate the sediment spreading in MIKE. The fall velocity and jet movement has been in focus as this is important aspects in the disposal phase of the dredging operations and the processes that creates the turbidity which has to be evaluated in this case.

In the report it was chosen to let the environmental aspect be one of the focuses throughout all the chapters. This was done due to the responsibility that all engineers have while doing projects that could harm the environment, and because of the possible negative impacts this project could have on the environment, in terms of contaminated sediments being spread, habitats being damaged due to the turbidity caused by the dredging and the possible damage of habitats due to the change of the morphology.

It was decided to neglect waves in the numerical model. This has been done in communication with Tore Lundestad from Borg Port Authority and Ragnhild Daae from SINTEF. The area where the dredging will take place is relatively protected from the waves, as can be seen in Figure 4.2. This allows us to assume that the waves that enter the harbor is small enough to neglect when calculating and evaluating the sediment transport in relation to the dredging operations. Therefore it has not been presented any wave theory nor the effect of current and

waves together on the sediment transport in this report.

7.4.2 Data analysis and operating window

The data analysis showed that the month with the most extreme events regarding discharge is June, with April and May also having some extreme events. For wind it's mainly fall and winter. Therefore the hydrodynamic module was tested for extreme cases in June.

Discharge was found to be the governing factor for the current speed, while wind speed and wind direction had little impact or both current speed and current direction. These results were used as basis for further analysis.

Dredging is an operation that can be stopped in extreme events and therefore we don't have to model for extreme events. Knowing what these limits are by experiencing the effects of different parameters helps us narrow down which cases needs to be analysed, and which cases we need to stop the operations. Based on the results from this research dredging operations should not be performed when the discharge is larger than 3000 kg/s.

7.4.3 Validation

The validation process shows that the modelled results are similar enough to conclude that the model created in MIKE is validated. In these kind of projects the variations are rather large between what is modelled and the reality of the actual dredging projects. It is therefore expected that there are differences in the results for the two models. This is based on communication with Jens Laugesen, Chief Specialist Environment, from DNV GL, who has worked with dredging projects involving contaminated sediments for many years.

As the modeled hydrodynamics are different and the bathymetry might be different these are sources for differences between the results from SINTEF and the results in this thesis.

There are large differences between the 2D and 3D model. This might have several causes. With the 3D model there are more parameters and a more detailed way of modelling, which should give a more correct representation of the physical events. In addition the 2D results are depth-averaged, which makes it difficult to directly compare the results.

7.4.4 Results - Sensitivity analysis

The sensitivity analysis has only been performed at the top of Borg 1. This is due to the fact that Borg 1 is where most of the dredging will happen and has the largest possibility of spreading (compared to the turning basin). The dredging process will most likely begin at the top of Borg 1 (closest to the port), and the simulations has therefore been run from there.

We can see that there are variations in the results when changing the parameters settling velocity and release rate. As there are still many uncertainties in such a dredging project this is important to be aware of and take in to account when evaluating the consequences of the dredging operations.

The simulations for April and May is based on the year that the discharge from the river was at its highest, therefore it is most probably a worse situation than for the upcoming dredging project. The timeseries was used for this simulations. This allowed for an analysis of the variation throughout the first ten days, with fluctuations during the days in discharge from the river, wind speed and wind direction. However those values never exceeded the 100 year value for discharge nor wind speed. It is therefore important to evaluate these conditions during the dredging operations, to be able to stop the dredging processes early enough in case of extreme events. The operating window should be investigated closely and be a governing factor for when the operations should take place.

When the current speed is strong we see that the sediments spread over a large area, both as suspended particles and as they sediment. This leads to the level of suspended sediments

being below the threshold ($3ppm$) over most of the area. Which could be a problem as it could be classified as good timing to dredge, while there is no knowledge of how far the sediments are spread. It should therefore be considered what is the evaluation parameters for doing such dredging operations.

With the strong currents, especially in May and June, the spreading of the sediments exceeds the area that has been used for the simulations. A larger area was set-up for this study, but due to the long simulation time for this area it was not done simulations in the particle tracking module for it. This set-up should be further explored and used, to see how far the particles spread while suspended.

If a backhoe with specifications that are not well controlled are used and the release rate are higher than 5% there is a large risk that the spreading will be a much larger problem than what has been modelled so far, based on the results of the sensitivity analysis.

When the settling velocity is very low the sediments spread in a large area and are moved in different patterns. This makes it hard to calculate how the spreading will be in reality for very low settling velocities. In the analysis the settling velocity was changed with a factor of ten both up and down, it is not likely that it will vary more than that.

Lastly, as mentioned in Chapter 5, one of the assumptions of the particle tracking module is neglecting Fick's dispersion law. This was explained as could lead to more suspended sediments on the sides than in the middle, which is not physically possible according to Fick's dispersion law. From the results we see that this has happened in some of the cases. Where this is the case it should be taken into account by knowing that the suspended and sedimented sediments at the sides are less than what the results depict.

The area around Øra has been simplified by removing the channel towards the east. This might be the reason for why there are a lot of sedimentation in that area. It could be solved by detailing that area of th model.

Chapter 8

Conclusion and recommendations for further work

This research has attempted to learn how sediments spread and sediment during dredging projects, by using the planned dredging project at Borg Port as a case study. A two-dimensional (2D) model with flexible mesh was created using the hydrodynamic module of MIKE21, powered by DHI. It was calibrated using local measurement and personal communication with experienced people at Borg Port Authority. The particle tracking module created in MIKE21 were calibrated and validated by comparing it to results from previous modelling done by SINTEF in their in-house software"DREAM". A sensitivity analysis for two parameters, settling velocity and release rate, was performed for April and May. The important findings can be summarized as follows:

- The governing factor for the current speed is the discharge from the river.
- The calculated current speed for the 100-year discharge from the river was between 2 and 2.5 m/s in the narrow areas of the fairway.
- The current speed is the governing factor for the spreading of the sediments.
- The analysis excludes June and parts of May from the operating window as the current speed is too high.
- The sensitivity analysis revealed that both settling velocity and release rate has a large effect on the spreading of sediments.
- When the release rate is doubled both the suspended and sedimented sediments are over the threshold (3 ppm for suspended sediments). The release rate is a combination of the capacity and the spill percentage of the dredging equipment, and can therefore be controlled to some extent.
- A reduction of the settling velocity with a factor of ten leads to a spreading of the sediments that are hard to control and leaves contaminated sediments at all locations of the fairway.
- Increasing the settling velocity with a factor of ten gives a situation with is easy to control. However, the settling velocity is only decided by the sediments and flocculations, which makes it a parameter that is difficult to control.
- In general the sensitivty analysis in May gives a clear indication that the current speed is too high, leading to conditions where it will be hard to control the spreading of the sediments.
- Due to the uncertainties in these type of simulations it's important to monitor the settling velocity, the release rate and the turbidity throughout the whole dredging process.

8.1 Further work

The following points should be considered for any further research to be carried out for the location:

- A sensitivity analysis has been performed for settling velocity and release rate. There are several other parameters that are valuable to investigate. For example the distance between two backhoes, the difference between using one or two backhoes at the same time,
- Both horizontal and vertical dispersion have been neglected in the Particle Tracking module in this case study, as well as erosion and resuspension. These are effects that should be considered to be analysed.
- The particles spread beyond the modelled area. A larger area has been set-up and should be used for further modelling.
- Only a few simulations were run with the MIKE3 model due to time limitations. For the future all the dredging simulations should be performed with the MIKE3 model, due to the different layers with different salinity levels.
- The planned deposit sites for the deposition of clean sediment is in the large model and should be simulated accordingly.
- There are other dredging tools that has not been modelled for, and could be interesting to use for further analysis. For example could the Pneuma Pump be used as it is suitable for environmental dredging where low turbidity and low spreading of contaminants are important (Høy-Petersen, 2008).
- The area around Øra should be refined to obtain more accurate results.

References

Ansa Ebinimi J., Akinrotimi Ojo A. The Political Ecology of Oil and Gas Activities in the Nigerian Aquatic Ecosystem. 2018.

Arntsen Øivind A., McClimans Thomas A. Excerpt from "The marine physical environment of Coastal and Shelf seas". 2003.

Bach Lis, Nielsen Morten Holtegaard, Bollwerk Sandra M. Environmental Impact of Submarine Rock Blasting and Dredging Operations in an Arctic Harbor Area: Dispersal and Bioavailability of Sediment-Associated Heavy Metals // Water Air Sollut Pollut. 2016.

Borg Havn IKS . Om Borg Havn. 2018. https://www.borg-havn.no/om-borg-havn/.

Carson Bob. Eolian Geomorphology. 2011.

Chan S. N., Lee Joseph H. W. A Particle Tracking Model for Sedimentation from Buoyant Jets // Journal of Hydraulic Engineering. 2016.

Daae Ragnhild L., Hoff Jan Van 't, Pennekamp Johan. Innseiling til Borg havn – modellering av mudrings- og deponeringsoperasjoner*Spredning av finpartikulært materiale.* May 2018.

Elliot Michael, Hemingway Krystal. Fishes in Estuaries. 2018.

European Dredging Association . Types of dredger. 2018. https://www.european-dredging.eu.

Ferziger Joel H., Peric Milovan. Computational Methods of Fluid Dynamics. 2002.

Fettweis Michael, Baeye Matthias, Francken Frederic, Lauwaert Brigitte, Eynde Dries Van den, Lancker Vera Van, Martens Chantal, Michielsen Tinne. Monitoring the effects of disposal of fine sediments from maintenance dredging on suspended particulate matter concentration in the Belgian nearshore area (southern North Sea) // Marine Pollution Bulletin. 2011.

Galappatti R. A depth-integrated model for suspended sediment transport. 1985.

Gildeh H. Kheirkhah, Mohammadian A., Nistor I., Qiblawey H. Numerical Modeling of Turbulent Buoyant Wall Jets in Stationary Ambient Water // Journal of Hydraulic Engineering. 2014.

Goda Yoshimi. Random seas and design of maritime structures 3rd edition. 2010.

Google Earth . Image from Google Earth, Fredrikstad, Norway. 2018.

Google Maps . Image from Google Maps, Fredrikstad, Norway. 2018.

Götz Flöser Rolf Riethmüller Hans Burchard. Observational evidence for estuarine circulation in the German Wadden Sea // Continental Shelf Research. 2011.

Helland Aud. MILJØKONSEKVENSVURDERING VED FARLEDSUTBEDRING TIL BORG HAVN. 2018.

Hjermann Dag Ø. Statistisk analyse av volum av forurenset sediment i Borg 1 og Flyndregrunnen, basert på samlet kjemisk analysemateriale fram til 2017. May 2018.

Høy-Petersen Carl Erik. Salvage of U864 *Supplementary studies - Dredging.* July 2008.

Jan de Nul . Backhoe Dredger. 2014. https://www.jandenul.com/en/equipment/fleet/backhoe-dredger.

Jirka Gerhard H. Integral Model for Turbulent Buoyant Jets in Unbounded Stratified Flows. Part I: Single Round Jet // Environmental Fluid Dynamics. 2004.

Johansen Øistein. Spredning av forurensning i luft og vann. 1993. Forelesnings-notat til studieretning for miljø- og ressursteknikk, Bergavdelingen, NTH.

Kamphuis J. William. Introduction to coastal engineering and management. 2010.

Kartverket . sehavniva. 2019. https://www.kartverket.no/sehavniva.

Liu Zhou. Sediment Transport. 2001.

Lund University . Buoyant Jets and Plumes: Theory and model. 2010. http://www.lth.se/fileadmin/tvrl/files/vvr176/lecture6.pdf.

MIKE, powered by DHI . MIKE21 - 2D modelling of coast and sea. 2017a.

MIKE, powered by DHI . MIKE21 Flow Model FM - Hydrodynamic Module - User Guide. 2017b.

MIKE, powered by DHI . MIKE21 Flow Model and MIKE21 Flood Screening Tool - Hydrodynamic Module - Scientific Documentation. 2017c.

MIKE, powered by DHI . MIKE21 Toolbox - Global Tide Model - Tidal Prediction. 2017d.

MIKE, powered by DHI . MIKE21 and MIKE 3 Flow Model, Advection-Dispersion Module, Scientific Documentation. 2017e.

MIKE, powered by DHI . MIKE21 and MIKE 3 Flow Model FM, Hydrodynamic Module, Short description. 2017f.

MIKE, powered by DHI . MIKE21 and MIKE 3 Flow Model FM, Hydrodynamic and Transport Module, Scientific Documentation. 2017g.

MIKE, powered by DHI . MIKE21 and MIKE 3 Flow Model FM, Mud Transport Module, Scientific Documentation. 2017h.

MIKE, powered by DHI . MIKE21 and MIKE 3 Flow Model FM, Particle Tracking Module, Scientific Documentation. 2017i.

MIKE, powered by DHI . MIKE21 and MIKE 3 Flow Model FM, Sand Transport Module, Scientific Documentation. 2017j.

MIKE, powered by DHI . Mesh generator - User Guide. 2017k.

Manap Norpadzlihatun, Voulvoulis Nikolaos. Environmental management for dredging sediments - The requirement of developing nations // Journal of Environmental Management. 2014.

Matthews John A. Encyclopedia of environmental change. 2014. 981.

Matthews John A., Boulton Mary A. Encyclopedia of environmental change. 2014. 1068.

Matthews John A., Owen Geraint. Encyclopedia of environmental change. 2014. 87.

Metha Ashish J. On estuarine cohesive sediment suspension behaviour // Journal of geophysical research. 1989.

Miljødirektoratet . Veileder for risikovurdering av forurenset sediment. 2016. http://www.miljodirektoratet.no/no/Publikasjoner/2016/September-2016/Veileder-for-risikovurdering-av-forurenset-sediment/.

MyNewsDesk . East Marine Launches New $10m^3$ Grab Dredger to Undertake Jurong Island West Extension Project (Dredging). 2014. http://www.mynewsdesk.com/sg/eastmarine/pressreleases/east-marine-launches-new-10m3-grab-dredger-to-undertake-jurong-island-west-extension-project-dredging-989350.

Norwegian Meterological Institute . eKlima. 2019. http://eklima.met.no.

Pike Jennifer. Encyclopedia of environmental change. 2014.

Roelvink Dano, Reniers A.J.H.M. A Guide to Modeling Coastal Morphology. 2011.

SNL - Great Norwegian Encyclopedia . Glomma. 2019. https://snl.no/Glomma.

Saremi Sina. Mixing, Transport and Fine sediments. 2016.

Swamee Prabhata K., Ojha Chandra Shakhar P. DRAG COEFFICIENT AND FALL VELOCITY OF NONSPHERICAL PARTICLES // Journal of Hydraulic Engineering. 1991.

The Norwegian Environment Agency . Kystverket søker om å utdype innseilingen til Borg havn (2013/2348). 2018. http://pp.miljostatus.no/no/Horinger/Landbasert-industri/Kystverket-soker-om-a-utdype-innseilingen-til-Borg-havn-201323481/.

Wang Xiao Yu, Feng Jiang. Assessment of the Effectiveness of Environmental Dredging, in South Lake, China // Environmenal Management. 2007.

Wikipedia . Atmospheric dispersion modeling. 2018a. https://en.wikipedia.org/wiki/Atmospheric_dispersion_mo

Wikipedia . Sediment. 2018b. https://en.wikipedia.org/wiki/Sediment.

Wohlfarth U. Barbara. Encyclopedia of environmental change. 2014.

Yuanahua . Jet Suction Dredger deepwater sand dredge. 2019.

Appendices

Appendix A

Results - Scenario 1 (April 2011)

A.1 Scenario 1 - April 2011

Results from running the model for a month.

A.1.1 1st run - 1.389 kg/s - 0.0001 m/s

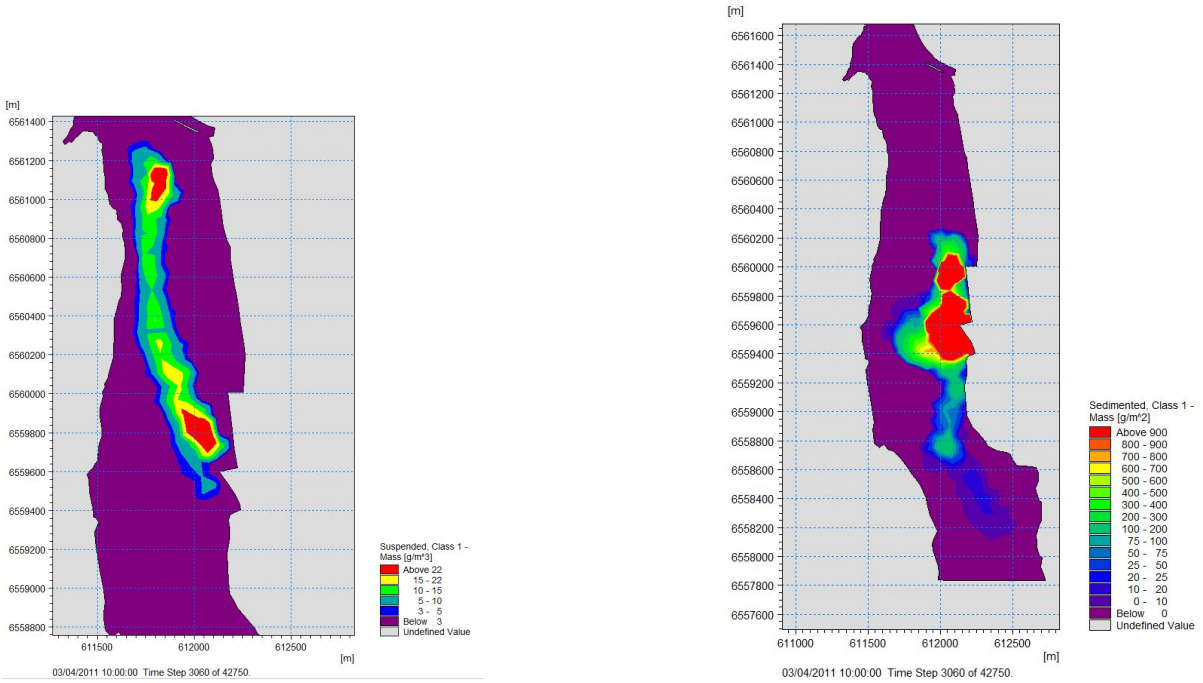

Figure A.1: Concentration of sediments at Borg 1 while dredging with a backhoe ($1g/m^3 = 1ppm$) - MIKE

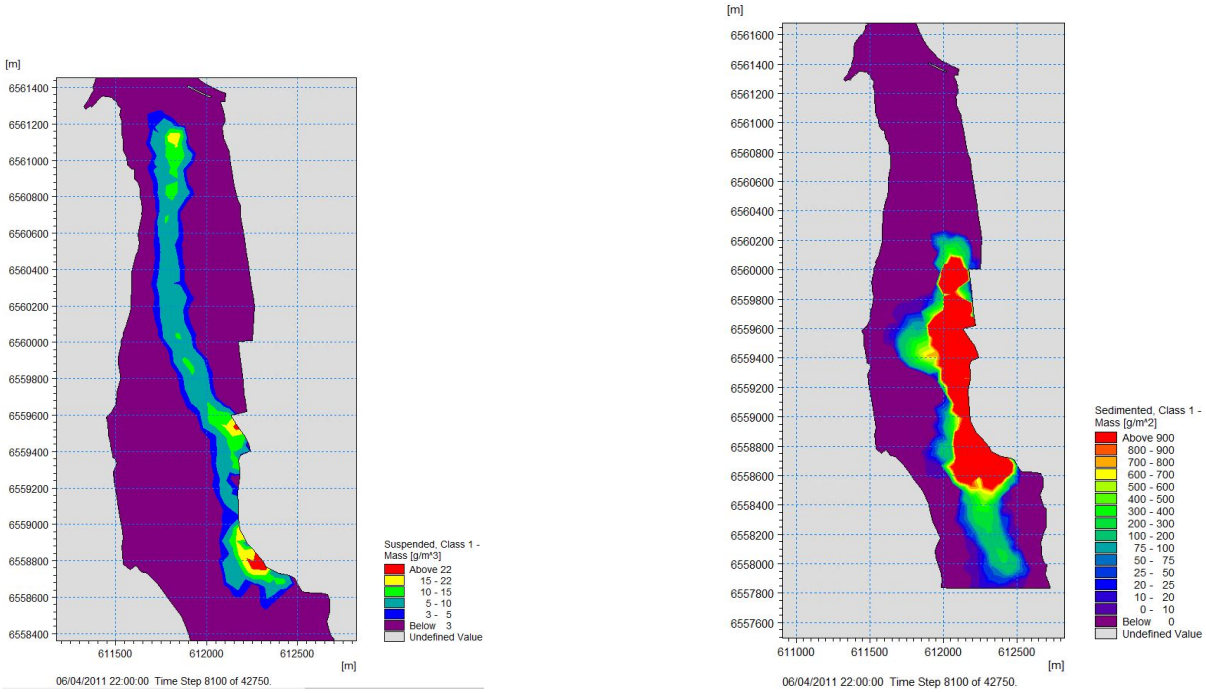

Figure A.2: Concentration of sediments at Borg 1 while dredging with a backhoe ($1g/m^3 = 1ppm$) - MIKE

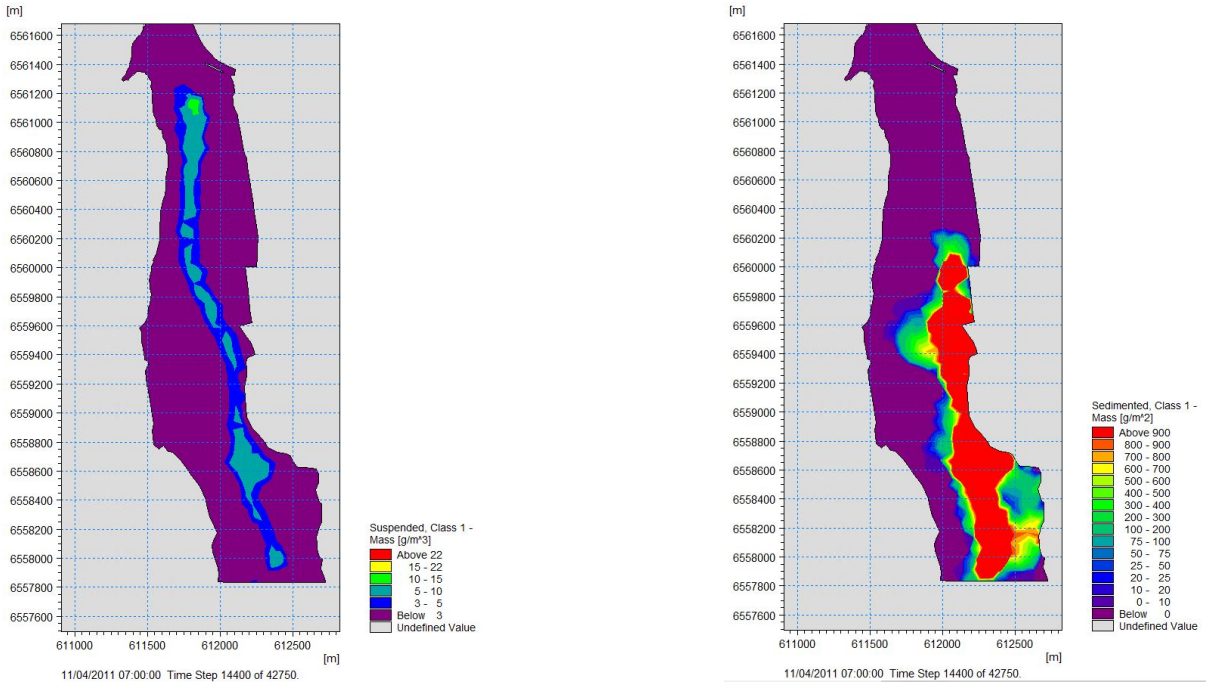

Figure A.3: Concentration of sediments at Borg 1 while dredging with a backhoe ($1g/m^3 = 1ppm$) - MIKE

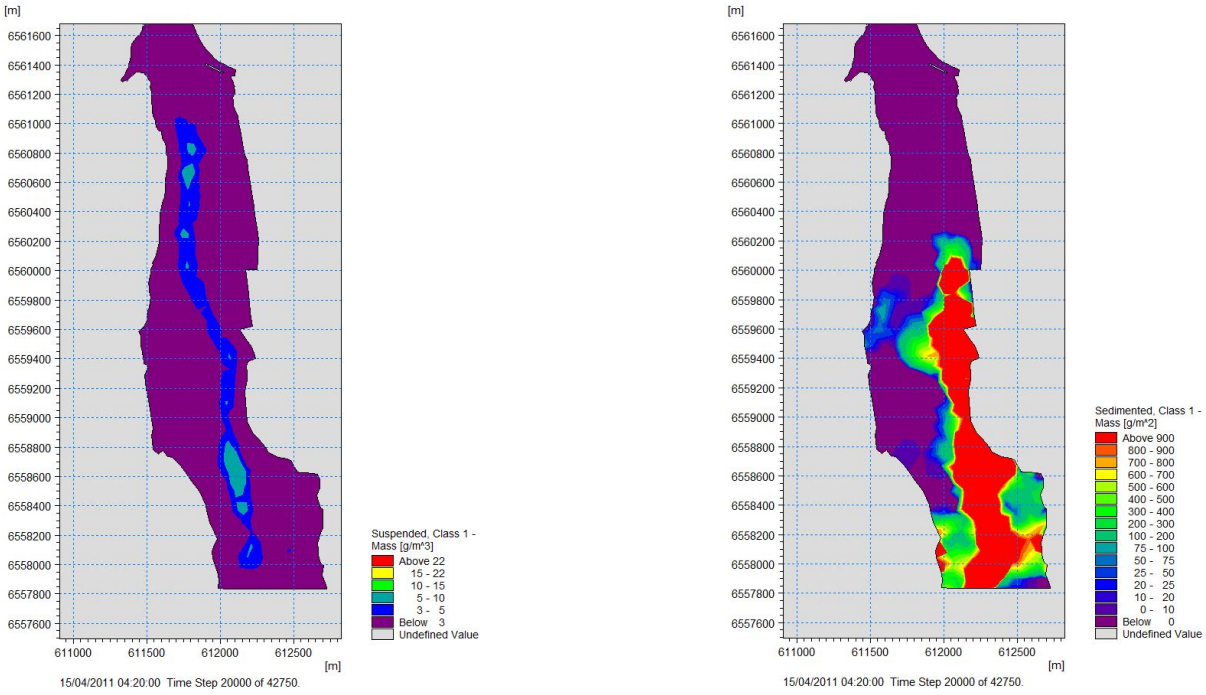

Figure A.4: Concentration of sediments at Borg 1 while dredging with a backhoe ($1g/m^3 = 1ppm$) - MIKE

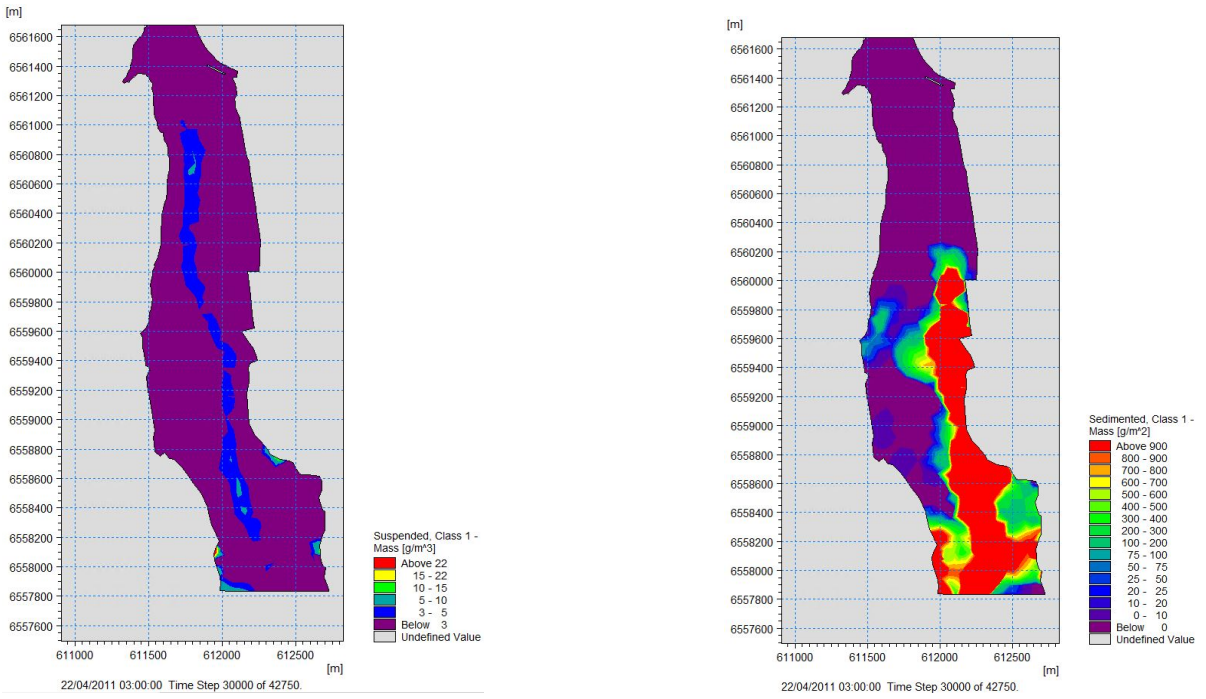

Figure A.5: Concentration of sediments at Borg 1 while dredging with a backhoe ($1g/m^3 = 1ppm$) - MIKE

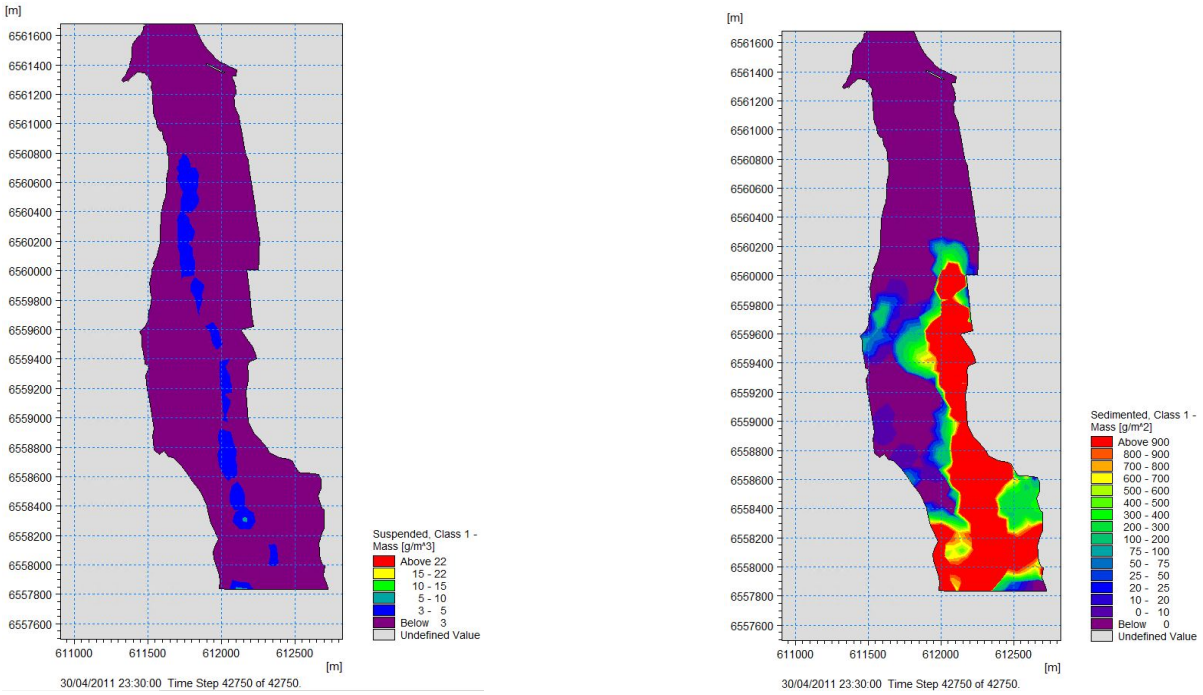

Figure A.6: Concentration of sediments at Borg 1 while dredging with a backhoe ($1g/m^3 = 1ppm$) - MIKE

A.1.2 2nd run - 1.389 kg/s - 0.00001 m/s

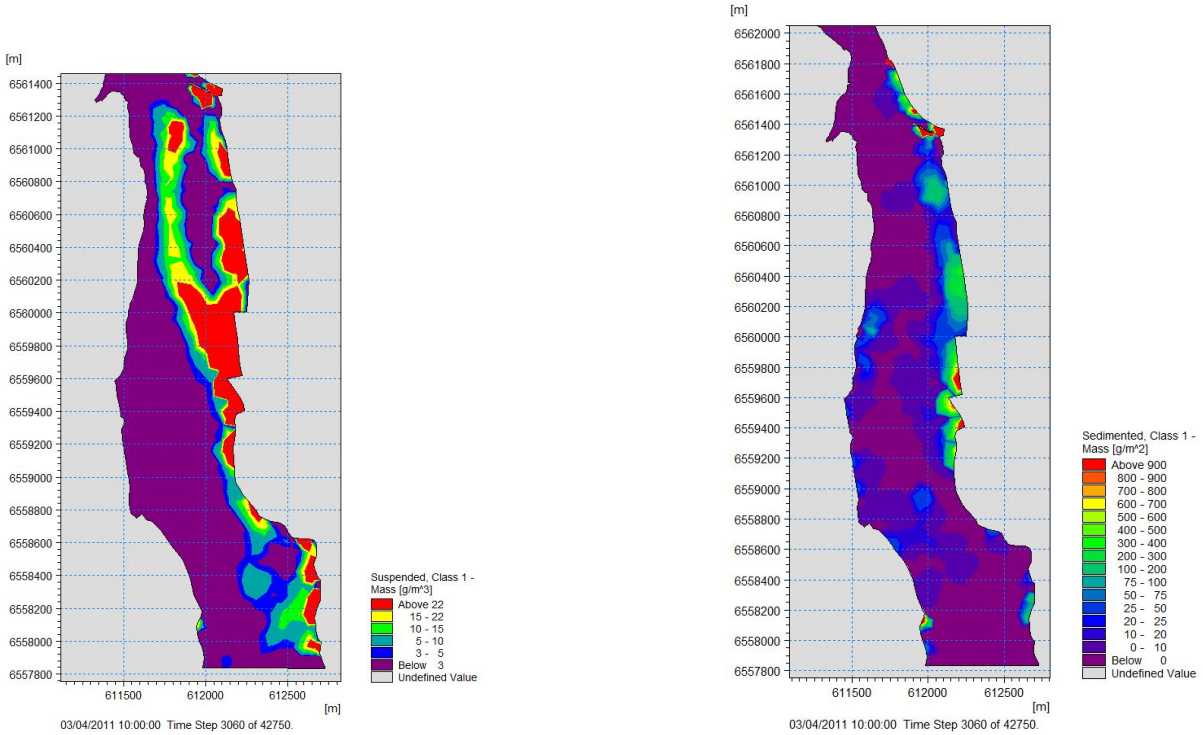

Figure A.7: Concentration of sediments at Borg 1 while dredging with a backhoe ($1g/m^3 = 1ppm$) - MIKE

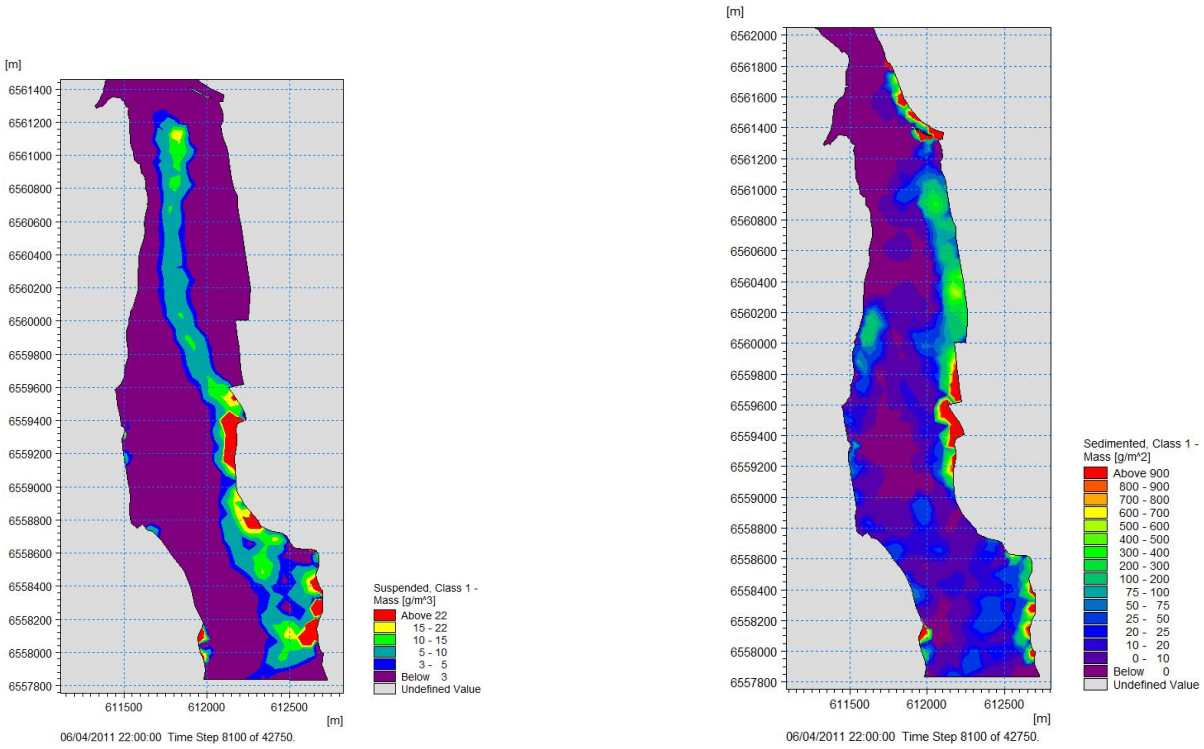

Figure A.8: Concentration of sediments at Borg 1 while dredging with a backhoe ($1g/m^3 = 1ppm$) - MIKE

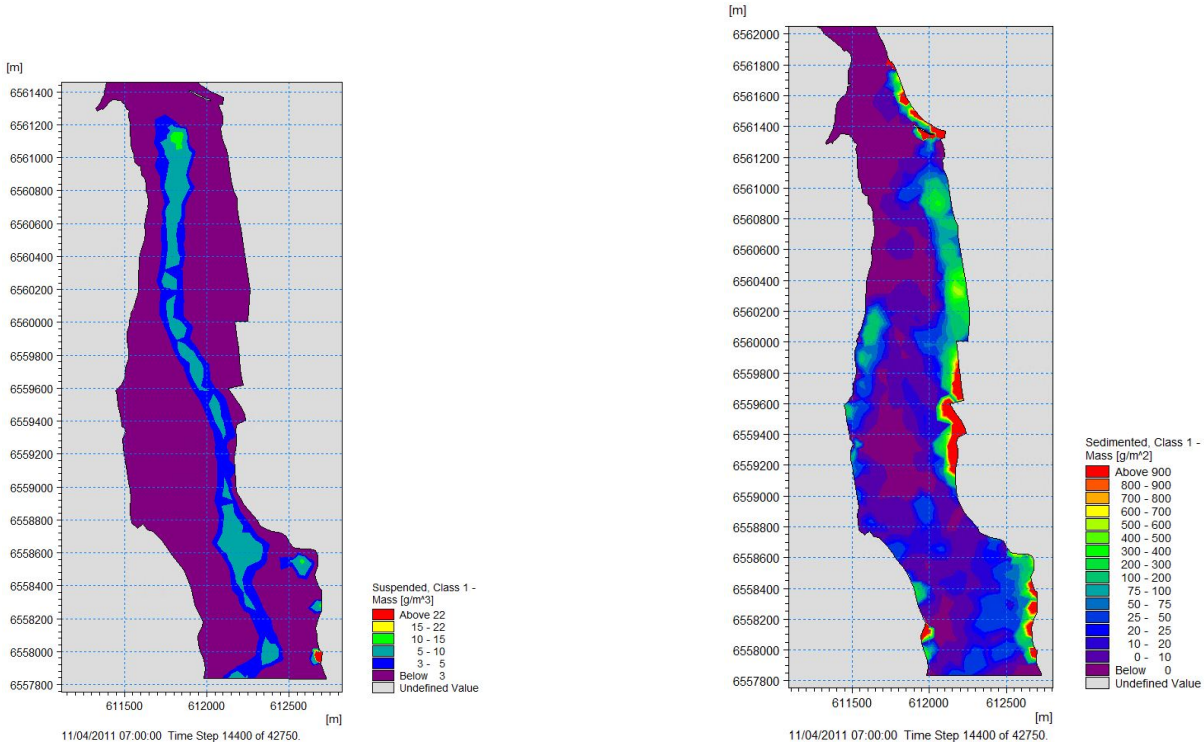

Figure A.9: Concentration of sediments at Borg 1 while dredging with a backhoe ($1g/m^3 = 1ppm$) - MIKE

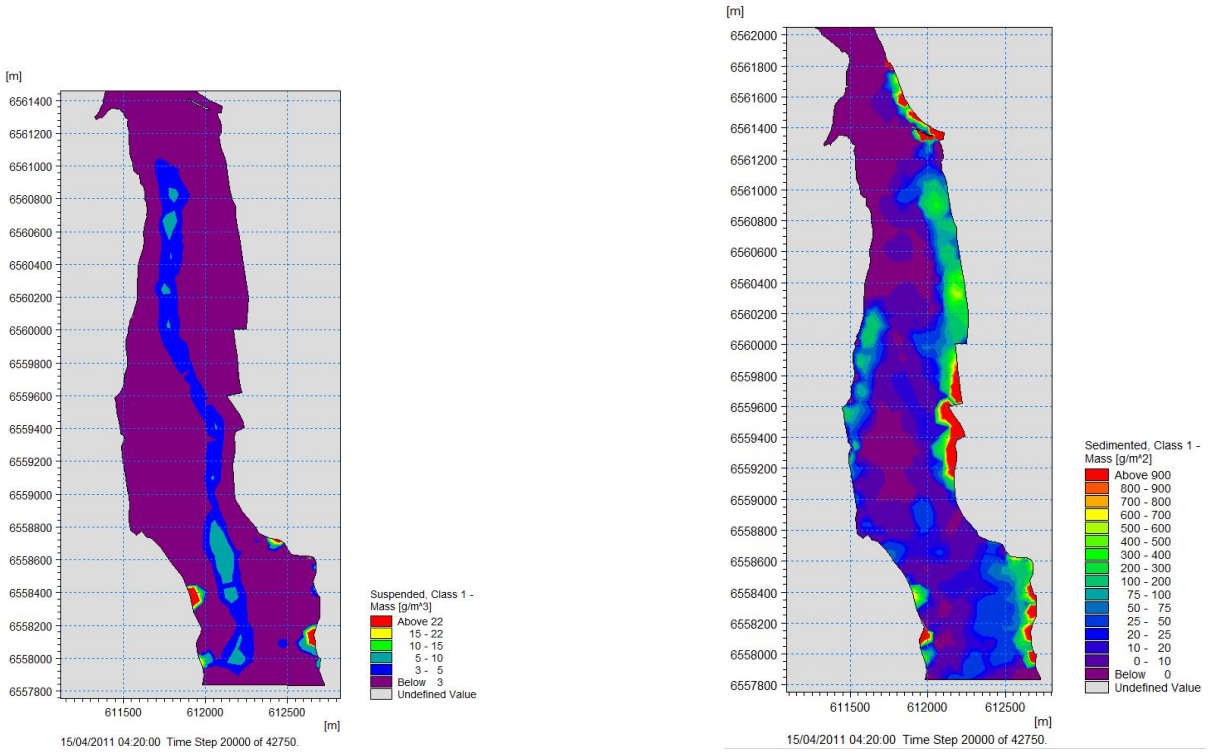

Figure A.10: Concentration of sediments at Borg 1 while dredging with a backhoe ($1g/m^3 = 1ppm$) - MIKE

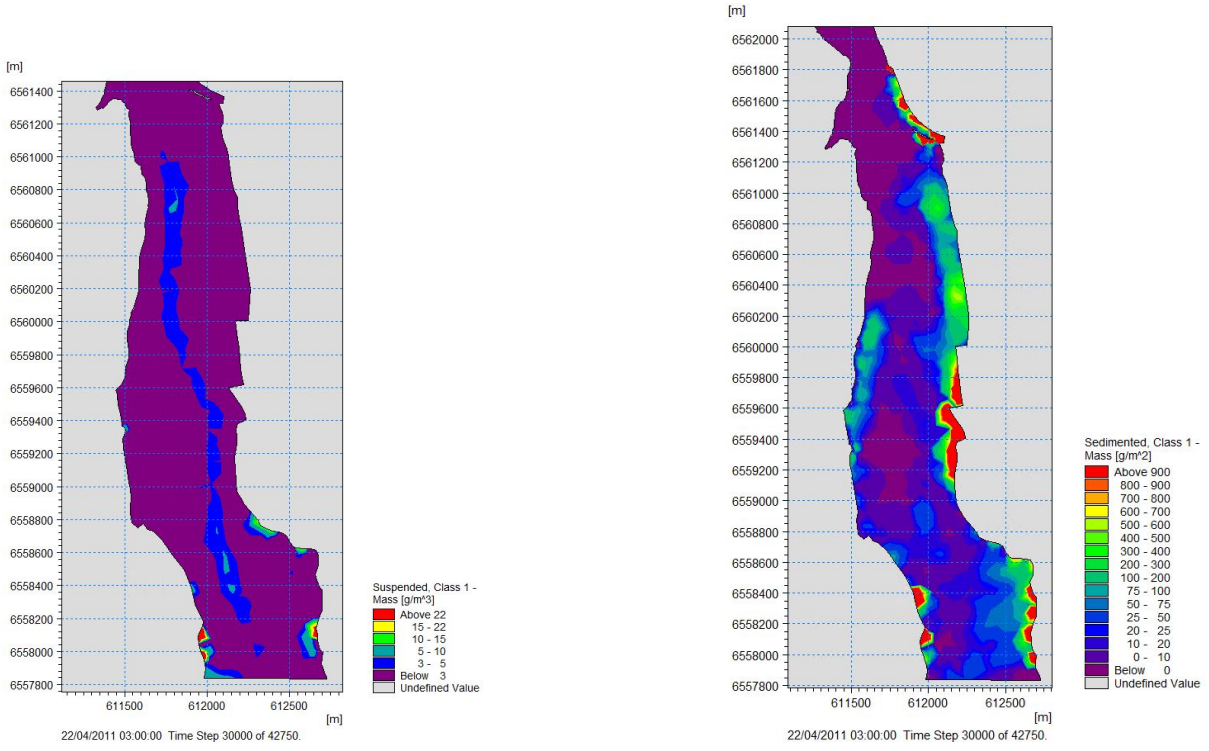

Figure A.11: Concentration of sediments at Borg 1 while dredging with a backhoe ($1g/m^3 = 1ppm$) - MIKE

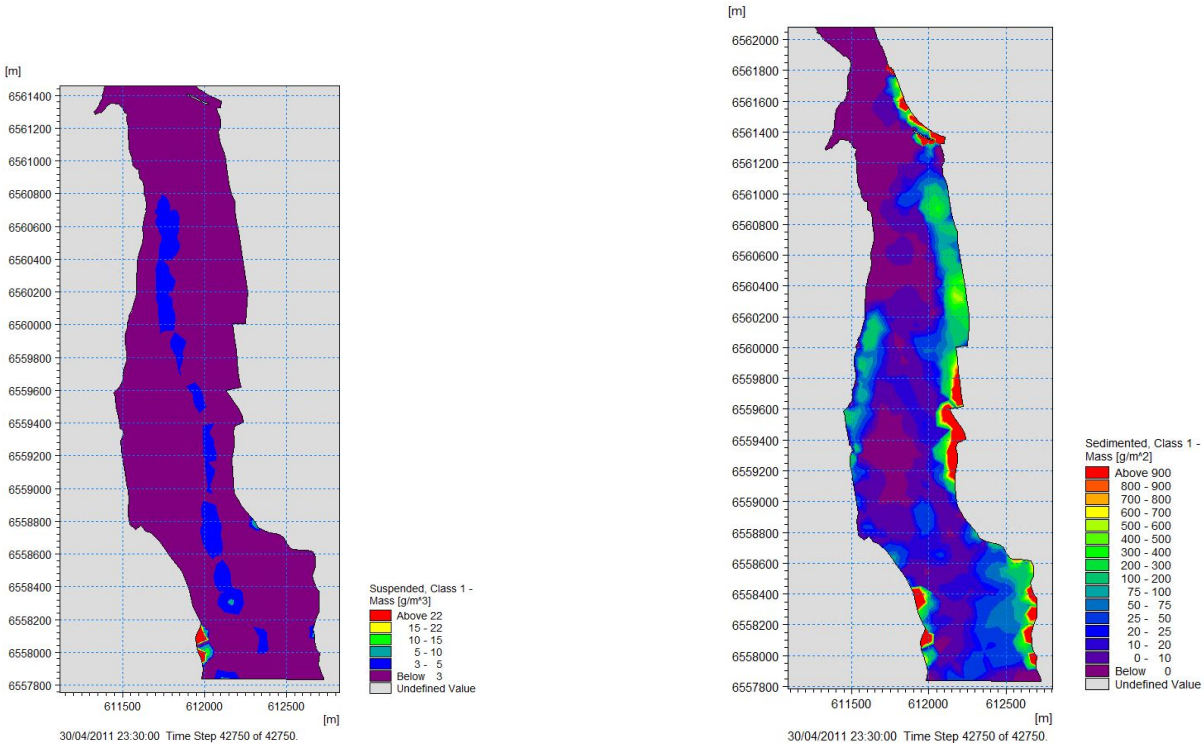

Figure A.12: Concentration of sediments at Borg 1 while dredging with a backhoe ($1g/m^3 = 1ppm$) - MIKE

A.1.3 3rd run - 1.389 kg/s - 0.001 m/s

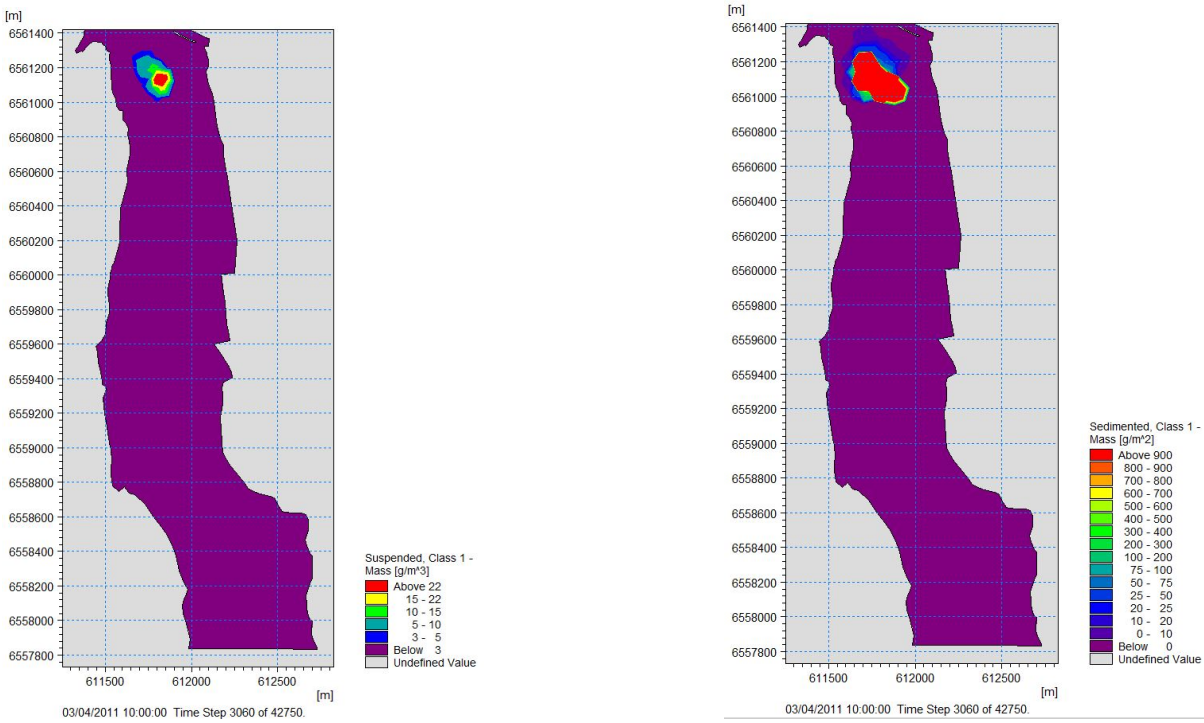

Figure A.13: Concentration of sediments at Borg 1 while dredging with a backhoe ($1g/m^3 = 1ppm$) - MIKE

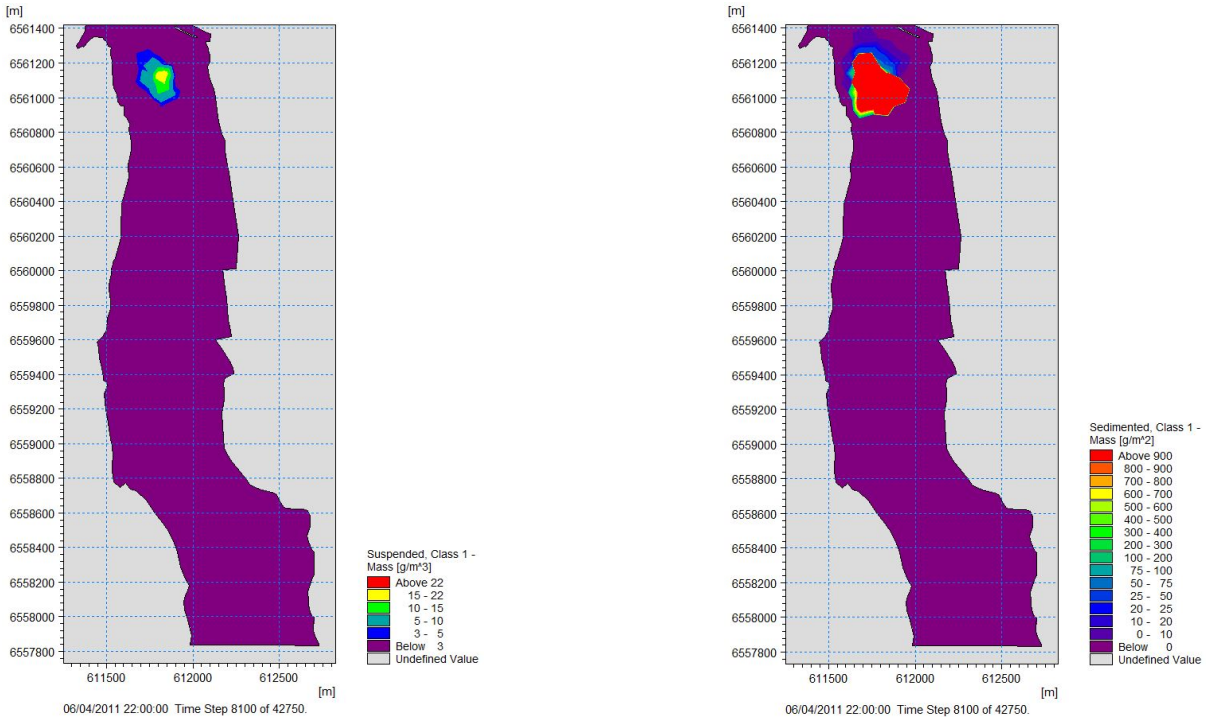

Figure A.14: Concentration of sediments at Borg 1 while dredging with a backhoe ($1g/m^3 = 1ppm$) - MIKE

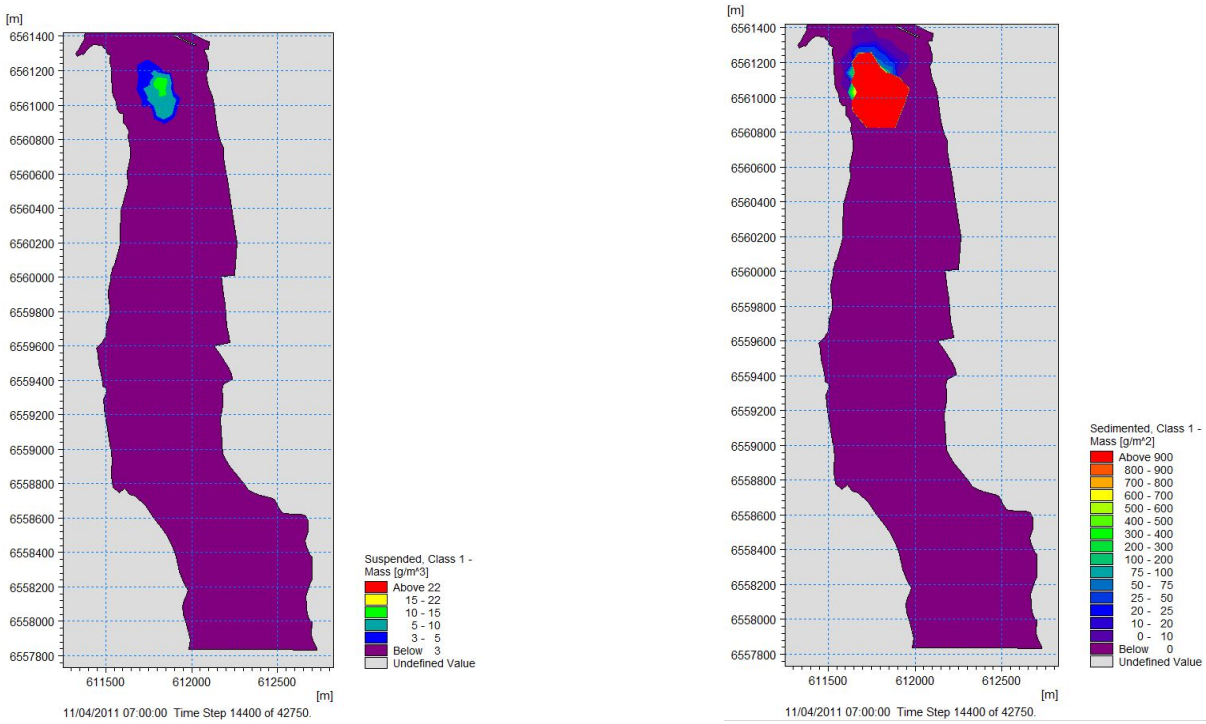

Figure A.15: Concentration of sediments at Borg 1 while dredging with a backhoe ($1g/m^3 = 1ppm$) - MIKE

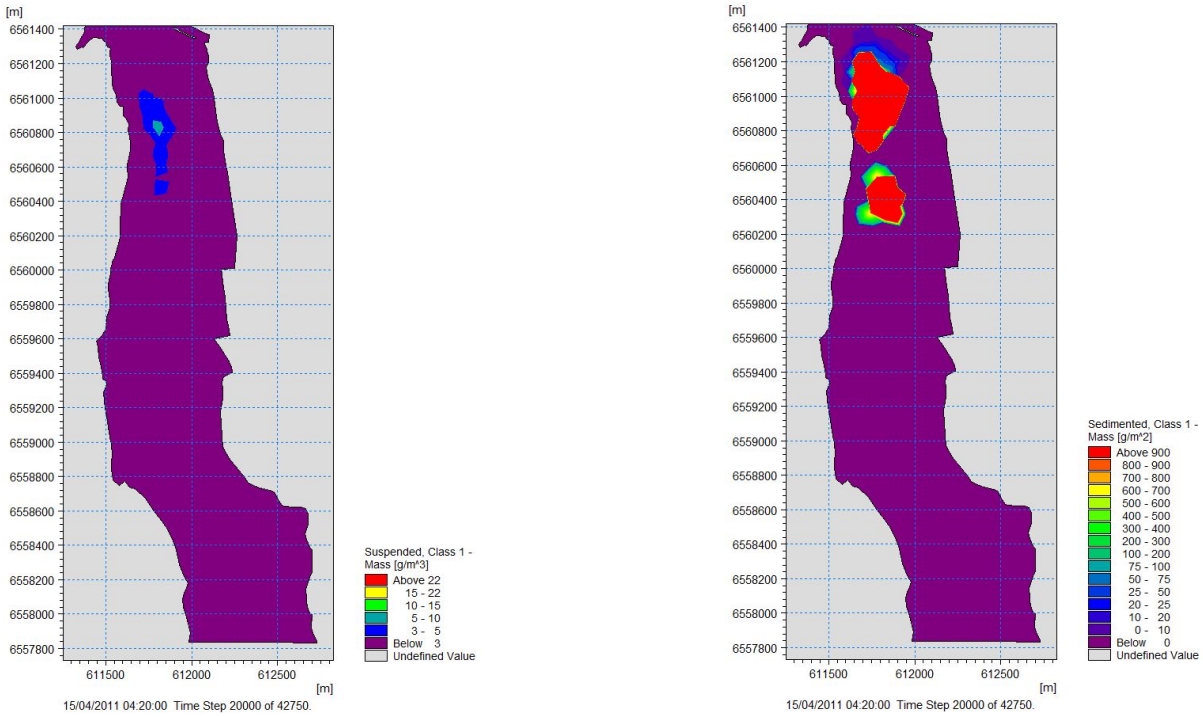

Figure A.16: Concentration of sediments at Borg 1 while dredging with a backhoe ($1g/m^3 = 1ppm$) - MIKE

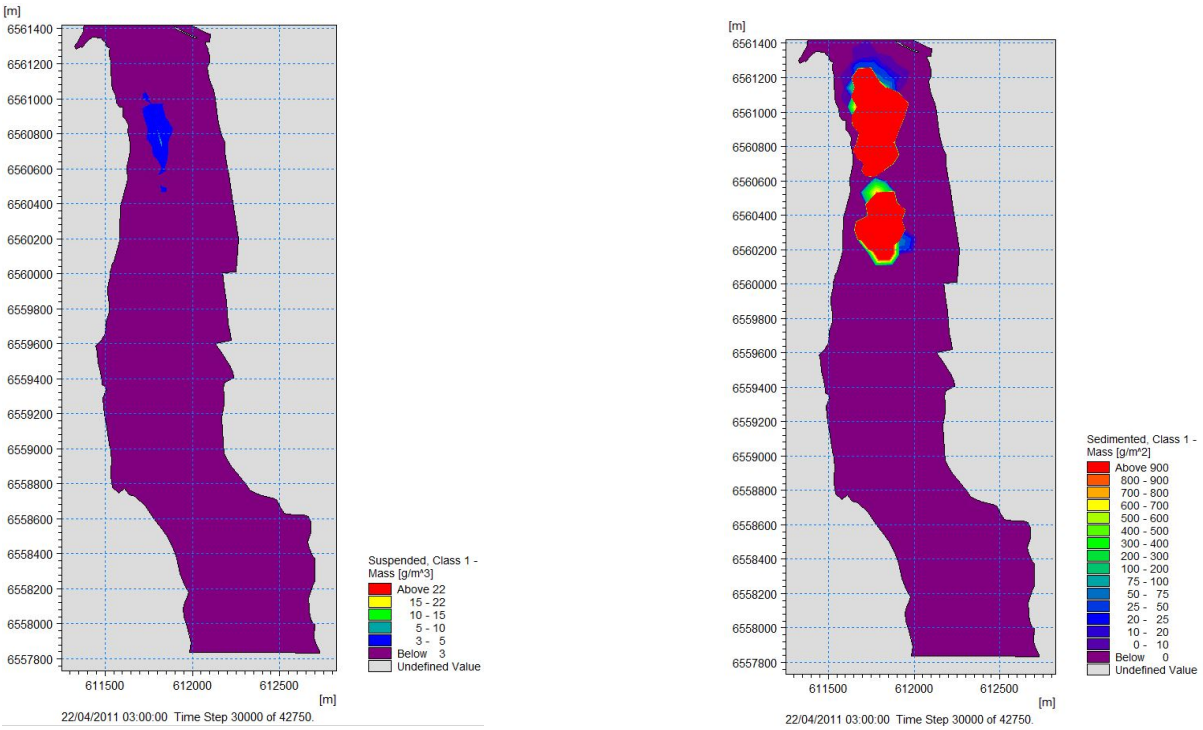

Figure A.17: Concentration of sediments at Borg 1 while dredging with a backhoe ($1g/m^3 = 1ppm$) - MIKE

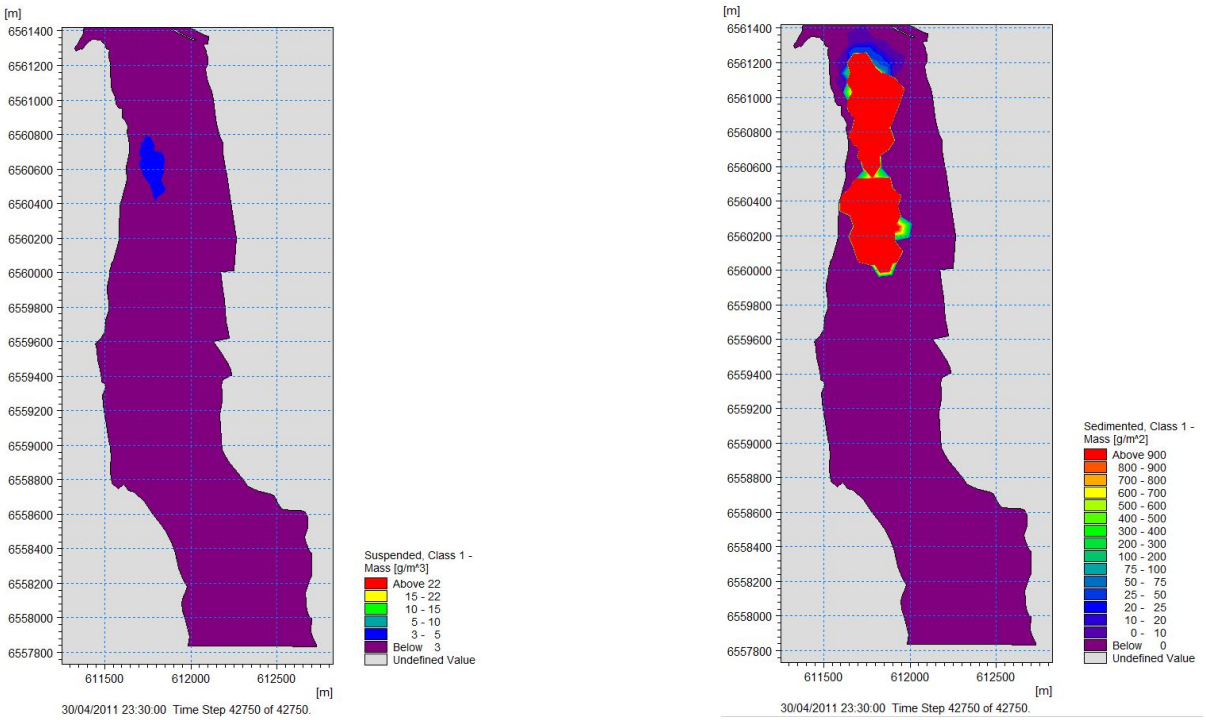

Figure A.18: Concentration of sediments at Borg 1 while dredging with a backhoe ($1g/m^3 = 1ppm$) - MIKE

A.1.4 4th run - 2.778 kg/s - 0.0001 m/s

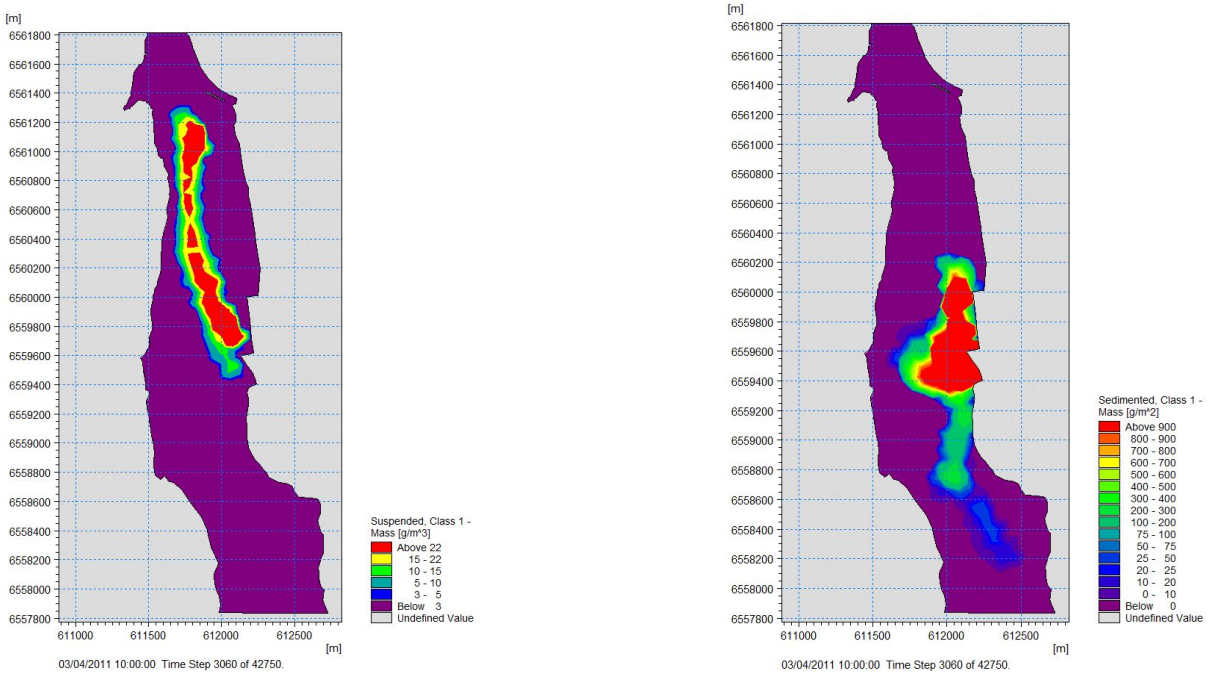

Figure A.19: Concentration of sediments at Borg 1 while dredging with a backhoe ($1g/m^3 = 1ppm$) - MIKE

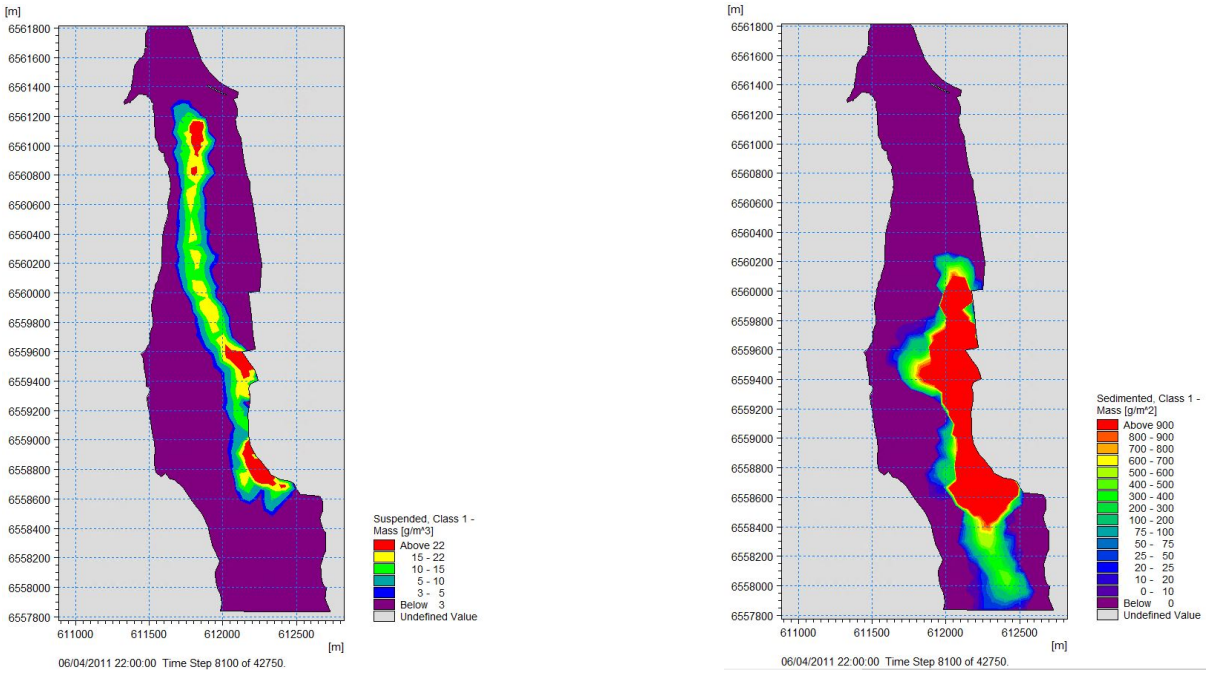

Figure A.20: Concentration of sediments at Borg 1 while dredging with a backhoe ($1g/m^3 = 1ppm$) - MIKE

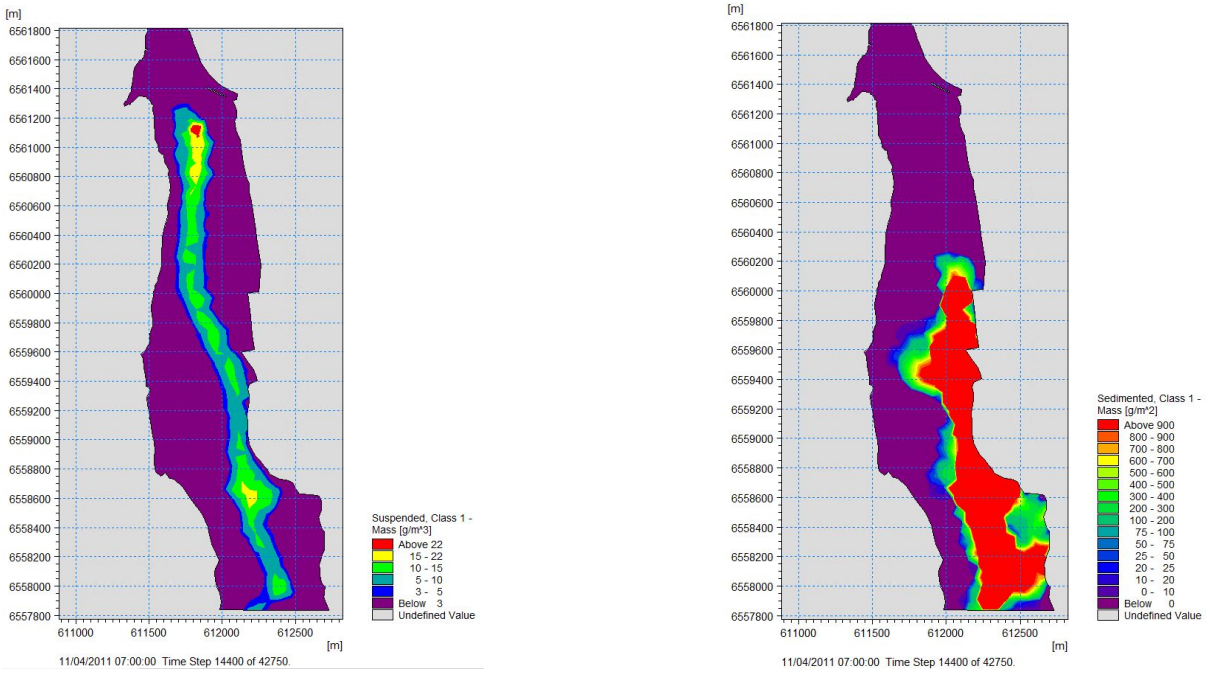

Figure A.21: Concentration of sediments at Borg 1 while dredging with a backhoe ($1g/m^3 = 1ppm$) - MIKE

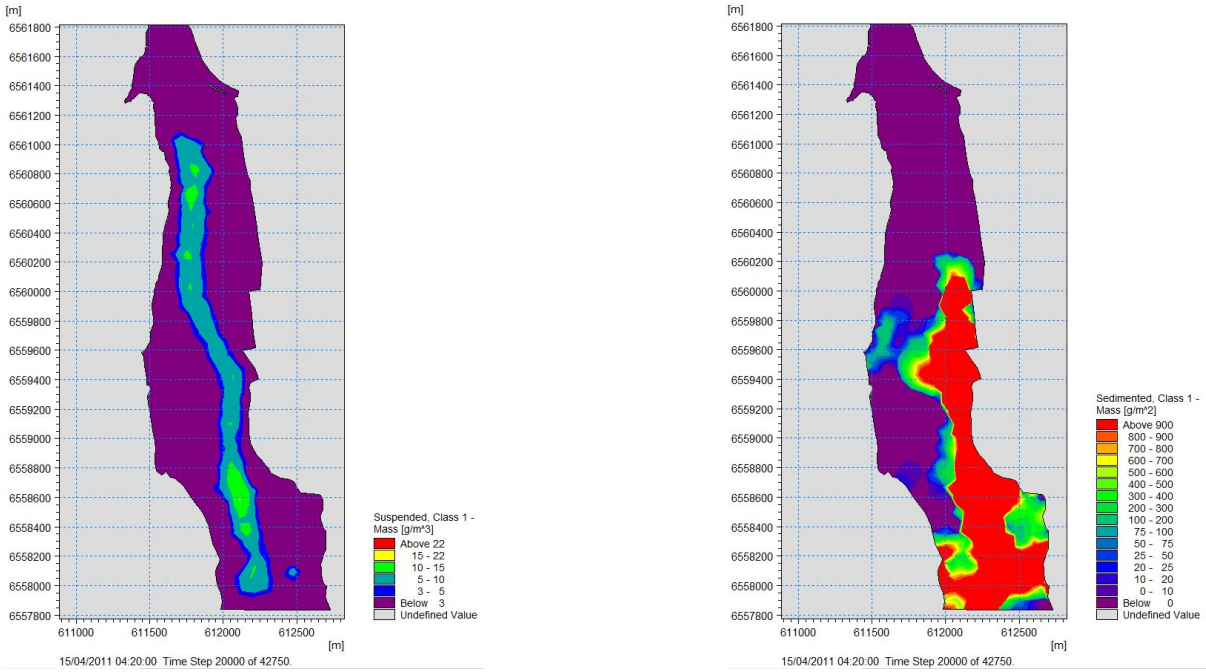

Figure A.22: Concentration of sediments at Borg 1 while dredging with a backhoe ($1g/m^3 = 1ppm$) - MIKE

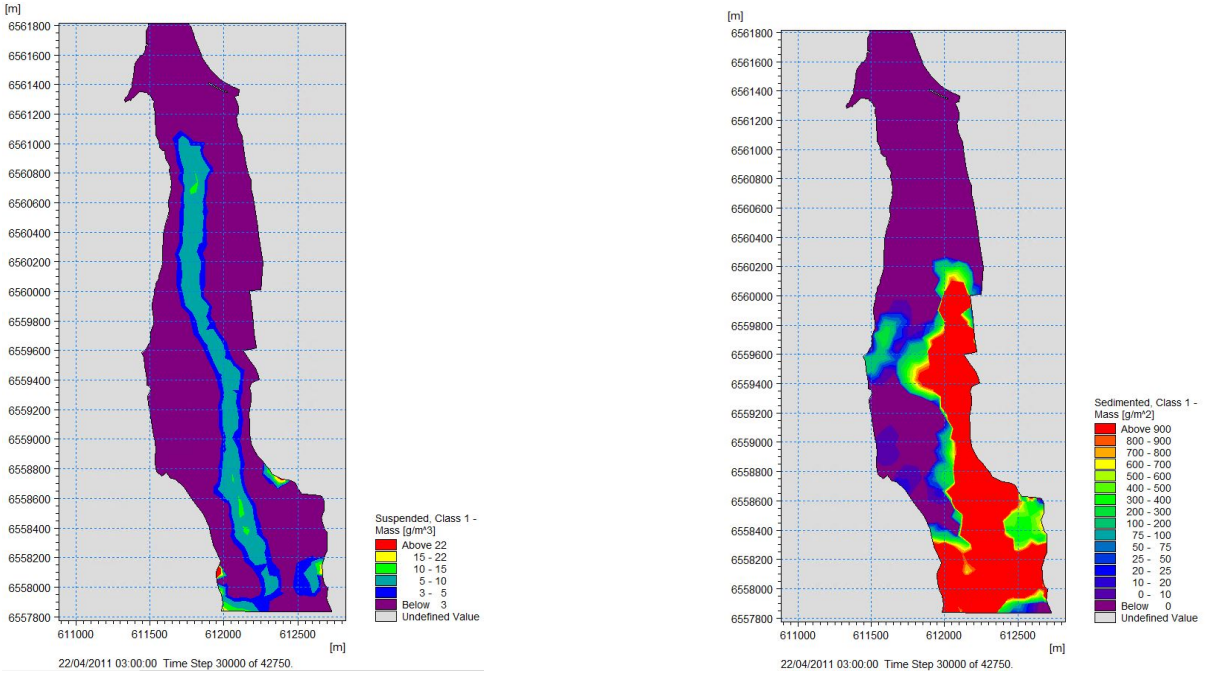

Figure A.23: Concentration of sediments at Borg 1 while dredging with a backhoe ($1g/m^3 = 1ppm$) - MIKE

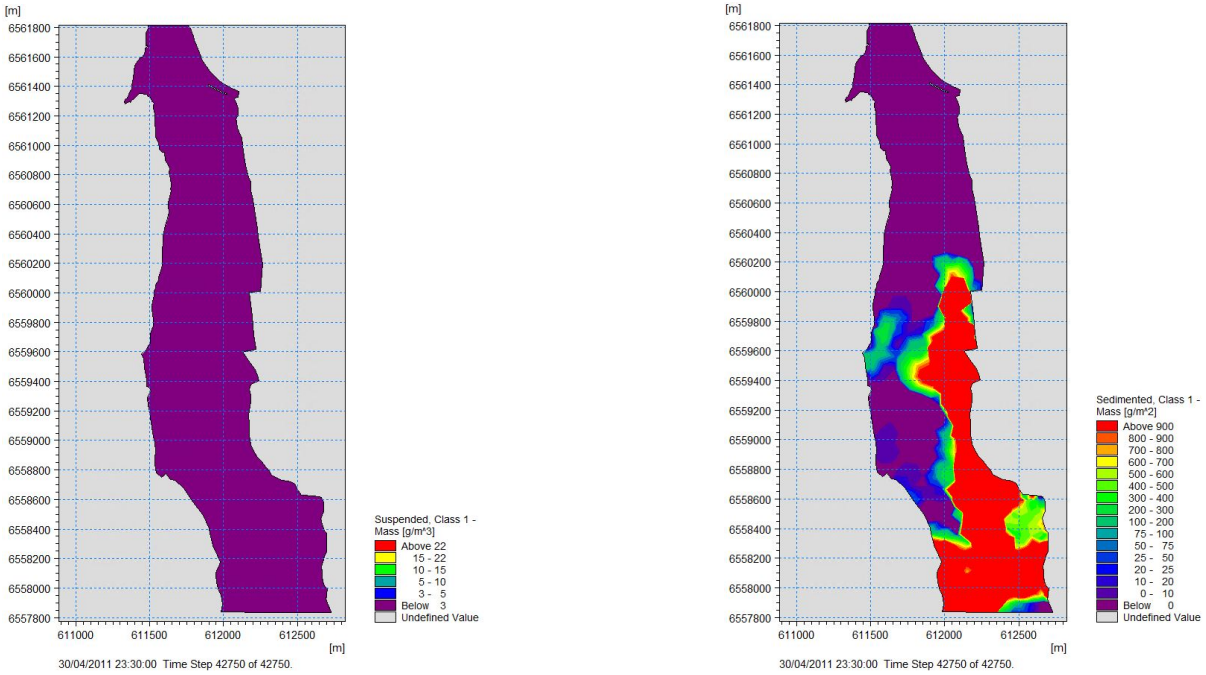

Figure A.24: Concentration of sediments at Borg 1 while dredging with a backhoe ($1g/m^3 = 1ppm$) - MIKE

A.1.5 5th run - 0.695 kg/s - 0.0001 m/s

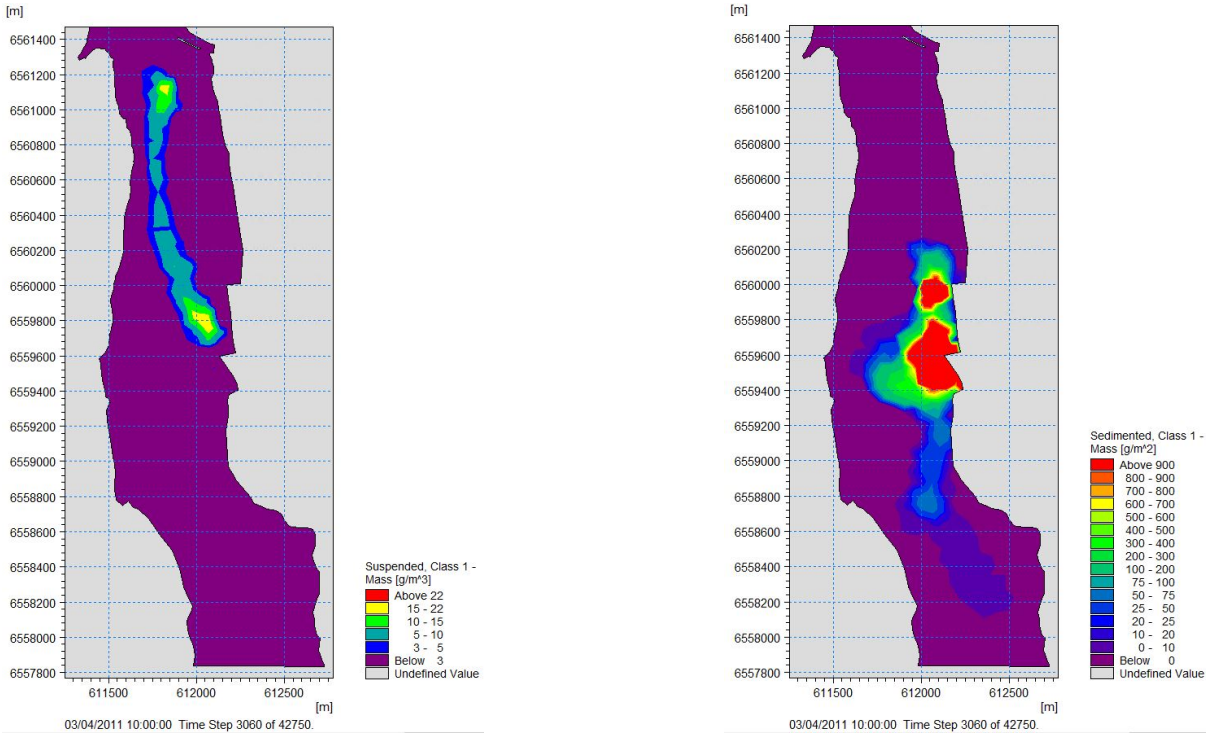

Figure A.25: Concentration of sediments at Borg 1 while dredging with a backhoe ($1g/m^3 = 1ppm$) - MIKE

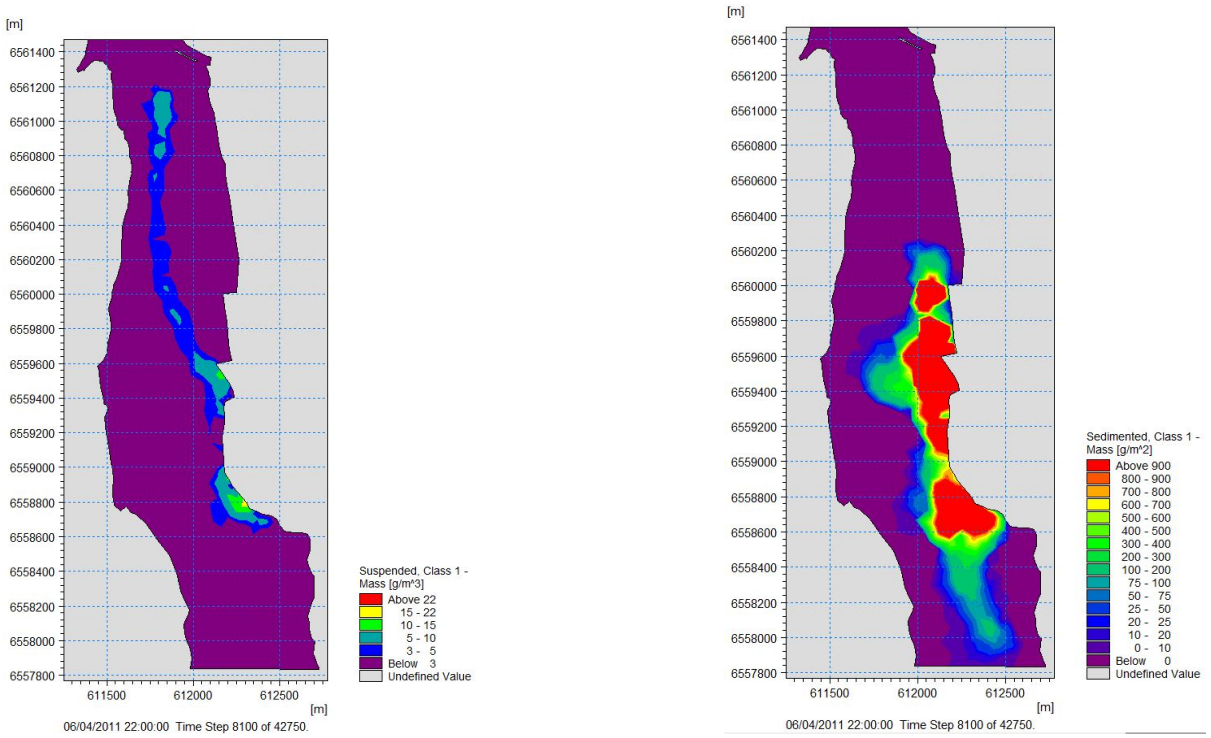

Figure A.26: Concentration of sediments at Borg 1 while dredging with a backhoe ($1g/m^3 = 1ppm$) - MIKE

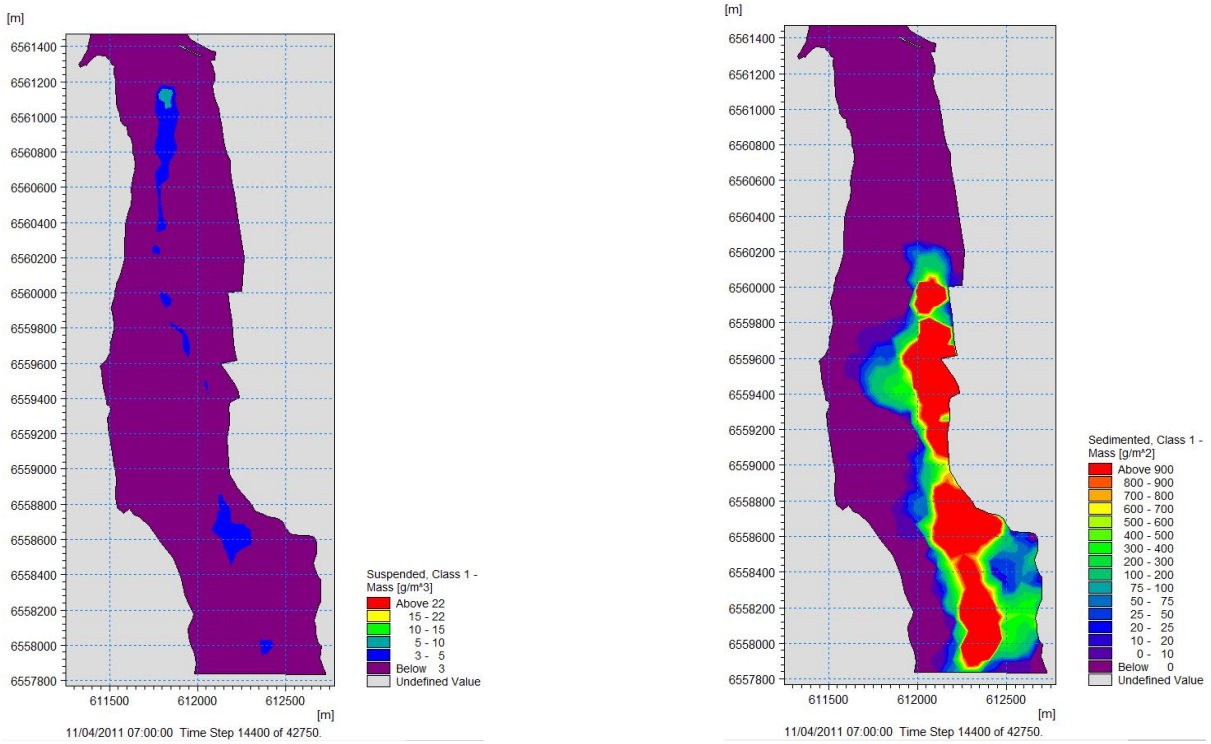

Figure A.27: Concentration of sediments at Borg 1 while dredging with a backhoe ($1g/m^3 = 1ppm$) - MIKE

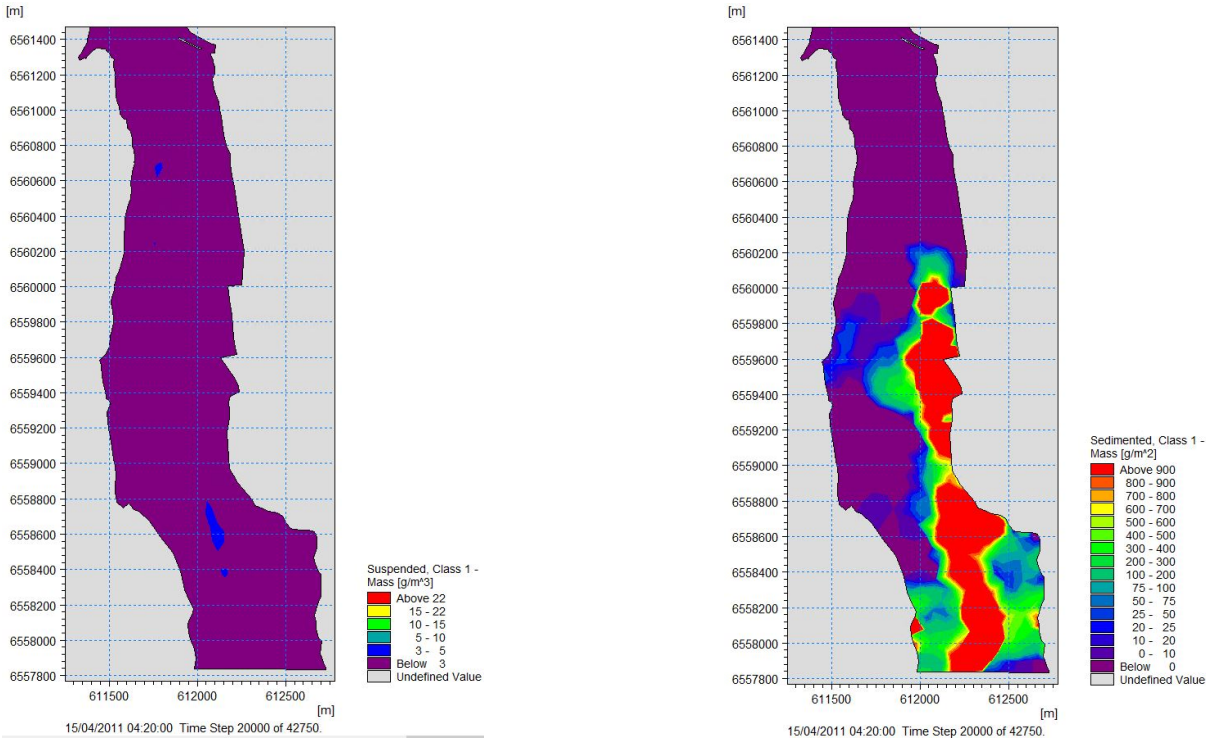

Figure A.28: Concentration of sediments at Borg 1 while dredging with a backhoe ($1g/m^3 = 1ppm$) - MIKE

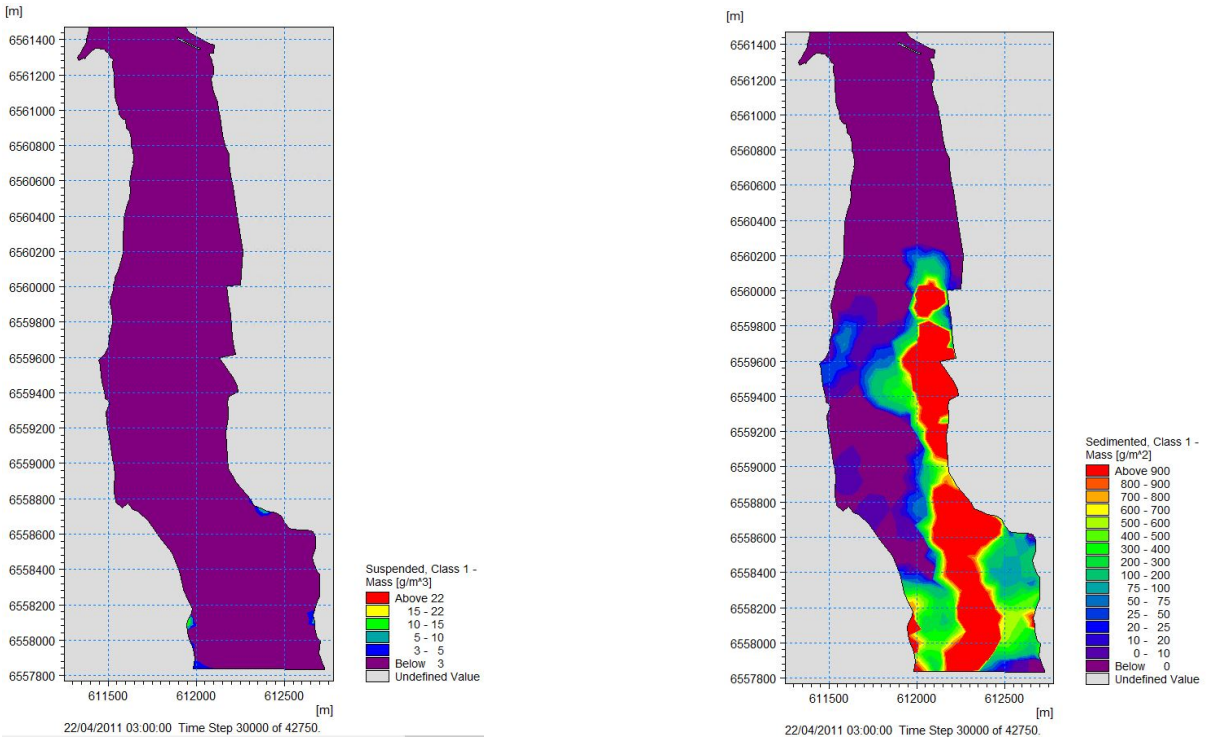

Figure A.29: Concentration of sediments at Borg 1 while dredging with a backhoe ($1g/m^3 = 1ppm$) - MIKE

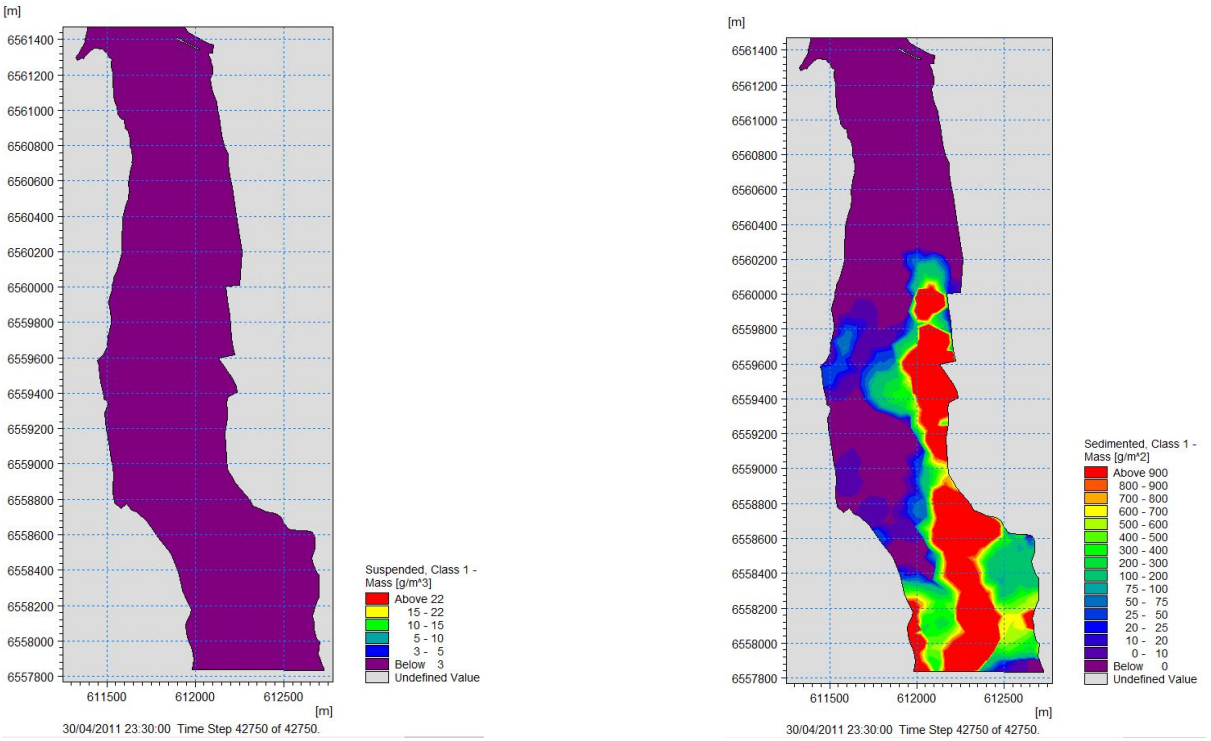

Figure A.30: Concentration of sediments at Borg 1 while dredging with a backhoe ($1 g/m^3 = 1 ppm$) - MIKE

Appendix B

Results - Scenario 2 (May 1966)

B.1 Scenario 2 - May 1966

Results from running the model for a month.

B.1.1 1st run - 1.389 kg/s - 0.0001 m/s

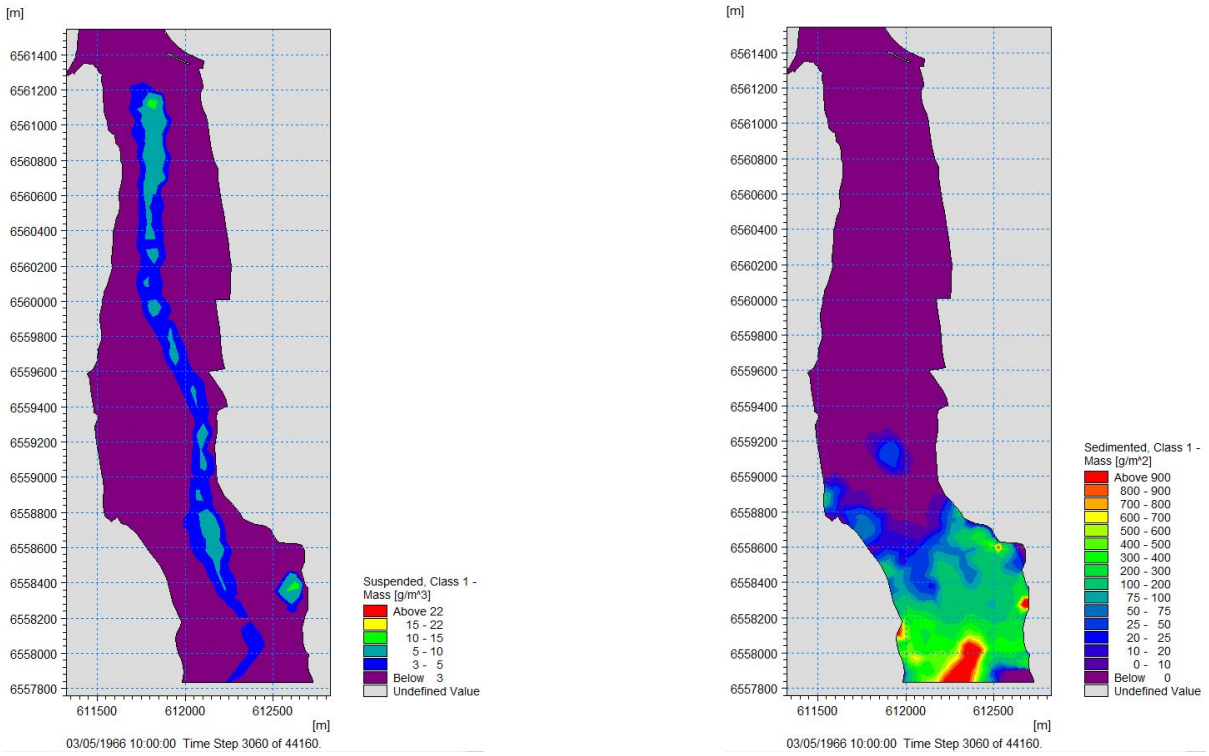

Figure B.1: Concentration of sediments at Borg 1 while dredging with a backhoe ($1g/m^3 = 1ppm$) - MIKE

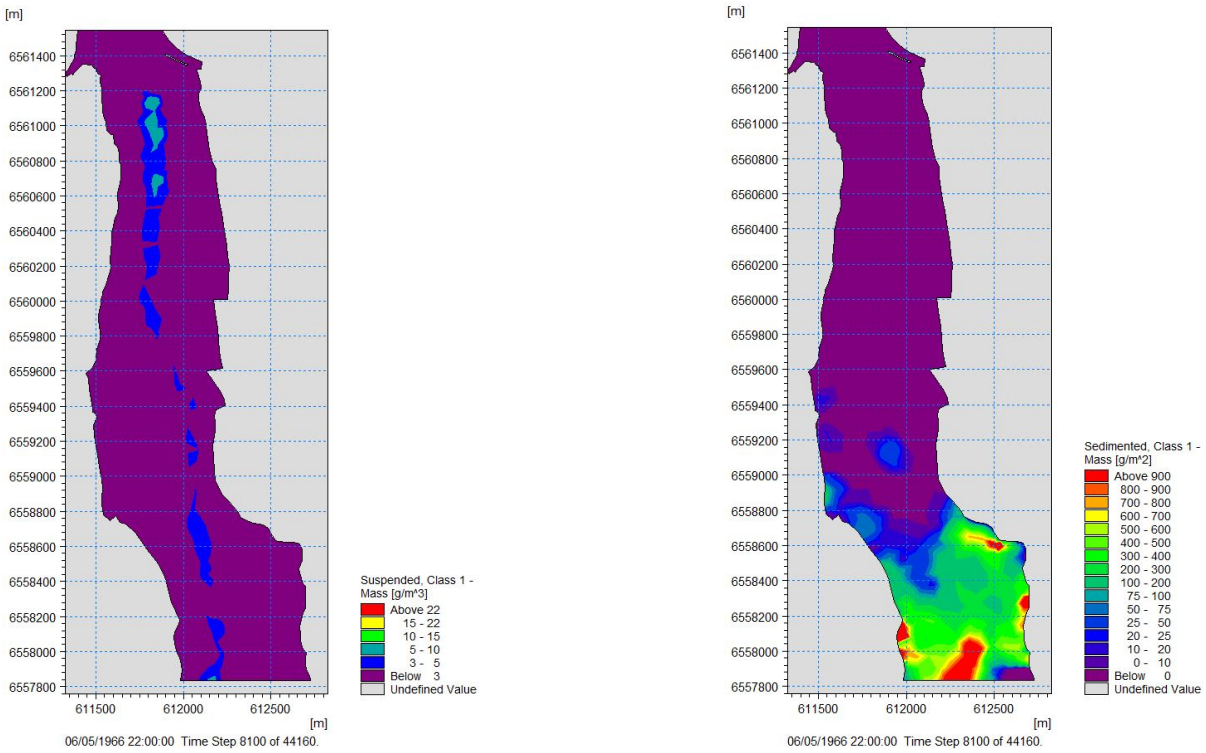

Figure B.2: Concentration of sediments at Borg 1 while dredging with a backhoe ($1g/m^3 = 1ppm$) - MIKE

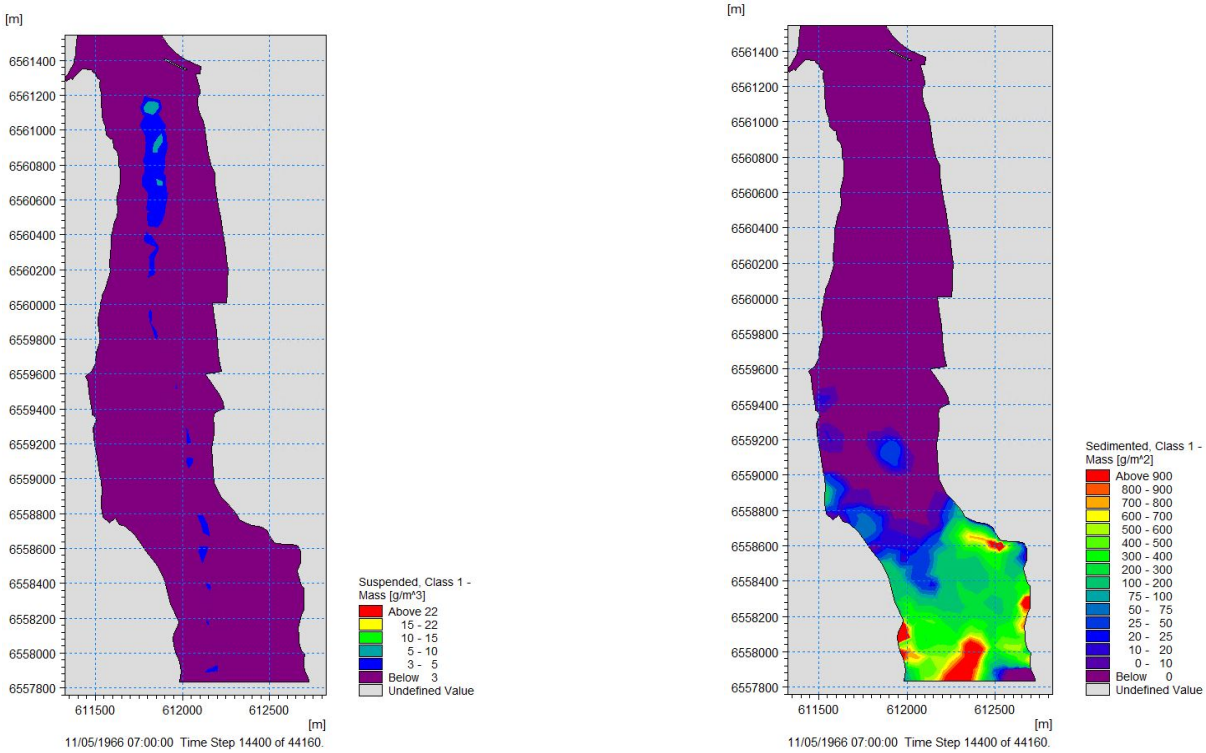

Figure B.3: Concentration of sediments at Borg 1 while dredging with a backhoe ($1g/m^3 = 1ppm$) - MIKE

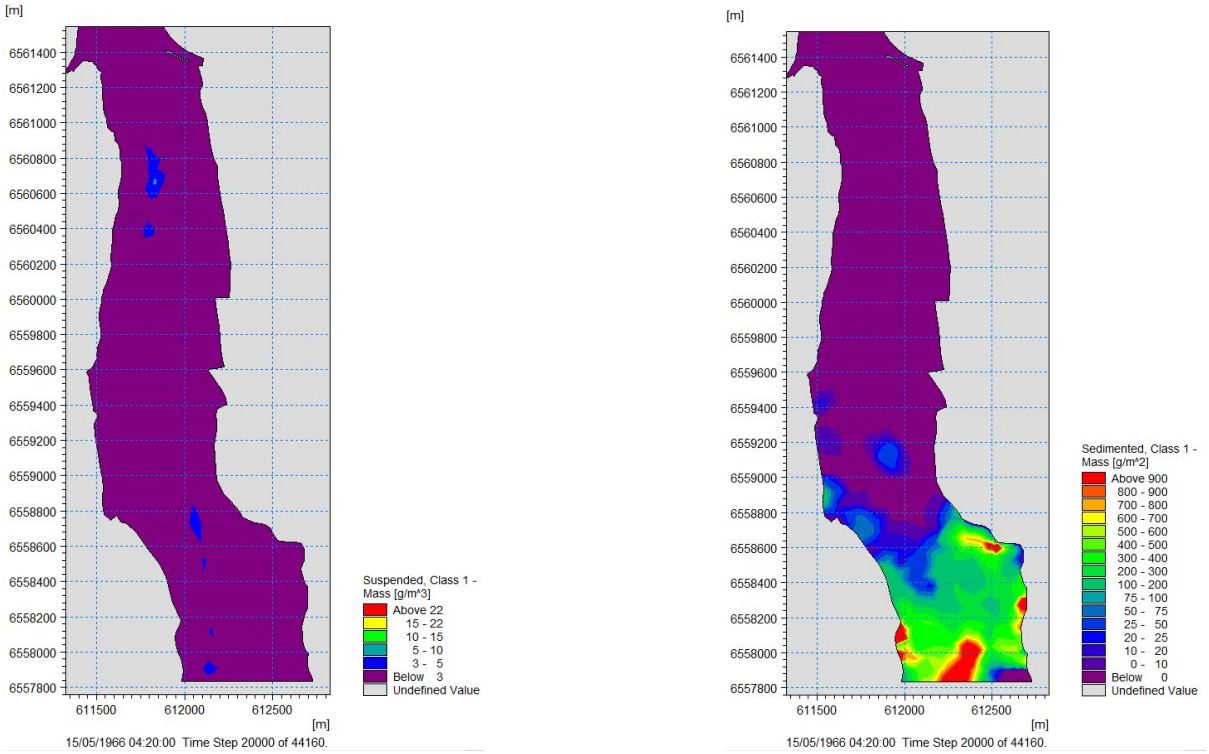

Figure B.4: Concentration of sediments at Borg 1 while dredging with a backhoe ($1g/m^3 = 1ppm$) - MIKE

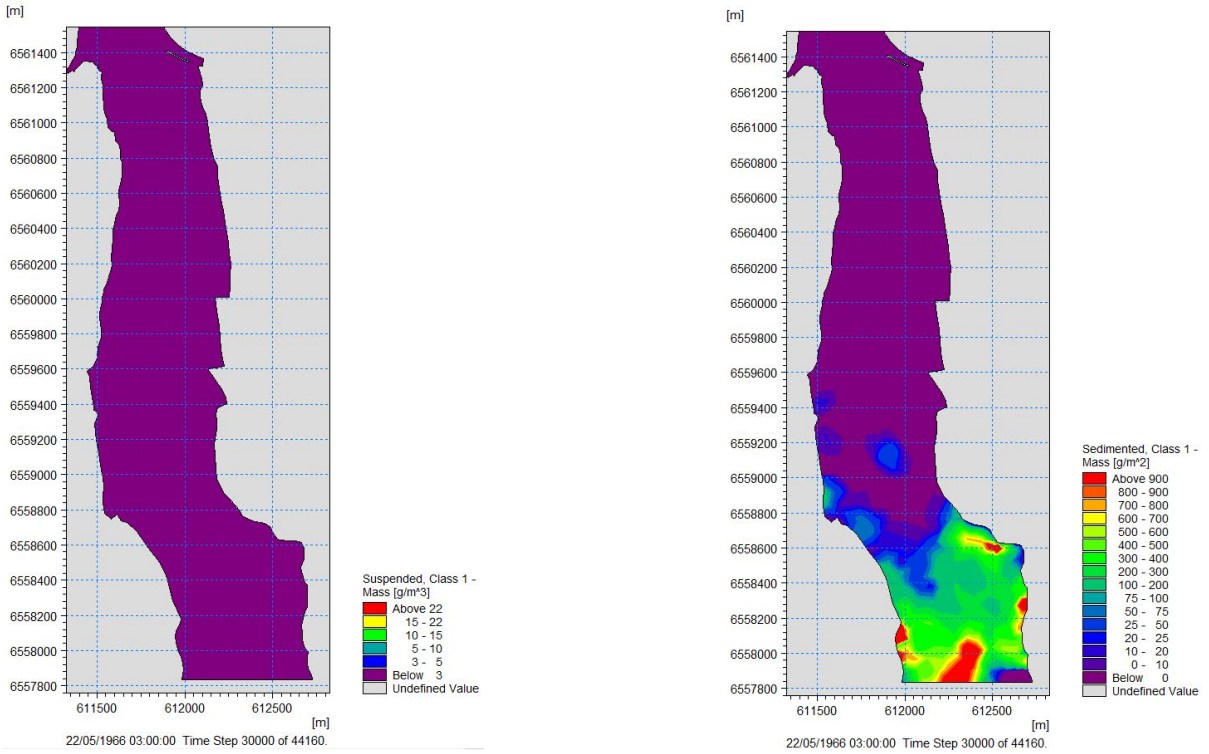

Figure B.5: Concentration of sediments at Borg 1 while dredging with a backhoe ($1g/m^3 = 1ppm$) - MIKE

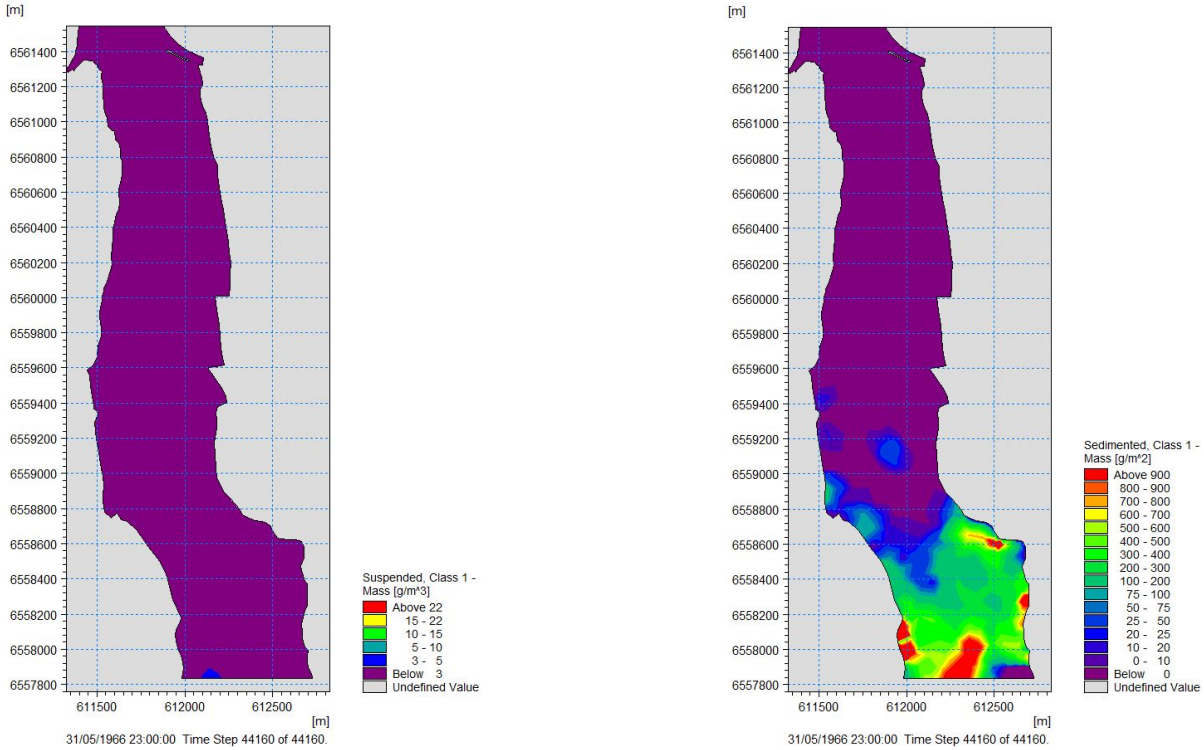

Figure B.6: Concentration of sediments at Borg 1 while dredging with a backhoe ($1g/m^3 = 1ppm$) - MIKE

B.1.2 2nd run - 1.389 kg/s - 0.00001 m/s

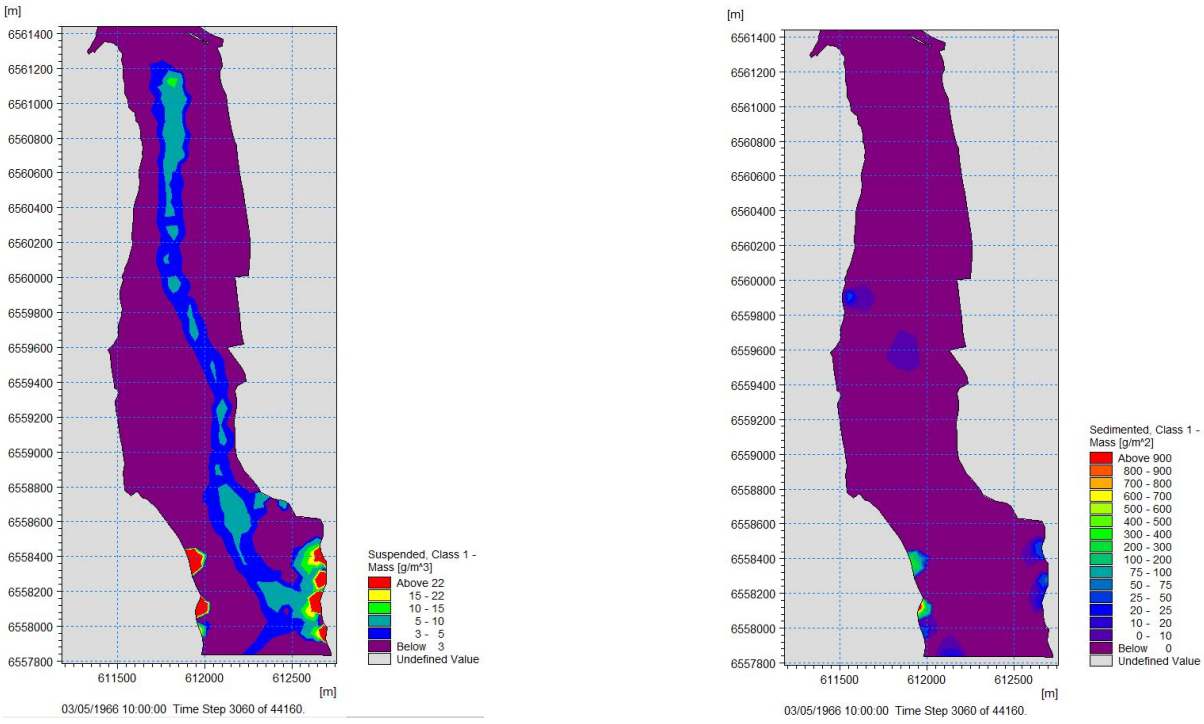

Figure B.7: Concentration of sediments at Borg 1 while dredging with a backhoe ($1g/m^3 = 1ppm$) - MIKE

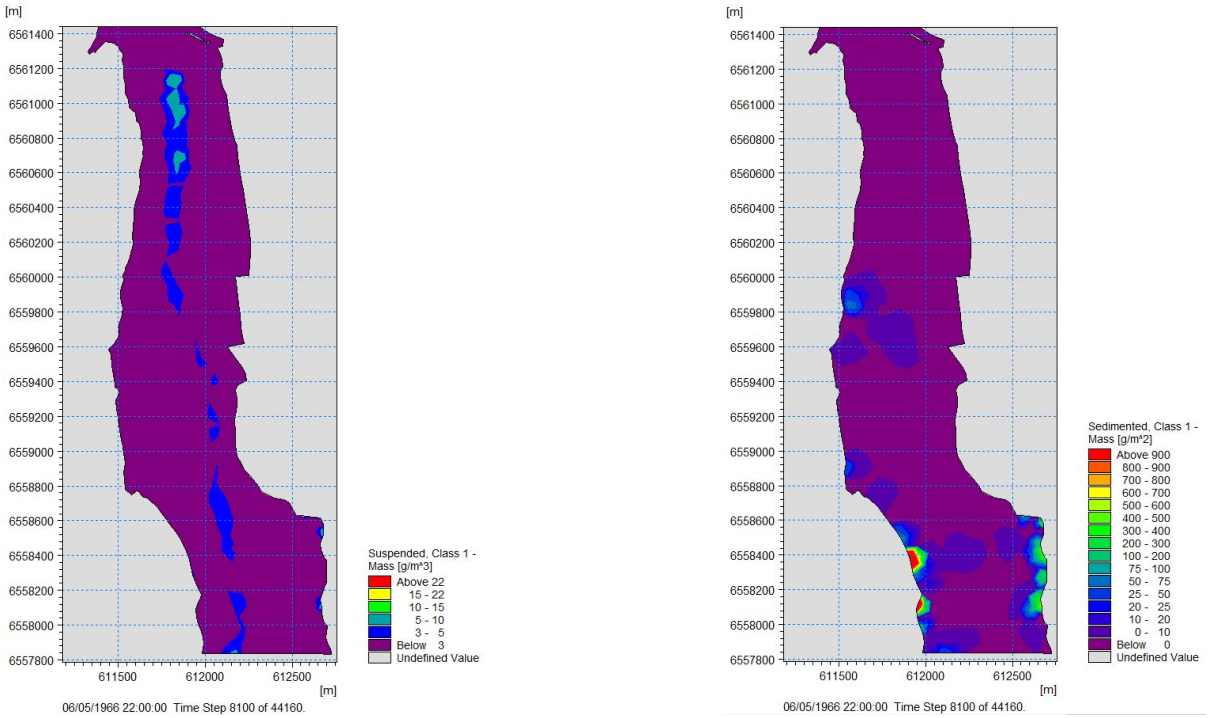

Figure B.8: Concentration of sediments at Borg 1 while dredging with a backhoe ($1g/m^3 = 1ppm$) - MIKE

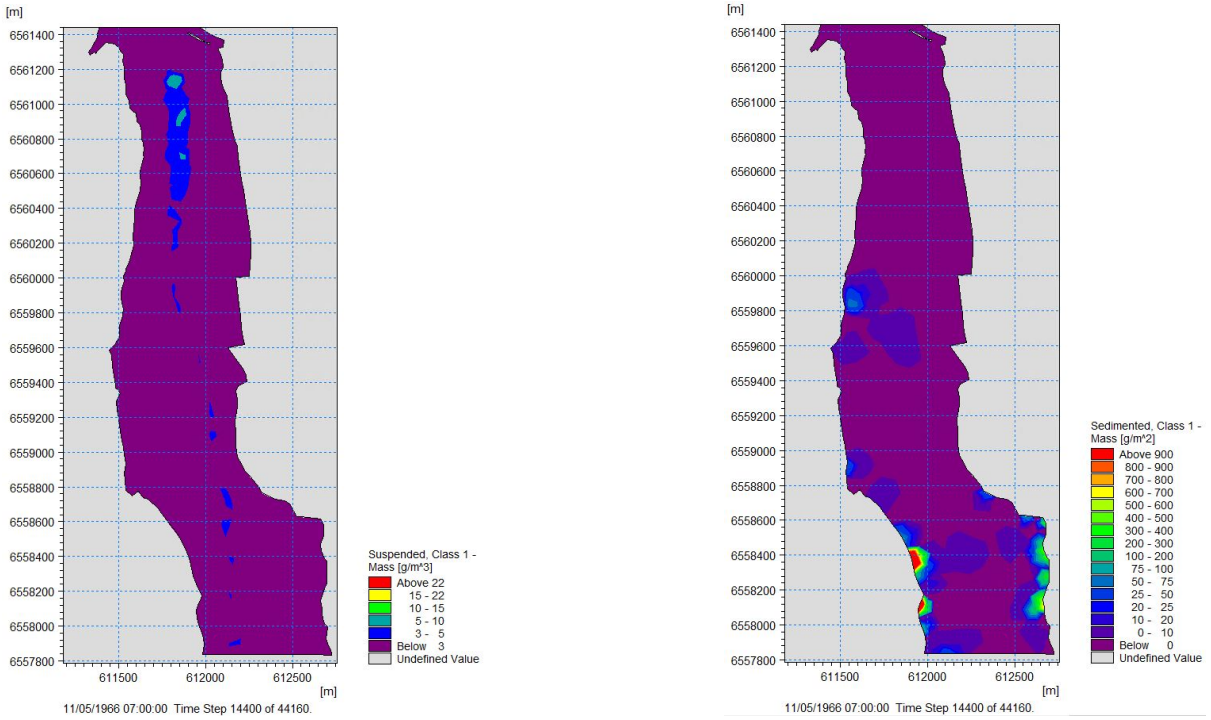

Figure B.9: Concentration of sediments at Borg 1 while dredging with a backhoe ($1g/m^3 = 1ppm$) - MIKE

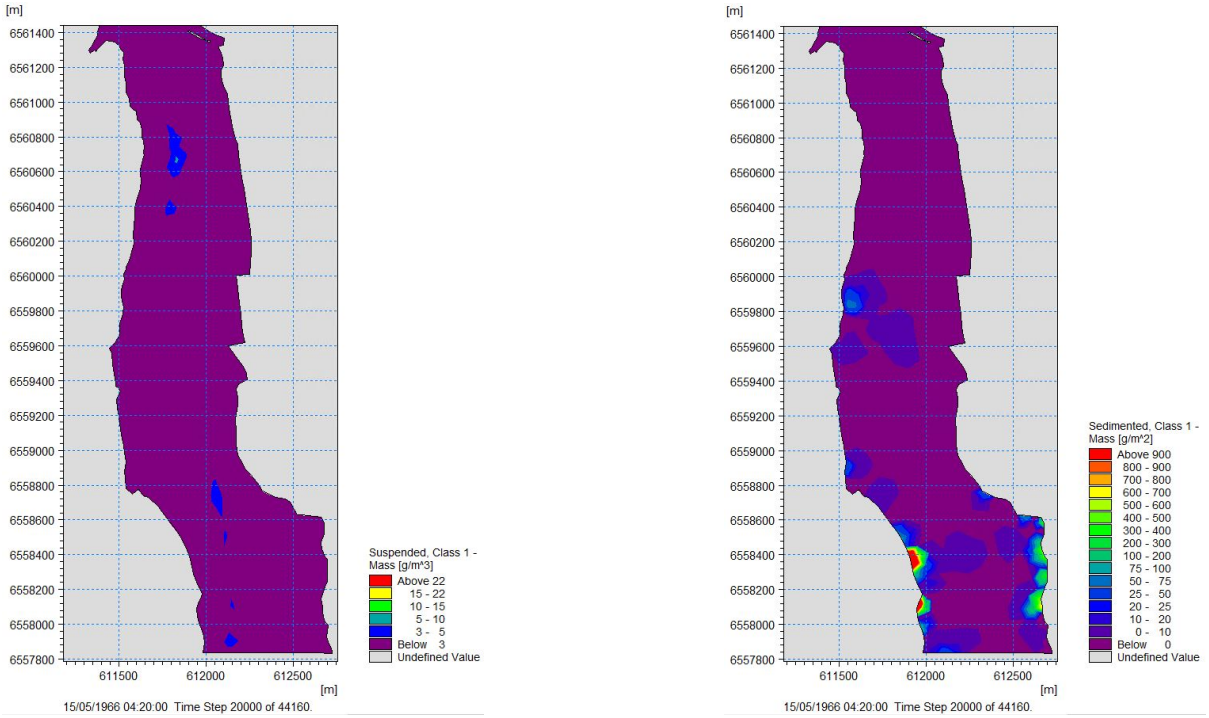

Figure B.10: Concentration of sediments at Borg 1 while dredging with a backhoe ($1g/m^3 = 1ppm$) - MIKE

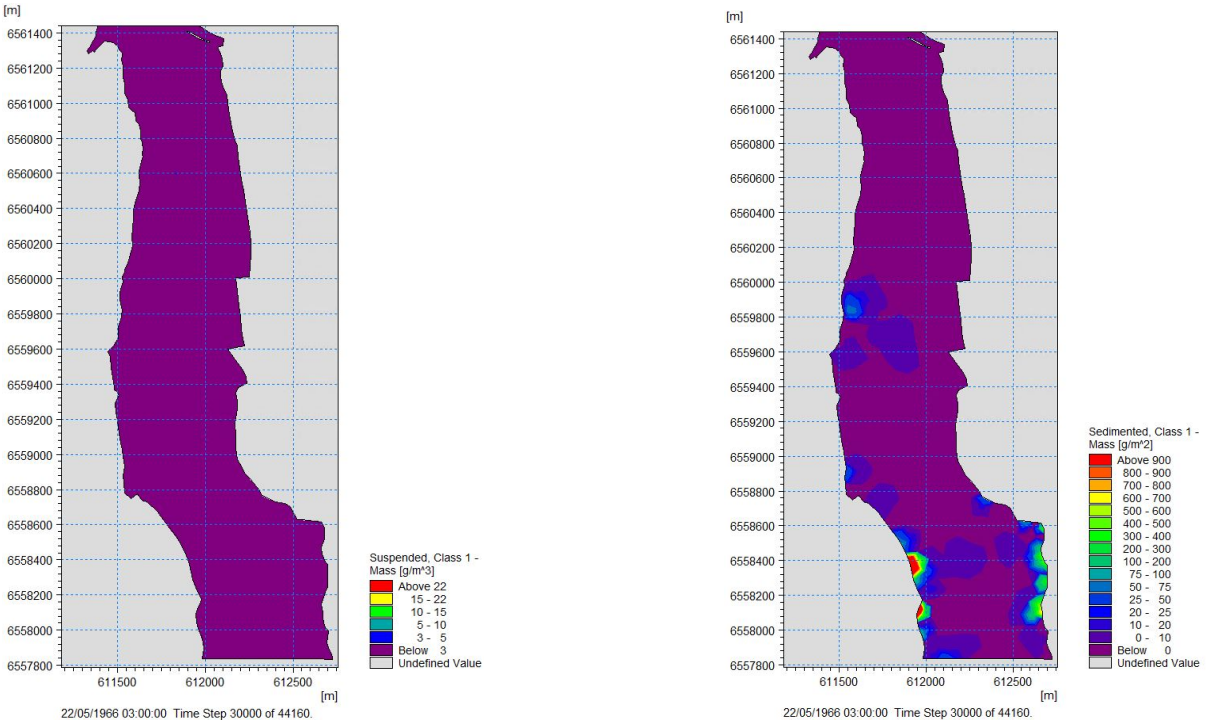

Figure B.11: Concentration of sediments at Borg 1 while dredging with a backhoe ($1g/m^3 = 1ppm$) - MIKE

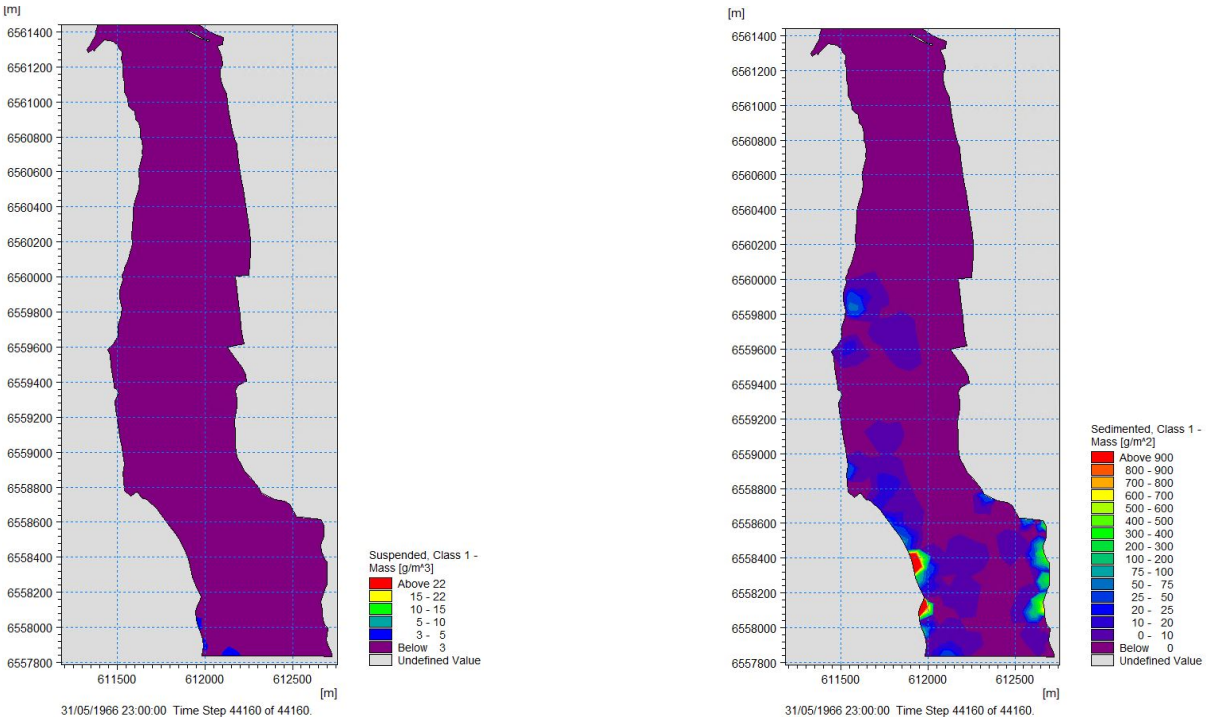

Figure B.12: Concentration of sediments at Borg 1 while dredging with a backhoe ($1g/m^3 = 1ppm$) - MIKE

B.1.3 3rd run - 1.389 kg/s - 0.001 m/s

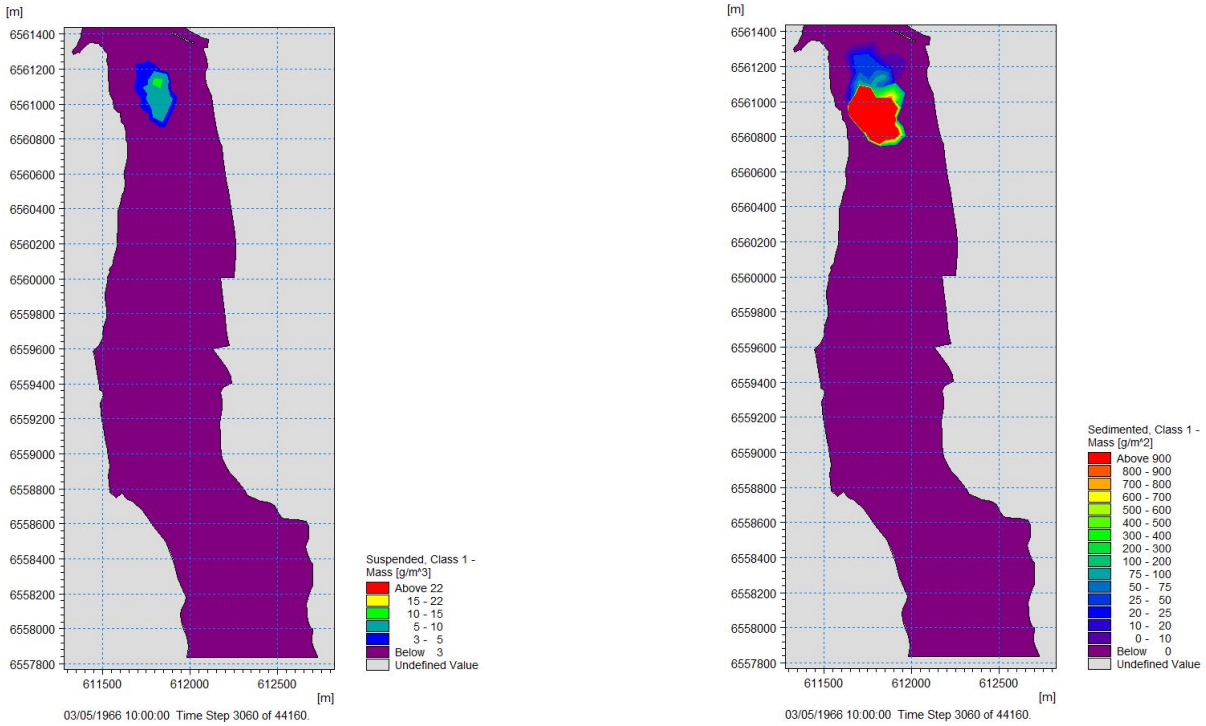

Figure B.13: Concentration of sediments at Borg 1 while dredging with a backhoe ($1g/m^3 = 1ppm$) - MIKE

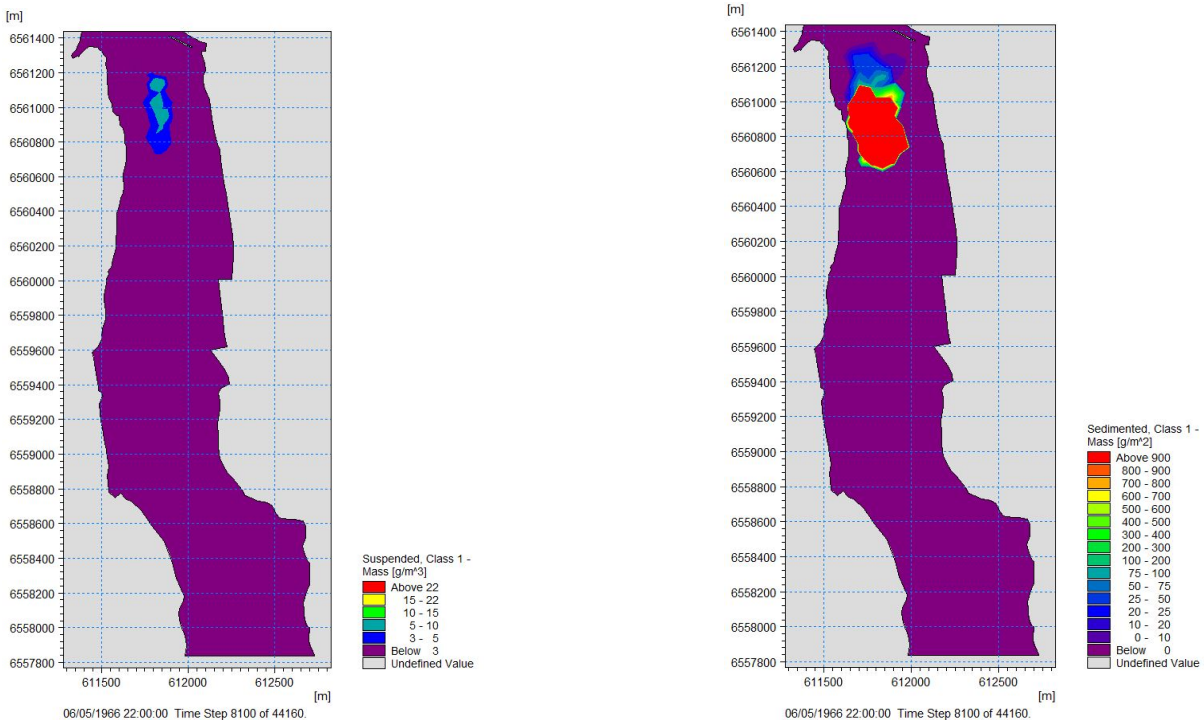

Figure B.14: Concentration of sediments at Borg 1 while dredging with a backhoe ($1g/m^3 = 1ppm$) - MIKE

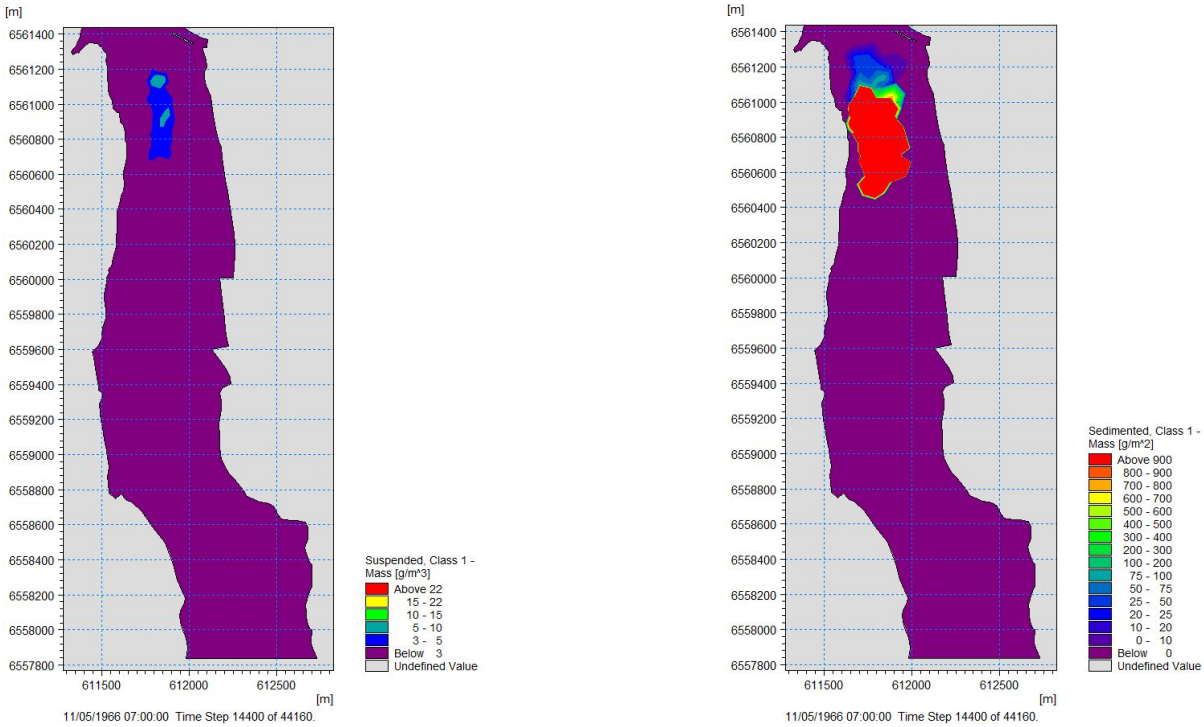

Figure B.15: Concentration of sediments at Borg 1 while dredging with a backhoe ($1g/m^3 = 1ppm$) - MIKE

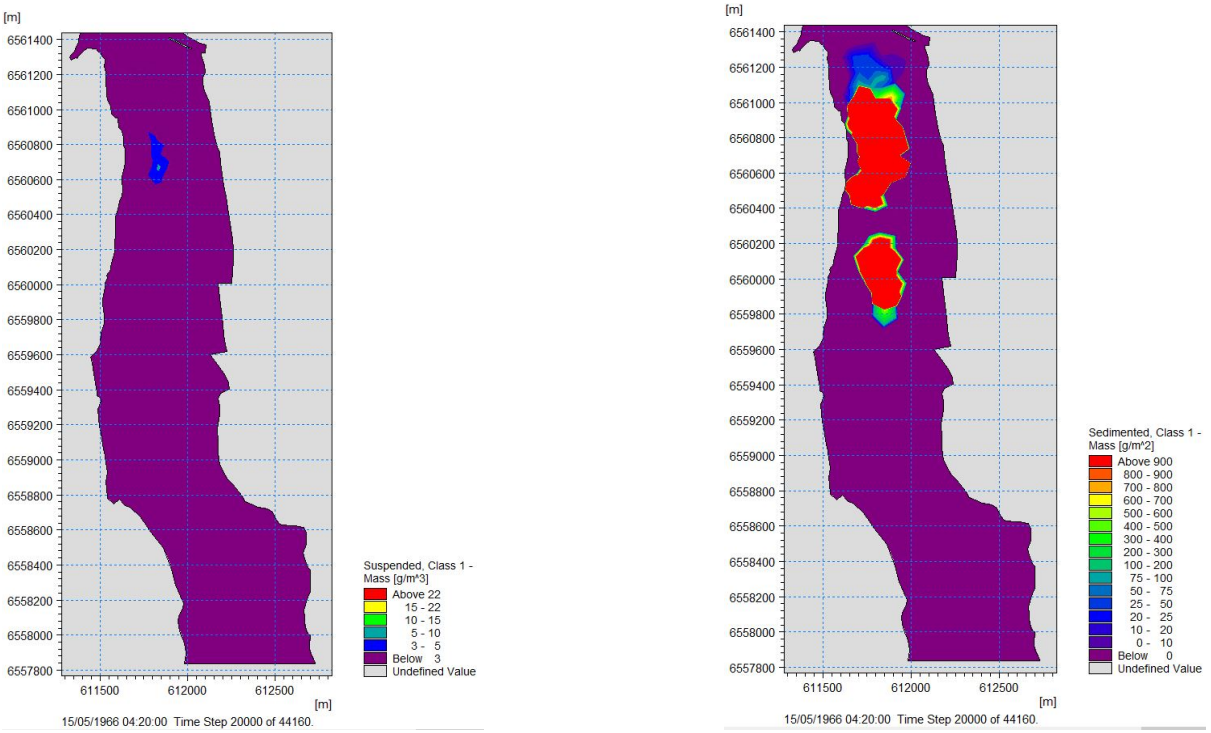

Figure B.16: Concentration of sediments at Borg 1 while dredging with a backhoe ($1g/m^3 = 1ppm$) - MIKE

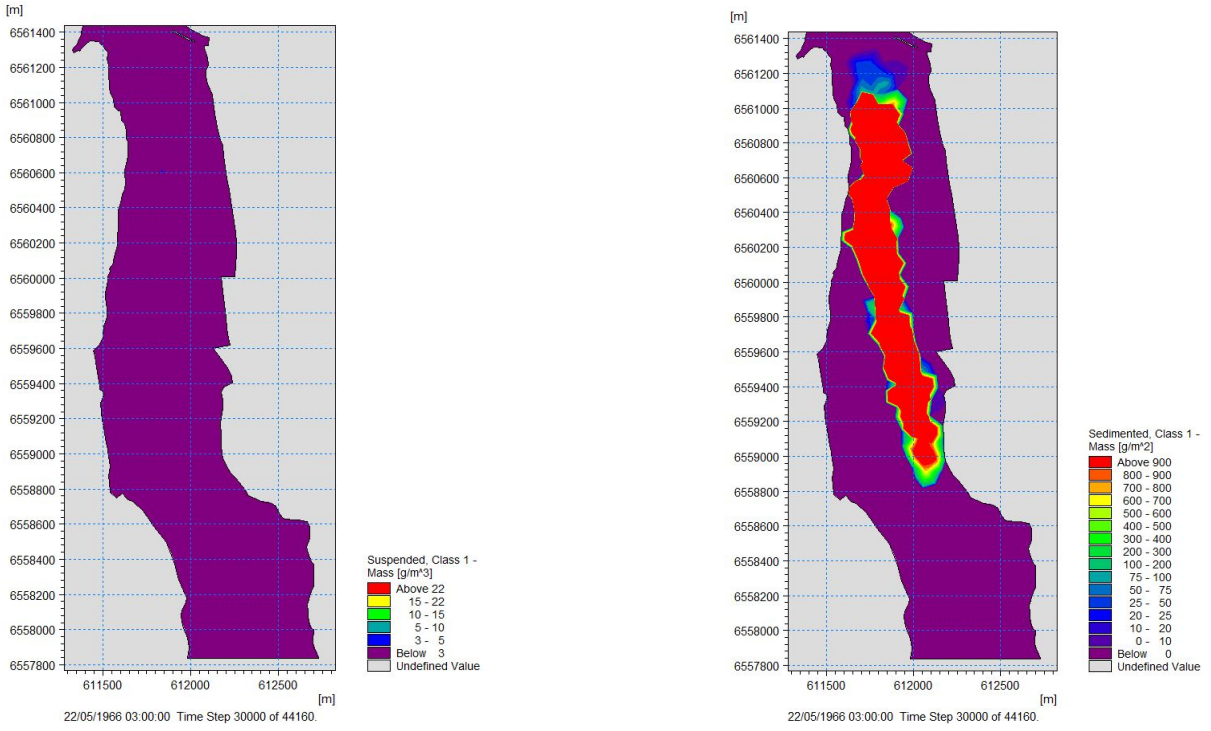

Figure B.17: Concentration of sediments at Borg 1 while dredging with a backhoe ($1g/m^3 = 1ppm$) - MIKE

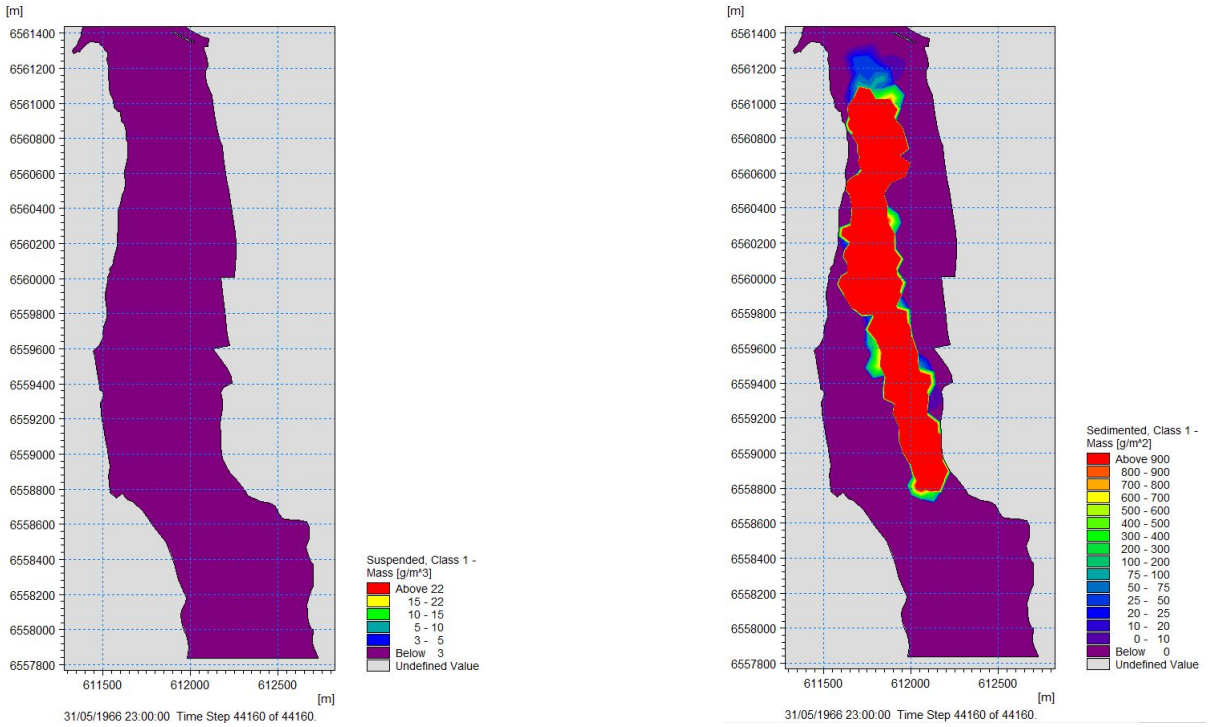

Figure B.18: Concentration of sediments at Borg 1 while dredging with a backhoe ($1g/m^3 = 1ppm$) - MIKE

B.1.4 4th run - 2.778 kg/s - 0.0001 m/s

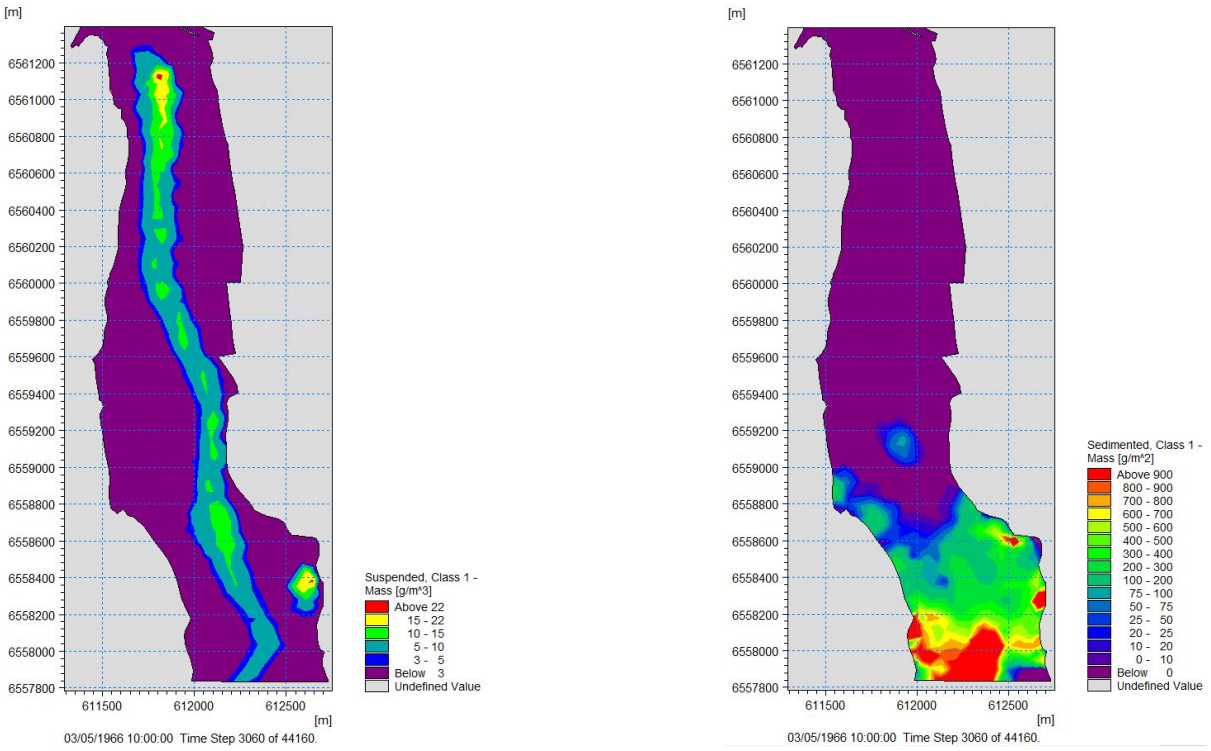

Figure B.19: Concentration of sediments at Borg 1 while dredging with a backhoe ($1g/m^3 = 1ppm$) - MIKE

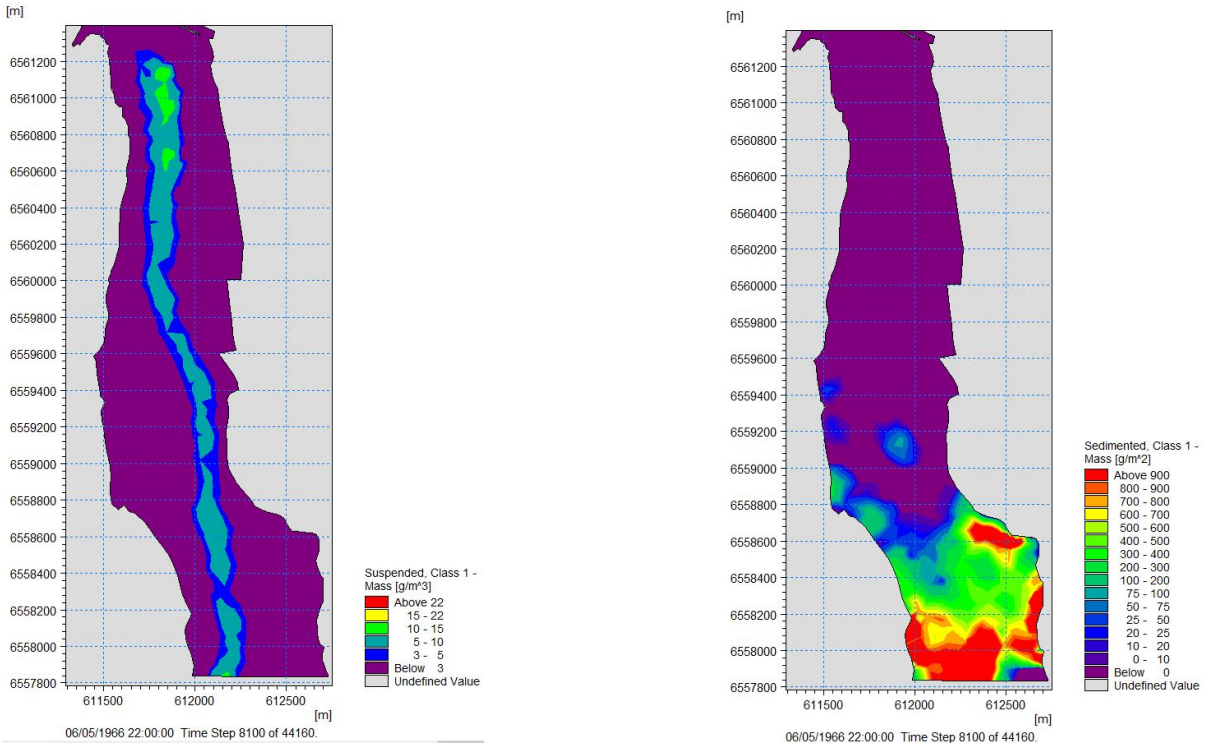

Figure B.20: Concentration of sediments at Borg 1 while dredging with a backhoe ($1g/m^3 = 1ppm$) - MIKE

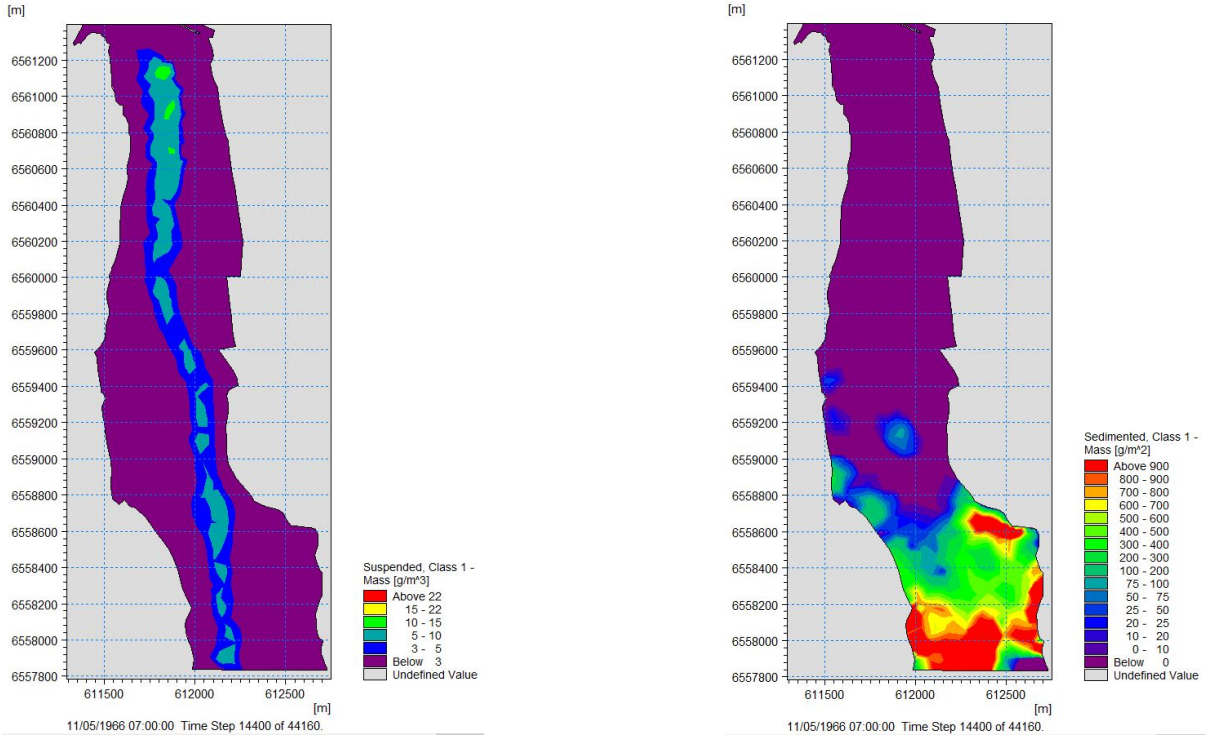

Figure B.21: Concentration of sediments at Borg 1 while dredging with a backhoe ($1g/m^3 = 1ppm$) - MIKE

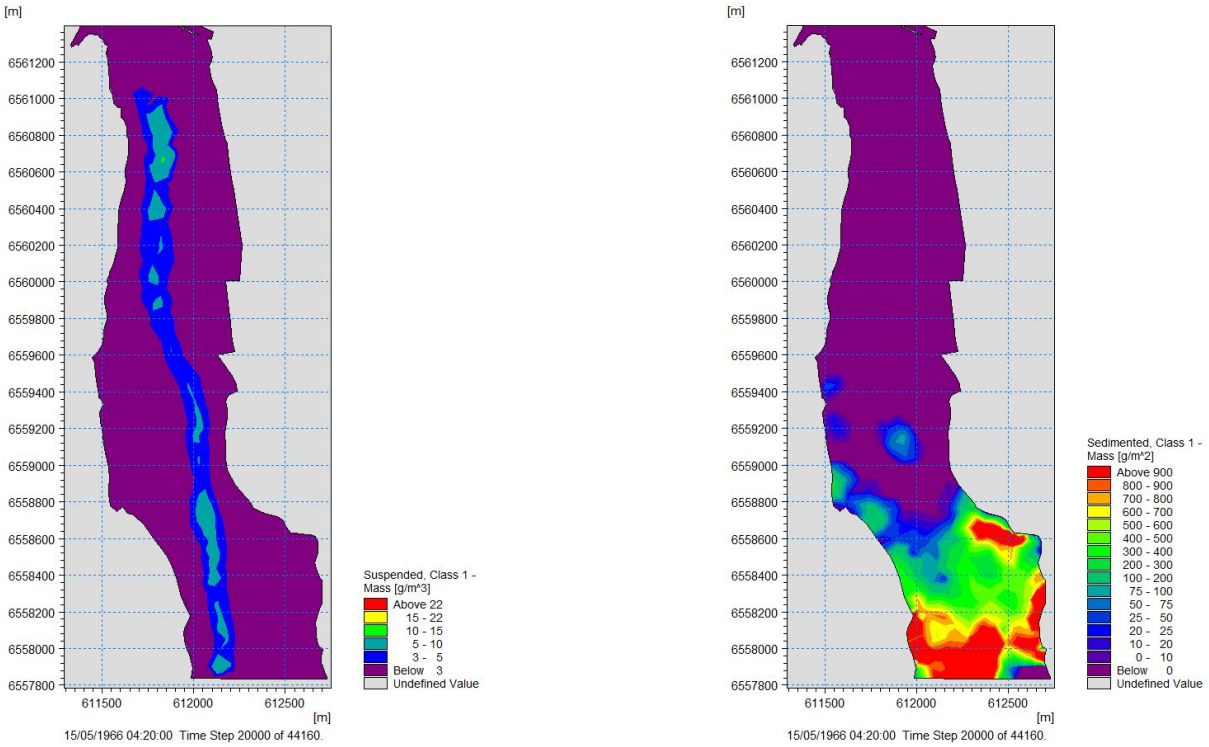

Figure B.22: Concentration of sediments at Borg 1 while dredging with a backhoe ($1g/m^3 = 1ppm$) - MIKE

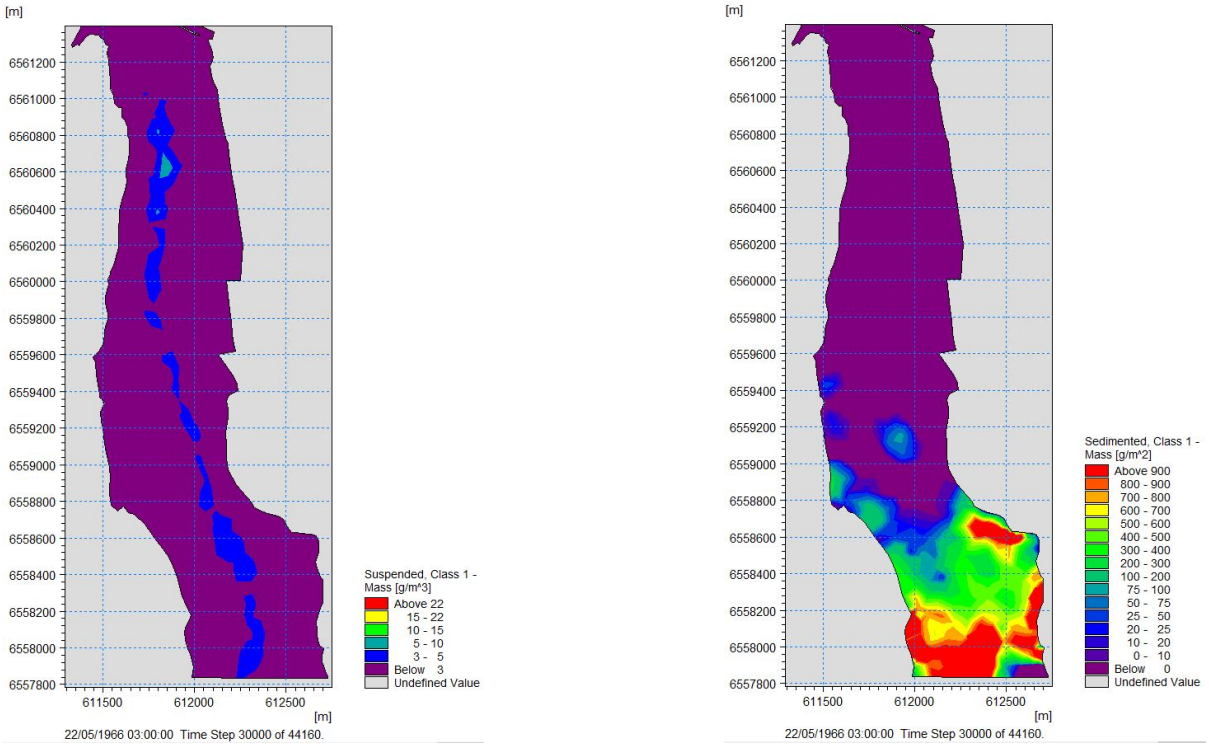

Figure B.23: Concentration of sediments at Borg 1 while dredging with a backhoe ($1g/m^3 = 1ppm$) - MIKE

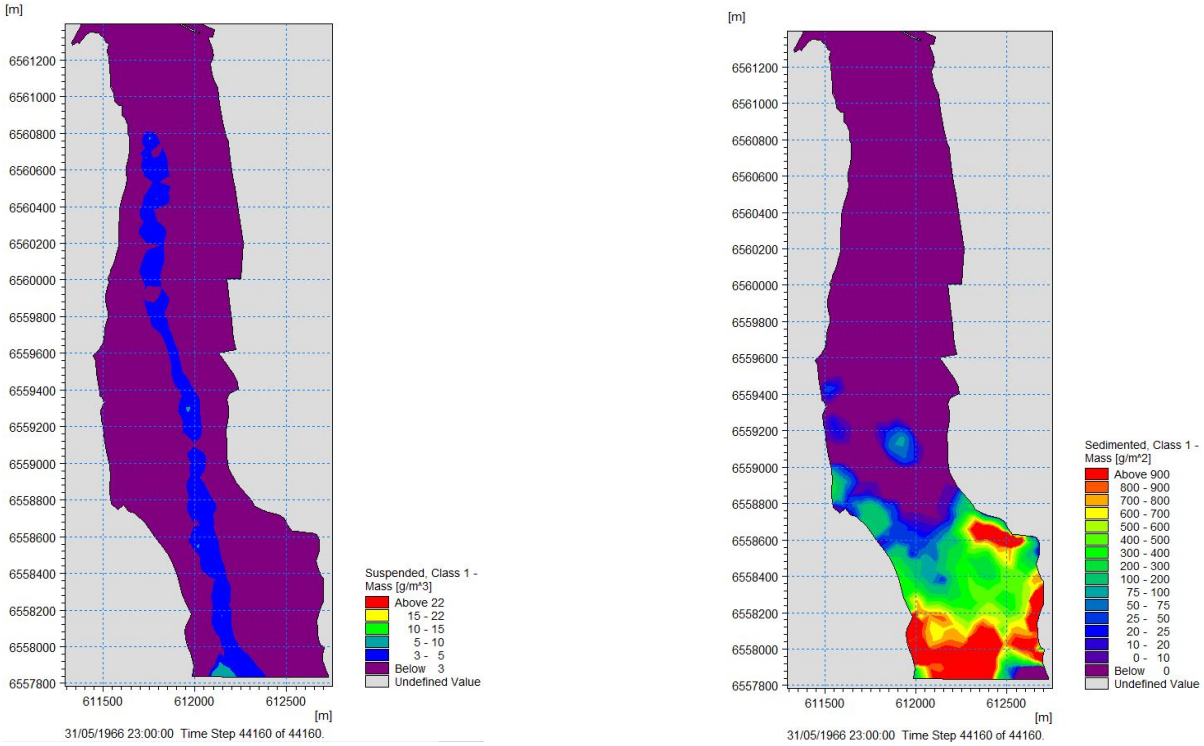

Figure B.24: Concentration of sediments at Borg 1 while dredging with a backhoe ($1g/m^3 = 1ppm$) - MIKE

B.1.5 5th run - 0.695 kg/s - 0.0001 m/s

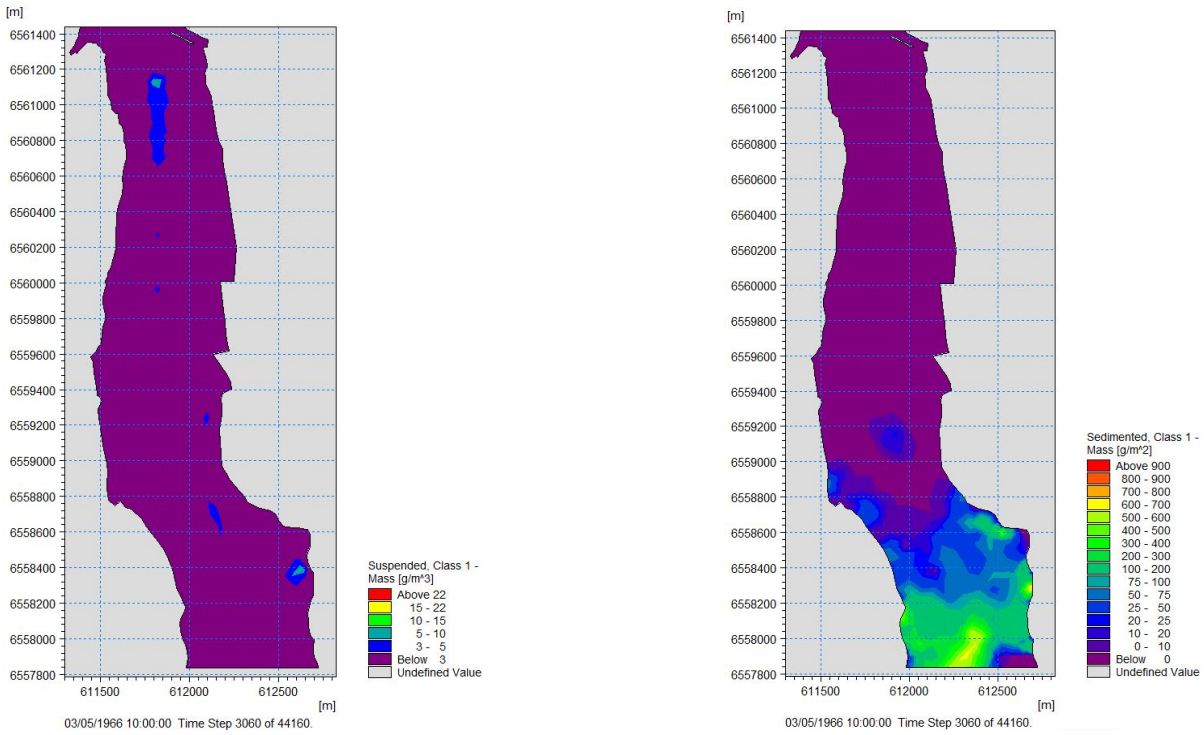

Figure B.25: Concentration of sediments at Borg 1 while dredging with a backhoe ($1g/m^3 = 1ppm$) - MIKE

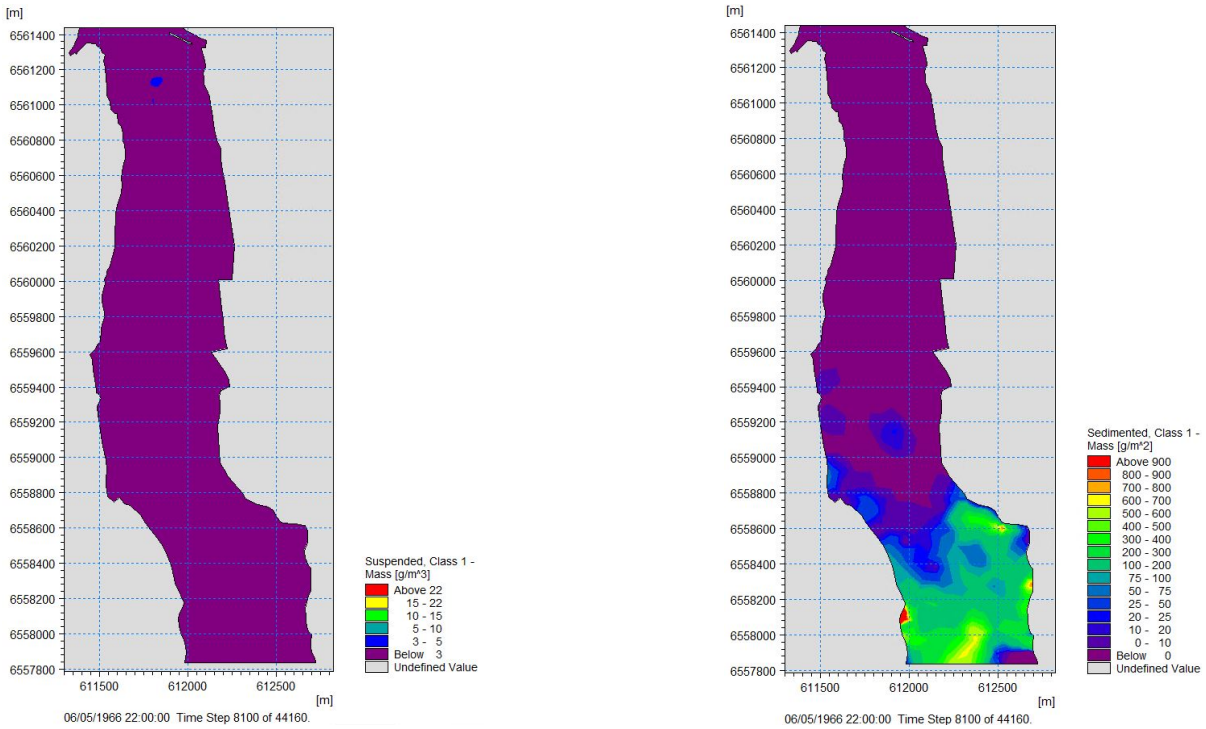

Figure B.26: Concentration of sediments at Borg 1 while dredging with a backhoe ($1g/m^3 = 1ppm$) - MIKE

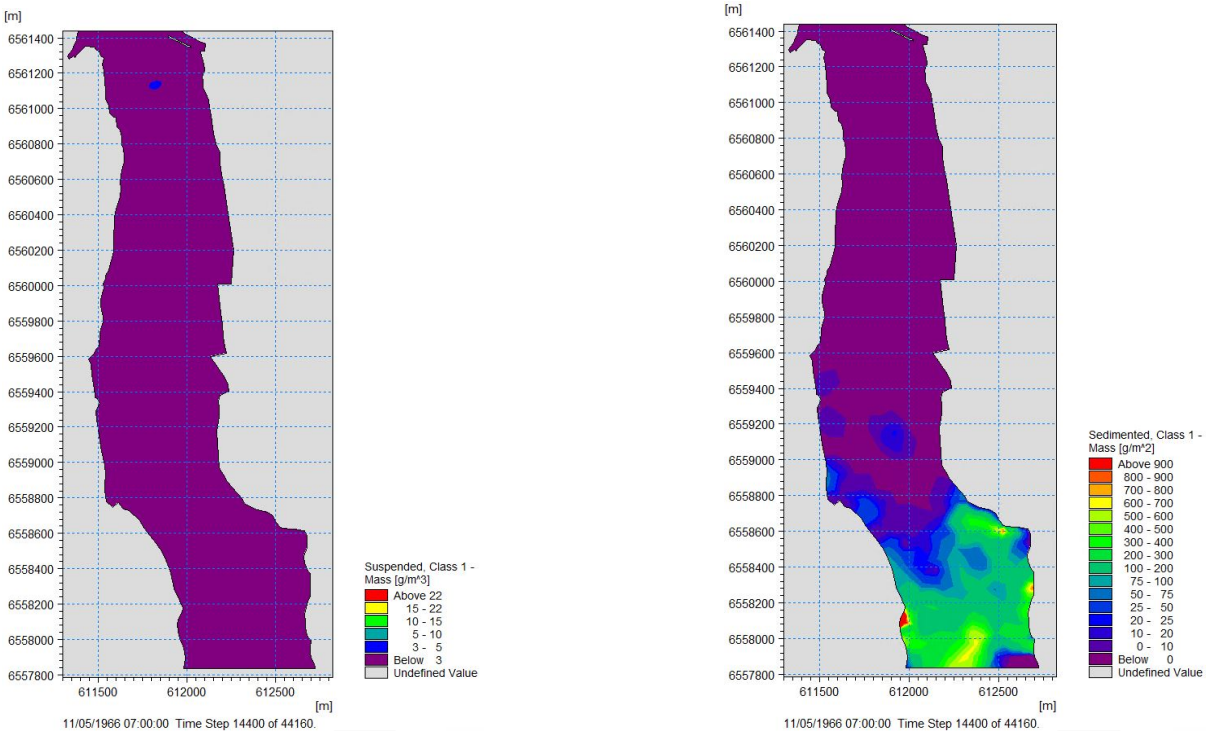

Figure B.27: Concentration of sediments at Borg 1 while dredging with a backhoe ($1g/m^3 = 1ppm$) - MIKE

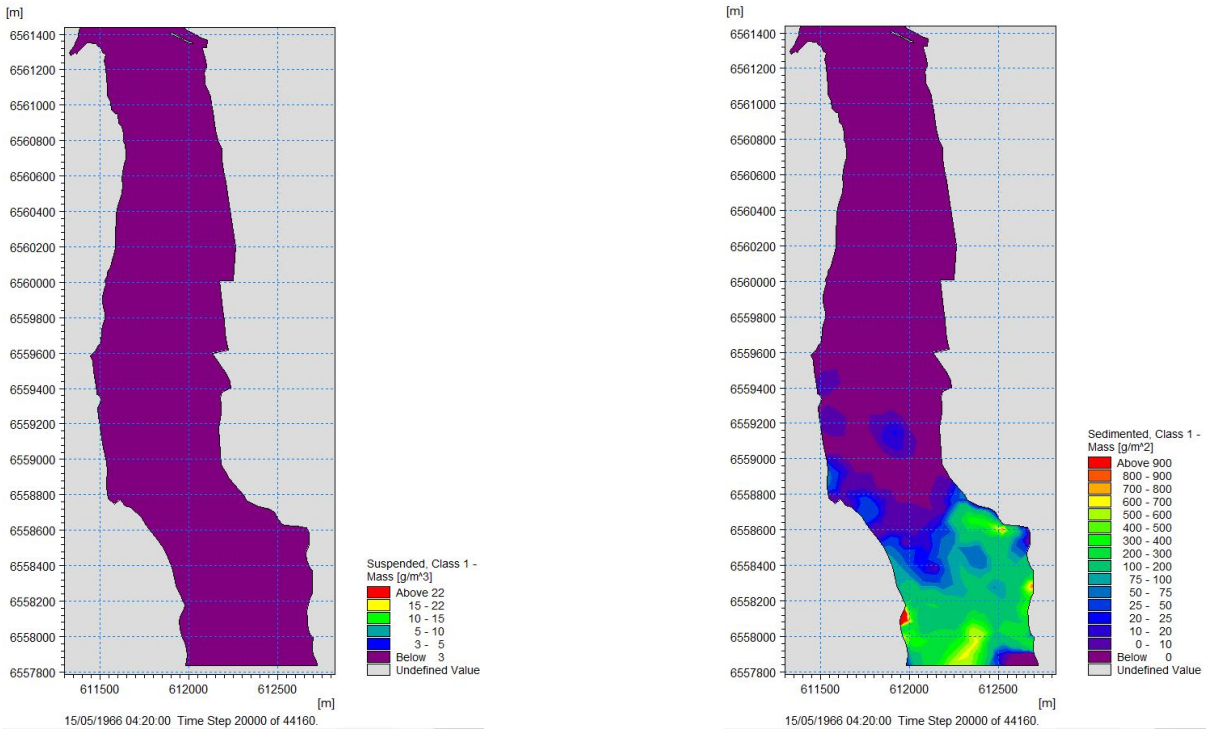

Figure B.28: Concentration of sediments at Borg 1 while dredging with a backhoe ($1g/m^3 = 1ppm$) - MIKE

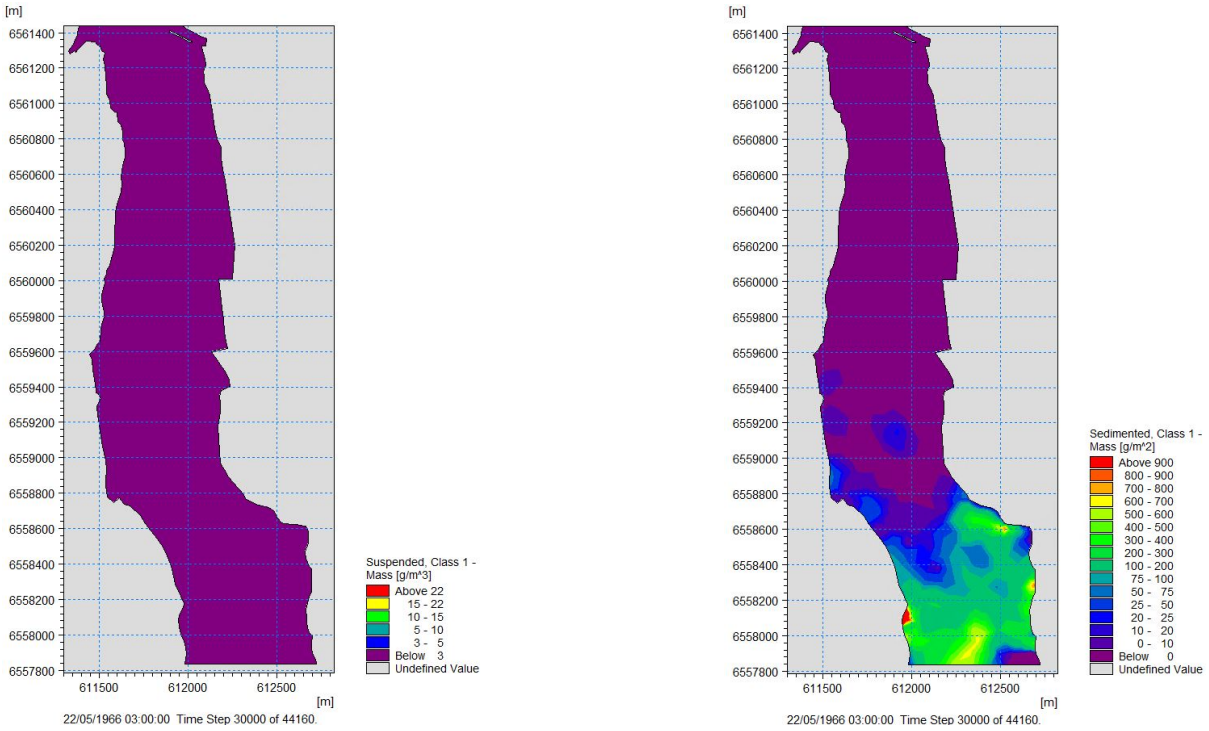

Figure B.29: Concentration of sediments at Borg 1 while dredging with a backhoe ($1g/m^3 = 1ppm$) - MIKE

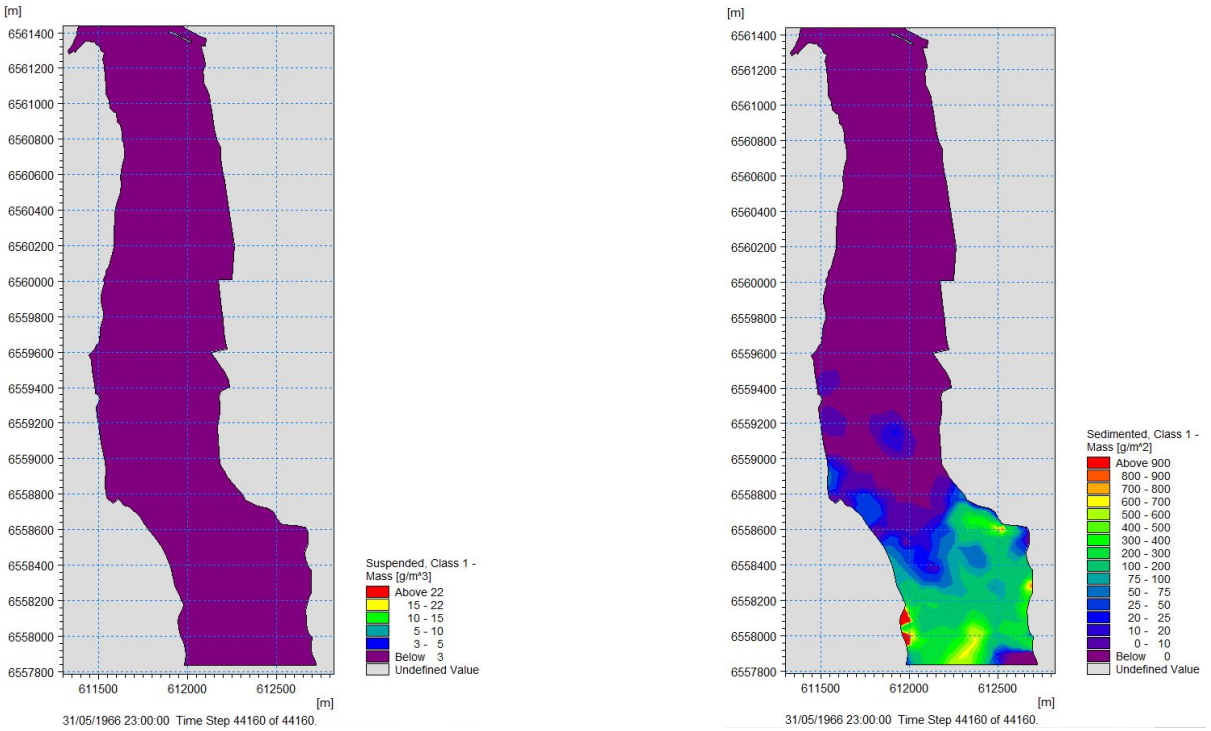

Figure B.30: Concentration of sediments at Borg 1 while dredging with a backhoe ($1g/m^3 = 1ppm$) - MIKE

Maren Elise Bengtson

Assessment of Impact of Dredging on Sediment Transport at Borg Port

NTNU
Norwegian University of
Science and Technology